Discharges in the inlet region of a noble gas MHD generator

Document Version:
Publisher's PDF, also known as Version of Record (includes final page, issue and volume numbers)

Please check the document version of this publication:

DISCHARGES IN THE INLET REGION OF A NOBLE GAS MHD GENERATOR

CARLO A. BORGHI

DISCHARGES IN THE INLET REGION OF A NOBLE GAS MHD GENERATOR

PROEFSCHRIFT

TER VERKRIJGING VAN DE GRAAD VAN DOCTOR IN DE TECHNISCHE WETENSCHAPPEN AAN DE TECHNISCHE HOGESCHOOL EINDHOVEN, OP GEZAG VAN DE RECTOR MAGNIFICUS, PROF. IR. J. ERKELENS, VOOR EEN COMMISSIE AANGEWEZEN DOOR HET COLLEGE VAN DEKANEN IN HET OPENBAAR TE VERDEDIGEN OP DINSDAG 1 JUNI 1982 TE 16.00 UUR

DOOR

CARLO ANGELO BORGHI

GEBOREN TE MASSA LOMBARDA (ITALIE)

Dit proefschrift is goedgekeurd
door de promotoren

Prof.dr. L.H.Th. Rietjens
en
Prof.dr. J.F. Uhlenbusch

co-promotor
Dr. A. Veefkind

to Irene,
whose love, sacrifice and
patience made possible the
completion of this work

CONTENTS

SUMMARY

In this work the onset of the development of the non-equilibrium conductivity in the entrance region of a noble gas MHD generator is investigated both theoretically and experimentally. The relaxation process that leads to the non-equilibrium regime, depends mainly on the ionization rate. At low gas temperatures the ionization relaxation process becomes the limiting factor for the operation of the generator.

At low electron densities a discharge is influenced by deviations from the Maxwellian shape of the electron energy distribution. The non-elastic collisions which cause the transitions from the ground state to the first excited state of cesium yield a loss of highly energetic electrons. At low electron densities the thermalization process due to electron electron collisions is not efficient enough to neutralize this loss so that the tail of the electron distribution is depleted. As a consequence the ionization rate, resulting from collisions of Cs atoms with the more energetic electrons, decreases. Hence the electron density does not build up as fast as predicted by theories in which a Maxwellian distribution is assumed.

First a self consistent model of a stationary discharge in an Ar-Cs mixture at atmospheric pressure is set up. It predicts deviations from the Maxwellian electron distribution for electron densities below $10^{18} \div 10^{19}$ m^{-3} in cases where radiation can escape.

In chapter III deviations from the Maxwellian shape of the electron distribution are included in a model to calculate the time dependence of the electron density and of the populations of excited states following a change in electron energy. An increase of the characteristic time for ionization relaxation is predicted by this theory.

In a discharge experiment two conditions are investigated: a stationary arc discharge and its afterglow. In the stationary situation values of the electron density from 4×10^{20} down to 1×10^{20} m^{-3} have been obtained. During the stationary discharge L.T.E. has been observed. Lower electron densities have been measured during the afterglow. The values of n_e and T_e realized here, agree with those present in the entrance

region of the MHD generator. During the afterglow, conditions for devi-
ations from the Maxwellian electron energy distribution are realized.

An experimental investigation on the transition from low to high
current in the MHD generator, is described in chapter IV. The conditions
during the onset of the non-equilibrium regime correspond to the condi-
tions at the transition from the non-Maxwellian to the Maxwellian regime.
For a low inlet value of n_e ($\lesssim 5 \times 10^{18}$ m^{-3}) a non-Maxwellian electron
distribution is expected so that the non-equilibrium regime becomes diffi-
cult to be built up. As a result the relaxation length becomes longer.
For a magnetic induction of 3 T and an inlet value of n_e lower than
5×10^{18} m^{-3} relaxation lengths larger than 50 cm are obtained. When
the inlet value of n_e is 5×10^{18} m^{-3} the relaxation length is 15 cm.
Higher inlet values of n_e result in shorter relaxation lengths.

NOMENCLATURE

a	transmission of the discharge tube
a'	fitting coefficient for the momentum transfer cross section of argon
a_o	radius of the first Bohr orbit for hydrogen
A_{ji}	Einstein coefficient for spontaneous emission for the j to i transiton
A'_{ji}	Einstein coefficient for spontaneous emission corrected for the radiation trapping
$A_{\lambda i}$	rate integral for two body recombination to the ith state
$A'_{\lambda i}$	rate integral for two body recombination corrected for the radiation trapping
b_{ij}	fitting coefficient for the excitation cross section from i to j
$\vec{B}$	magnetic induction
c	velocity of light ($c = 2.998 \times 10^8$ m/sec)
C_6	van der Waals constant
C_d	correction factor for the critical electron density
d	plasma dimension
D_a	ambipolar diffusion coefficient
D_{Cs}	diffusion coefficient of the ground state atoms of cesium
D_i	diffusion coefficient of Cs^+ ions
e	electron charge ($e = 1.602 \times 10^{-19}$ C)
$\vec{E}$	electric field
$f^b(\varepsilon_e)$, $f^t(\varepsilon_e)$	bulk and tail electron energy distribution function
g_i	degeneracy of the ith state
h	Plank's constant ($h = 6.626 \times 10^{-34}$ J sec)

I_W, I'_W	light intensity of the tungsten ribbon lamp measured with and without the discharge tube on the axis of the optical system
I	electrical current
I_p	pre-ionization current
I_T	minimum current
k	Boltzmann's constant ($k = 1.381 \times 10^{-23}$ J/K)
k_o	assorption coefficient at the line center
K_{ij}	rate integral for excitation for the j to i transiton
K_{ij}	rate integral for deexcitation for the j to i transiton
$K_{i\lambda}$	rate integral for ionization from the ith state
K_{Ri}	rate integral for three body recombination to the ith state
$\vec{J}$	current density
J_c	critical current density for the transition from Maxwellian to non-Maxwellian regime
J_p	pre-ionization current density
J_T	minimum current density
L_R	relaxation length
m_e	electron mass ($m_e = 9.11 \times 10^{-31}$ Kg)
m_i	mass of the particle i
m_{Ar}	mass of the Ar atom ($m_{Ar} = 6.63 \times 10^{-26}$ Kg)
m_{Cs}	mass of the Cs atom ($m_{Cs} = 2.21 \times 10^{-25}$ Kg)
n_{Ar}	argon number density
n_{Cs}	cesium number density
n_e	electron density
n_i	population density of the ith state
$\tilde{n}_e$	normalized electron density
$\tilde{n}_i$	normalized population density of the jth state
p_{Cs}	partial pressure of cesium

2

p_g	gas pressure
p_s	stagnation pressure
P_C^{bt}, P_C^{tb}	energy transfer due to the electron electron collisions from the bulk electrons to the tail electrons and from the tail electrons to the bulk electrons
P_{el}	electrical power output
P_{el}^{b}, P_{el}^{t}	loss of energy due to elastic collision,of the bulk and the tail electrons
P_E^{b}, P_E^{t}	gain of energy due to the electric field,of the bulk and the tail electrons
P_{ij}^{b}, P_{ij}^{t}	energy transfer due to the non elastic collisions to the bulk and the tail electrons
P_{Nel}	total electron energy loss due to non-elastic collisions
P_p	pre-ionization power
P_{th}	thermal power input
r	discharge raduis
R	Rydberg's constant (R = 13.6 eV)
R_L	load resistance
s	seed ratio
T_e	electron temperature
T_g	gas temperature
T_p	population temperature
T_S	stagnation temperature
T_t	tail electron temperature
T_w	wall temperature
u_g	gas velocity
v	velocity of the emitting part of the plasma
v_e	electron velocity
v_s	streak velocity
V	voltage
V_B	battery voltage

V_T	minimum voltage
V_H	Hall voltage
α	streak angle
α_R	recombination coefficient
β_{ij}, $\beta_{\lambda i}$	radiation escape factors
$\Delta\nu$	half width for total broadening
$\Delta\nu_R$, $\Delta\nu_W$	half width for resonance and van der Waals broadening
ε_e	electron energy
ε_{ij}	energy separation between the ith state and the jth state
$\varepsilon_{i\lambda}$	ionization energy for the state i
ε_o	permittivity of free space ($\varepsilon_o = 8.854 \times 10^{-12}$ F/m)
ξ_i	number of equivalent electrons in the ith state
λ	wave length
λ_{Ar}	thermal conductivity of argon
λ_{ji}	wave length corresponding to the transition from the jth to the ith state
Λ, Λ'	arguments of the Coulomb logarithm
μ_i	Cs^+ ions mobility
ν_i	momentum transfer collision frequency for the collisions between electrons and i particles
ν_{ji}	radiation frequency corresponding to the transition from the jth to the ith state
σ	electrical conductivity
σ_{Ar}, σ_{Cs}	momentum transfer cross section for collisions of the electrons with argon and cesium
σ_{ei}	electron ion momentum transfer cross section
σ_i	momentum transfer cross section for collisions between electrons and particles i
σ_{ij}	inelastic collision cross section for the i to j transition
$\sigma_{\lambda i}$	radiative recombination cross section for recombination to the ith state

τ characteristic time for the electron density relaxation

ω_p plasma frequency

INTRODUCTION

I.1 BACKGROUND

When a charged particle moves through a magnetic field it experiences a Lorentz force directed perpendicularly to the velocity of the particle and to the magnetic field. The conversion of thermodynamical energy into electrical energy is based on this phenomenon. In conventional turbo-generators the electrical power is produced by the rotation of a solid conductor between the poles of a magnet. The rotational energy is supplied by a turbine driven by a high speed flow of gas or steam. The energy required to produce the high speed flow is obtained from the combustion of a fossil fuel or by a nuclear reactor. The MHD (magneto-hydrodynamic) generator produces electrical energy by enthalpy extraction from a conducting fluid which moves through a magnetic field. In this device the rotor is eliminated and the energy of the plasma flow is directly converted into electrical energy. The conversion can start at the temperature of the heat source. The Carnot efficiency of a ther-modynamical system can be increased by increasing the ratio between in-let and outlet temperature. The high inlet temperature used in MHD generators gives the possibility to produce electrical power at high efficiencies. The potential offered by the combined MHD steam cycle has been demonstrated by studies (Energy Conversion Alternative Studies) showing conversion efficiencies approaching 50% with a cost of electri-city lower than that of competitive systems (1).

A first type referred as open cycle MHD, employs the combustion products directly as working medium. The oxydized fossil fuel, usually seeded with potassium and heated to about 2800 K, results in a plasma of sufficiently high conductivity. At present the work along this line, has reached the stage of engineering development and the stage of design, construction and operation of large scale facilities.

In the United States the development program consists of a two step approach to commercialization. Phase I is mainly based on investigations carried out in the Component Development and Integration Facility (CDIF), a 100 MWt facility in full operation in the state Montana. For phase II an Engineering Test Facility (ETF) of 200 MWe is proposed to be built.

The USSR National Program pursues the construction (to be completed in 1985) of a commercial MHD combined cycle power plant in Ryazan to be followed by the construction of similar plants in the metropolitan areas. The design of the U 500 Ryazan Power Station (250 MWe MHD topping, 250 MWe steam bottoming cycle) is based on the results of the U 25 facility which, connected to the net of Moscow, has generated 20.4 MWe.

The closed cycle system (CCMHD) utilizes a seeded noble gas as the working medium. The heat is obtained from fossil fuel combustion. CCMHD allows to obtain a plasma by non-equilibrium ionization at a relatively low temperature (2000 K). This eliminates the severe material problemes present in the open cycle MHD. Besides a fossil fuel combustor the noble gas MHD system can be coupled to a solar heater [2] or to a thermonuclear reactor [3].

During the late sixties electrical power generation in CCMHD generators has been demonstrated by blow-down experiments [4] with test times of about 10 sec. Electrical outputs up to 8 kWe were obtained in these experiments. In shock tunnel MHD experiments with noble gases (test time ∿ 5 msec) power densities over 100 MWe/m^3 and enthalpy extractions of over 20% have been achieved. At an inlet stagnation temperature of 2000 K and a magnetic induction of 3 T, an enthalpy extraction of over 10% has been detected [5]. Stimulated by these results the work on CCMHD was focussed on a system which utilizes a fossil fuel heat source [6]. A 5 MWt blow-down facility coupled to a propane fired heat exchanger, has been constructed at the Eindhoven University of Technology. During the first series of runs the electric power of the generator was 270 kWe. Later the electrical output has been increased to 360 kWe [7].

The study of the present work is devoted to the processes occurring in plasmas for CCMHD generators at the low current density regime in the entrance region of the generator. A high enthalpy extraction depends on the level of non-equilibrium conductivity which can be attained in a noble gas plasma with a temperature of 2000 K. The required level of conductivity has to be built up in a sufficiently short distance behind

the entrance of the generator. The non-equilibrium ionization caused by
the Joule heating of the electrons produces the charge carriers. Hence
it permits the transition from the low current regime present at the
inlet of the generator, to the high current regime substained by the
non-equilibrium conductivity. As a consequence the possibility of
building up the non-equilibrium regime is strongly dependent on the
phenomena that affect the plasma during the ionization when the current
is still low.

I-2 RELATED WORKS

One nor two dimensional numerical calculations (8) can explain
the long relaxation region observed in linear generators (see Veefkind
et al. in Ref. 5). The two dimensional calculations, carried out at
low stagnation temperature, predict relaxation lengths of a few centi-
meters up to the channel height whereas relaxation regions with lengths
up to the generator length are observed at low temperatures or low mag-
netic inductions. The calculations assume a Maxwellian electron energy
distribution.

The experimental data of Kerrebrock and Hoffman (9) on an alkali
seeded noble gas discharge show a transition from low to high current
densities where a peak in the required electric field occurs (Fig. I-1).
The anomalous behaviour is attributed by the authors to a non-Maxwellian
electron energy distribution. They argue that the high energy tail is
depleated owing to collisional ionizations faster than it can be re-
plenished by thermalization. The thermalization time is long because
of the low electron electron collision frequencies at these low elec-
tron densities. The depletion of the high energy tail of the electron
distribution causes a slower building up of the current density.

The electron energy distribution in a low current discharge in
cesium vapour, determined by means of a Langmuir probe, has been
measured by Postma (10). The measurements, carried out at a gas densi-
ty of about 10^{21} m^{-3} and electron densities in the range $10^{16} \div 10^{17}$ m^{-3},
show that the distribution function decreases steeply above 1.4 eV.
That is in agreement with the theoretical prediction based on the so-
lution of the Boltzmann equation.
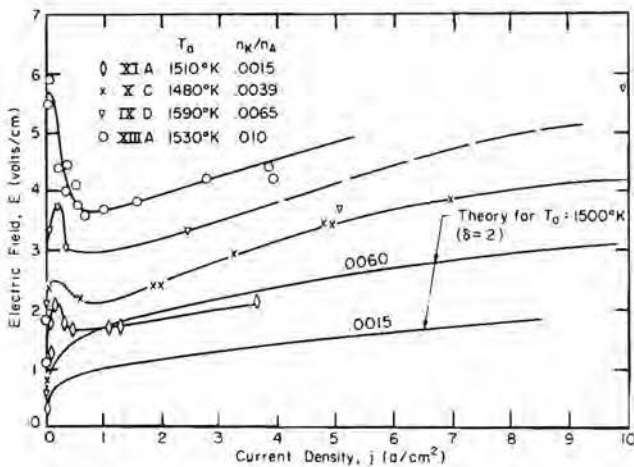
Figure I-1.
Experimental electric field vs current density characteristics
for four different seeding fractions but all at about 1500 K gas
temperature using an argon gas seeded with potassium at 1 atm total
pressure (from Ref. 9).

Calculations which attempt to solve the kinetic equation for the
free electrons are presented in Ref. 11. They indicate substantial
deviations from a Maxwellian electron distribution when the non-elastic
terms are taken into account in the calculations. The solution of the
Boltzmann equation for the free electrons, coupled to the rate equations
for the populations of the excited states of cesium, is given by Dugan.
It yields a decreased ionization degree in comparison with that obtained
with Maxwellian models for electron densities lower than 10^{19} m^{-3}.
However these calculations suffer from numerical problems. Shaw pre-
sents in Ref. 12 a self consistent solution of the free electron Boltz-
mann equation coupled to the rate equations yielding numerical results
for hydrogen plasmas.

Up to now no work includes the effect of a non-Maxwellian electron
distribution on the ionization relaxation process in plasmas for noble
gas MHD generators.

The aim of the present study is to get a better understanding of the processes which govern the discharge at the entrance of a noble gas MHD generator. At low electron densities the discharge seems to be affected by a non-Maxwellian electron distribution. The main questions to which this work is devoted are:

1. Is the electron distribution in the entrance region of the generator non-Maxwellian?

2. Can the non-Maxwellian electron distribution be the cause of the observed long ionization relaxation at low stagnation temperatures?

In Chap. II a self-consistent model of a stationary discharge in an Ar-Cs mixture at atmospheric pressure, is set up. It includes the possibility of deviations from a Maxwellian electron energy distribution. The model allows to calculate at what discharge parameters deviations from the Maxwellian electron distribution will become important. In Chap. III the relaxation of the plasma to a new equilibrium situation following a sudden change in the electron thermal energy is calculated by a model which can take radiation and a non-Maxwellian distribution into account. In Chap. IV an Ar-Cs discharge experiment is described with plasma parameters similar to those present in the entrance region of the generator. A stationary arc discharge for current densities of $2.5 \times 10^4 \div 4 \times 10^4$ Am^{-2} is investigated to cover electron densities between 1×10^{20} and 4×10^{20} m^{-3}. Lover electron densities are obtained in the afterglow of the discharge . In order to see if the plasma during the afterglow is affected by deviations from the Maxwellian electron energy distribution, terms of the energy balance equation of the higly energetic electrons, obtained from the experiment, are compared. The ionization relaxation process in a noble gas MHD generator is experimentally studied and described in Chap. V. In this chapter the relaxation ionization region with and without pre-ionization is investigated. Current voltage characteristics are obtained by varying the applied voltage or the external load. The results are confronted with the theoretical results of the non-Maxwellian model developed in Chap. II. Conclusions of this work are drawn in Chap. VI.

REFERENCES

1. RIETJENS, L.H.Th., RUDINS, G., SLUYTER, M.M., "The present status of MHD for large scale electrical power generation", Proc. 11th World Energy Conference, WG 7, Munich, (1980).

2. NEGRINI, F., GENTILINI, M., MONTANARI, I., "Study of solar heat exchanger-closed cycle pulsed MHD system", Proc. 7th Int. Conf. on MHD Power Generation, Vol. 2, p. 171, Cambridge, Mass., (1980).

3. BREEV, V.V., VELIKHOV, E.P., VOLKOV, Yu.M., GOLUBEV, V.S., PANCHENKO, V.P., CHERNUKHA, V.V., YAKUSHEV, A.A., "Problems of building optimum conductive-type MHD generators for thermonuclear power plants", Proc. 6th Int. Conf. on MHD Power Generation, Vol. 5, p. 155, Washington, (1975).

4. BERTOLINI, E., GASPAROTTO, M., GAY, P., and TOSCHI, R., "Subsonic constant area MHD generator experiments with the CNEN blow-down loop facility", Proc. 4th Int. Symp. on MHD, Vol. 2, p. 957, (1968); DECHER, R., HOFFMAN, M.A., KERREBROCK, J.L., "Behaviour of a large non-equilibrium MHD generator", AIAA Jour., Vol. 9, p. 357, (1971).

5. VEEFKIND, A., HOUBEN, J.W.M.A., BLOM, J.H., and RIETJENS, L.H.Th., "High-power density experiments in a shock-tunnel MHD generator", AIAA Jour., Vol. 14, p. 1118, (1976); MARSTON, C., TATE, E., and ZAUDERER, B., "Large enthalpy extraction results in a non-equilibrium MHD generator", Proc. 6th Int. Conf. on MHD Power Generation, Vol. 3, p. 89, Washington, (1975); VEEFKIND, A., HELLEBREKERS, W.M., BORGHI, C.A., RIETJENS, L.H.Th., "Noble gas MHD generator experiments at low stagnation temperatures", Proc. 17th Symp. Eng. Asp. of MHD, p.H. 3.1, Stanford, Calif., (1978).

6. RIETJENS, L.H.Th., "Fossil fired closed cycle MHD", Proc. Specialists Meeting on Coal Fired MHD Power Generation, p. 511, Sydney, (1981).

7. MASSEE, P., et al., "Gasdynamic performance in relation to the power extraction of the Eindhoven MHD Blow-Down Facility", to be published, Proc. 20th Symp. Eng. Asp. of MHD, Irwine, Calif., (1982). FLINSENBERG, H.J., et al., "Instability analysis of the first power runs with the Eindhoven MHD blow-down facility" to be published, Proc. 20th Symp. Eng. Asp. of MHD, Irwine, Calif., (1982).

8. BERTONLINI, E., TOSCHI, R., Mc NAB, I.R., "Relaxation phenomena in MPD generators", Proc. 3rd Int. Symp. on MHD, Vol. 1, p. 533, Salzburg, (1966);

TAKESHITA, T., GROSSMAN, L.M., "Excitation and ionization processes in non-equilibrium MHD plasmas", Proc. 4th Int. Symp. on MHD, Vol. 1, p. 191, Warsaw, (1968);

BLOM, J.H., and HOUBEN, J.W.M.A., "Relaxation length calculations in Ar-Cs mixtures for one- and two-dimensional pre-ionizer geometries", Proc. 5th Int. Symp. on MHD, Vol. 2, p. 65, Munich, (1971);

HARA, T., VEEFKIND, A., RIETJENS, L.H.Th., "A numerical investigation of the inhomogeneous discharge structure in noble gas MHD channels", Proc. 19th Symp. on Eng. Asp. of MHD, p. 7.2.1, Tullahoma, Tenn., (1981).

9. KERREBROCK, J.L., and HOFFMAN, M.A., "Non-equilibrium ionization due to electron heating: II. Experiments", AIAA Jour., Vol. 2, p. 1080, (1964).

10. POSTMA, A.J., "Measurements on the electron energy distribution function in a low pressure cesium discharge", Physica, Vol. 49, p. 77, (1970);

POSTMA, A.J., "Calculations of the momentum-transfer cross section of electrons in cesium vapour from drift-velocity measurements", Physica, Vol. 43, p. 465, (1969).

11. POSTMA, A.J., "Influence of several types of inelastic collisions on the electron energy distribution in helium", Physica, Vol. 45, p. 609, (1970);

POSTMA, A.J., "Electron energy distributions in discharges in cesium-argon mixtures", Physica, Vol. 48, p. 447, (1970);

DUGAN, J.V., LYMAN, F.A., and ALBERS, L.V., "Solution of the Boltzmann and rate equations for the electron distribution function and state population in non-equilibrium MHD plasmas", Proc. 3rd Int. Symp. on MHD, Vol. 2, p. 85, Salzburg, (1966);

SHAW, J.F., KRUGER, C.H., MITCHNER, M., and VIEGAS, J.R., "Examination of the validity of the Saha equation in a gas discharge", Proc. 3rd Symp. on MHD, Vol. 2, p. 77, Salzburg, (1966);

VIEGAS, J.R., and KRUGER, C.H., "Electron distribution function for a non-equilibrium plasma in a strong electric field", Phys. of Fluids, Vol. 12, p. 2050, (1960).

12. SHAW, J.F., MITCHNER, M., and KRUGER, C.H., "Effects of non-elastic collisions in partially ionized gases. Part I and II", Phys. of Fluids, Vol. 13, p. 325, (1970).

MODEL OF THE STATIONARY DISCHARGE

II-1 INTRODUCTION

In this chapter a self consistent model for low current discharges will be set up. The model includes the possibility of deviations from the Maxwellian electron energy distribution function due to the excitations to the first excited level of the cesium atoms. For this purpose the two electron group model of Vriens (1,2) is used. In this model the electrons are divided into two energy groups, one for the electrons with energies smaller than the threshold energy of excitation to the first excited state of cesium, the other for the electrons with higher energies. Two different Maxwellian functions are assumed to describe the electron distribution in the two groups. That allows to replace the integro-differential Boltzmann equation for the electron energy by two algebraic equations. They represent the energy balance equations for the low energetic electrons and for the high energetic electrons. This method has been already applied to low pressure discharges (8). The comparison of the results with Boltzmann calculations gives a good agreement (3). In argon cesium plasmas at atmospheric pressure deviations from the Maxwellian distribution function due to non-elastic collisions play an important role at the electron densities investigated. In Fig. II-1 this effect is estimated. In the figure the energy transfer term from low to high energetic electrons, due to electron electron collisions, P_C^{bt}, and the energy loss term due to excitations to the first resonance level, P_{12}^t, are plotted as a function of the electron density. When the electron electron collision energy terms are the dominating terms in the energy balace of the high energetic electrons, the electron distribution is described by a Maxwellian function. For P_{12}^t of the same order as P_C^{bt} the tail of the electron distribution may become depleted. In the discharge under investigation P_{12}^t and P_C^{bt} are of the same order for $n_e \sim 10^{18}$ m^{-3}.
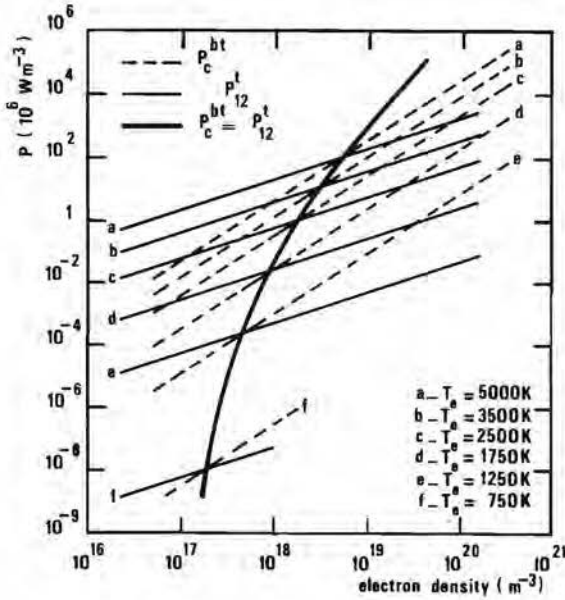
Figure II-1.

Energy flow from the bulk electrons to the tail electrons due to Coulomb interactions, P_C^{bt}, and energy loss P_{12}^t by excitations to the 6P level of cesium P_{12}^t, against the electron density for $n_{Cs} = 10^{22}\ m^{-3}$.

A three level model for the Cs atom is described in Sec. II-2. It includes electron collision transitions, radiative transitions and the effects of diffusion. The two electron group model is described in Sec. II-3. Based upon it, the rate coefficients for electron induced transitions will be dealt with. In Sec. II-4 the effects of resonance radiation trapping and radiative recombination will be considered. Further in Sec. II-5 a method to take into account the effects of ambipolar diffusion is described. A set of solutions for the plasma parameters of interest in MHD generators and a discussion of the typical results are given in Sec. II-6.

In the model the argon cesium discharge is considered axially uni-
form. The noble gas is assumed to act only as a buffer gas. The cesium
atom is described by a three level model (Fig. II-2) consisting of the
ground state $6S_{\frac{3}{2}}$ (state 1), the double degenerated 6P state (state 2),
and the singly ionized state (state 3). The energy differences between
the three levels are: ε_{12} = 1.432 eV, ε_{23} = 2.462 eV, and ε_{13} = 3.894 eV.
The statistical weights are g_1 = 2, g_2 = 6, and g_3 = 1. Electron
induced transitions, radiative transitions and diffusion processes
are taken into account. The transitions due to electron atom collisions
consist of 1) excitations from the ground to the excited level and the
reverse processes, 2) ionizations from the ground state and the excited
level, and 3) three body recombinations to the ground state and to the
excited level.
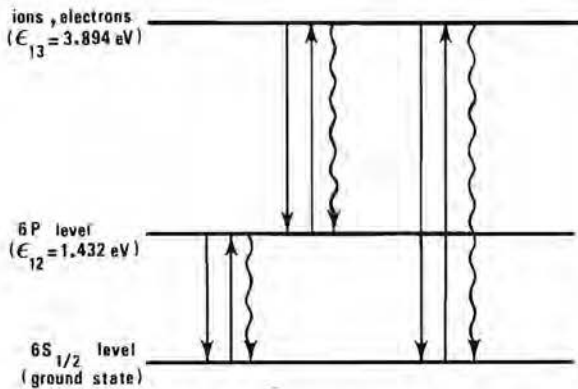
Figure II-2.
The three level model of the Cs atom where the wavy arrows indi-
cate radiative transitions and the straight arrows indicate elec-
tron induced transitions.

The radiative transitions are 1) radiative decay of the excited atoms,
2) absorption of radiation by ground state atoms and 3) radiative re-
combinations to the excited and the ground level. For the radiations
of the last kind the plasma is assumed to be optically thin. The
assumption of quasi-neutrality is made (i.e. the electron density is

assumed equal to the ion density) and the diffusion processes are
assumed to be ambipolar: the charged particles diffuse to the plasma
boundery where they recombine. After recombination the resulting neu-
tral particles return to the plasma.

The rate equations for the ground state density n_1, the excited
state density n_2, and the electron density n_e read:

$$\dot{n}_1 = D_{Cs}\nabla^2 n_1 - n_1 n_e (K_{12} + K_{13}) + n_2 (n_e K_{21} + \beta_{21}A_{21}) +$$

$$n_e^3 K_{R1} + n_e^2 A_{\lambda 1},\tag{II-1}$$

$$\dot{n}_2 = n_1 n_e K_{12} - n_2 \{n_e (K_{21} + K_{23}) + \beta_{21}A_{21}\} +$$

$$n_e^3 K_{R2} + n_e^2 A_{\lambda 2},\tag{II-2}$$

$$\dot{n}_e = D_a \nabla^2 n_e + n_e (n_1 K_{13} + n_2 K_{23}) - n_e^3 (K_{R1} + K_{R2}) -$$

$$n_e^2 (A_{\lambda 1} + A_{\lambda 2}),\tag{II-3}$$

where ∇^2 stands for the Laplace operator and $\dot{n}_i$ for the partial time
derivative of n_i. D_{Cs} is the diffusion coefficient of the ground state
atoms and D_a the ambipolar diffusion coefficient.
K_{ij} is the rate integral for the transition from the i-th to the j-th
state due to electron collisions. K_{Ri} and $A_{\lambda i}$ are the three body and
the radiative recombination coefficients respectively. $\beta_{21}A_{21}$ is the
radiative deexcitation coefficient from level 2 where A_{21} is the
Einstein coefficient and β_{21} accounts for reabsorption.

II-3 ELECTRON ENERGY MODEL

II-3-1- Basic relations

The two electron group model of Vriens (1) is used to describe the
energy distribution of the electrons. A subdivision of the electrons in-
to two groups, bulk electrons and tail electrons, is made. The elec-
trons with energies below the excitation energy threshold of the first
excited level ε_{12}, belong to the first group, the electrons with

energies $\varepsilon_e \geq \varepsilon_{12}$ belong to the second group. Two Maxwellian distribution functions are assumed to describe the two electron energy groups: $f^b(\varepsilon_e)$ for the bulk electrons with a temperature T_e, and $f^t(\varepsilon_e)$ for the tail electrons with a temperature T_t :

$$f^b(\varepsilon_e) = 2 \left\{ \frac{\varepsilon_e}{\pi(kT_e)^3} \right\}^{\frac{1}{2}} \exp\left(- \frac{\varepsilon_e}{kT_e}\right) \quad , \qquad\qquad (II-4)$$

$$f^t(\varepsilon_e) = 2 \left\{ \frac{\varepsilon_e}{\pi(kT_t)^3} \right\}^{\frac{1}{2}} \exp\left(- \frac{\varepsilon_e}{kT_t}\right) \quad , \qquad\qquad (II-5)$$

where ε_e is the energy of the electron, k is the Boltzmann constant. The electron distribution function has to fulfil the normalization condition. The expressions given in eqs. II-4 and II-5 do fulfil this condition in a good approximation as discussed in Appendix A.

Separate energy conservation equations can be written for either group of electrons. In the stationary case they read for tail and bulk electrons respectively:

$$P_E^t + P_{21}^t + P_{31}^t + P_{32}^t + P_C^{bt} = P_{el}^t + P_{12}^t + P_{13}^t + P_{23}^t + P_C^{tb} \, , \quad (II-6)$$

$$P_E^b + P_{12}^b + P_{13}^b + P_{23}^b + P_C^{tb} = P_{el}^b + P_{21}^b + P_{31}^b + P_{32}^b + P_C^{bt} \, , \quad (II-7)$$

where the terms on the left hand side and right hand side of eq. II-6 and eq. II-7 stand for the local energy gain and loss respectively. The subscripts E, 21, 31, 32, el, 12, 13, 23, C denote: electric field, deexcitation from level 2 to 1, recombination to level 1 and to level 2, elastic collision with the heavy particles, excitation to level 2, ionization from level 1 and 2, electron electron Coulomb interaction. The superscript t (b) refers to the tail (bulk) electrons. The terms P_C^{bt} and P_C^{tb}, represent a flow of energy from the bulk to the tail and from the tail to the bulk due to electron electron interaction.

The contributions of the bulk and of the tail electrons to the average of the quantity A over the electron distribution, are indicated as:

$$\langle A \rangle^b = \int_0^{\varepsilon_{12}} A f^b(\varepsilon_e) d\varepsilon_e \quad , \tag{II-8}$$

$$\langle A \rangle^t = \int_{\varepsilon_{12}}^{\infty} A f^t(\varepsilon_e) d\varepsilon_e \quad . \tag{II-9}$$

The terms in eq. II-6 and eq. II-7 will be now defined. The electric field and elastic collision terms in the tail are:

$$P_E^t = \frac{n_e e^2 E^2}{3kT_t} < \frac{v_e}{\sum_i \sigma_i n_i} >^t \quad , \tag{II-10}$$

$$P_{el}^t = \sum_i n_e n_i \frac{2m_e}{m_i} < v_e \sigma_i (\varepsilon_e - \varepsilon_g) >^t . \tag{II-11}$$

P_E^b and P_{el}^b result from replacing the subscript t by b. In eq. II-10 and eq. II-11 E is the electric field, e and m_e the electron charge and mass, and $v_e = (2\varepsilon_e/m_e)^{\frac{1}{2}}$ the electron velocity; n_i and m_i are the density and the mass of the atomic species i which constitutes the plasma, σ_i its momentum transfer cross section for elastic collisions and ε_g is the gas energy. The formulas given in eq. II-10 and eq. II-11 are the standard expressions for the Joule heating and the elastic collision loss term [4] where the integration average in the whole region of the electron energy is replaced by the integrations in the tail and in the bulk region. In eq. II-11 the energy of the heavy particles is neglected when P_{el}^t is considered for the tail electrons.

The excitation and ionization terms are:

$$P_{ij}^t = n_e n_i \left\{ < v_e \sigma_{ij} \varepsilon_{ij} >^t + \int_{\varepsilon_{12}}^{(\varepsilon_{12} + \varepsilon_{ij})} v_e \sigma_{ij} (\varepsilon_e - \varepsilon_{ij}) f^t(\varepsilon_e) d\varepsilon_e \right\} \quad , \tag{II-12}$$

$$P_{ij}^{b} = n_e n_i \int_{\varepsilon_{12}}^{(\varepsilon_{12} + \varepsilon_{ij})} v_e \sigma_{ij} (\varepsilon_e - \varepsilon_{ij}) f^t(\varepsilon_e) d\varepsilon_e, \tag{II-13}$$

where $i < j$; $i, j = 1,2,3$.

Here σ_{ij} denotes the inelastic electron collision cross section for the transition $i \rightarrow j$. The first term in the right hand side of eq. II-12 accounts for the excitation energy difference between the levels i and j, the second term accounts for the fact that an energy $\varepsilon_e - \varepsilon_{ij}$ is transferred from the tail to the bulk during an excitation or an ionization. This energy is transferred to the bulk electrons as given by eq. II-13.

Similarly for superelastic collisions:

$$P_{ji}^{t} = n_e n_j \left\{ <v_e \sigma_{ji} \varepsilon_{ji}>^b + <v_e \sigma_{ji} \varepsilon_e>^b \right\} , \tag{II-14}$$

$$P_{ji}^{b} = n_e n_j <v_e \sigma_{ji} \varepsilon_e>^b . \tag{II-15}$$

The Coulomb terms are derived by Vriens in Ref. 5. The term P_C^{tb} is obtained as the summation of two expressions. The first one accounts for the almost continuous slowing down of all the tail electrons due to the collisions with the bulk electrons (small energy transfer) and is related to the stopping power averaged over the electron energy distribution $f^t(\varepsilon_e)$. The second term represents the abrupt energy loss ε_{12} when a tail electron is reduced below ε_{12}. For the case of interest in this investigation P_C^{tb} is given by the following expression:

$$P_C^{tb} = n_e^2 \left(\frac{e^2}{4\pi\varepsilon_0} \right)^2 (\varepsilon_{12} + kT_t) \left(\frac{8\pi}{m_e (kT_t)^3} \right)^{\frac{1}{2}} \ln \Lambda \exp \left(-\frac{\varepsilon_{12}}{kT_t} \right), \tag{II-16}$$

where

$$\Lambda = kT_t (\varepsilon_{12} - \frac{3}{2} kT_t)(\hbar\omega_p)^{-2}, \tag{II-17}$$

$\omega_p = (n_e e^2/m_e \varepsilon_0)^{\frac{1}{2}}$ is the plasma frequency, $\hbar = h/2\pi$ where h is Planck's constant, and ε_0 is the permittivity of free space. In equilibrium

20

$(T_e = T_t)$, the flow of energy from the tail to the bulk is balanced by an equal flow of energy from the bulk to the tail due to the electron electron collision, then P_C^{bt} is equal to the expression given by the eq. II-16 where T_t is replaced by T_e. The same experession of P_C^{bt} is assumed also to be valid for $T_e \neq T_t$.

II-3-2 Rate integrals

Excitations and ionizations depend on the tail electron energy. Hence assuming $i < j$, i, $j = 1$, 2, 3, it follows:

$$K_{ij} = < v_e \sigma_{ij} >^t . \tag{II-18}$$

The excitation and ionization cross sections for the Cs atom are known from several experiments (Refs. 6 and 7 respectively). The following analytic expression fit for experimental values is used:

$$\left| \begin{array}{ll} \sigma_{ij} = b_{ij}\left(1 - \dfrac{\varepsilon_{ij}}{\varepsilon_e}\right), & \text{for } \varepsilon_e \geq \varepsilon_{ij}, \\[2ex] \sigma_{ij} = 0 & \text{, for } \varepsilon_e < \varepsilon_{ij}. \end{array} \right. \tag{II-19}$$

Here the b_{ij} coefficients, obtained by the fit, are:
$b_{12} = 1.6 \times 10^{-18} \ m^2$, $b_{13} = 1.2 \times 10^{-19} \ m^2$, and $b_{23} = 5.8 \times 10^{-19} \ m^2$.

When the rate integrals (eq. II-18) are calculated with the cross sections of eq. II-19, it follows:

$$K_{ij} = b_{ij}\left(\frac{8kT_t}{\pi m_e}\right)^{\frac{1}{2}} \exp\left(-\frac{\varepsilon_{ij}}{kT_t}\right) . \tag{II-20}$$

In equilibrium $(T_t = T_e)$ the principle of detailed balancing yields:

$$K_{21} = K_{12}\left(\frac{n_1}{n_2}\right)^* , \tag{II-21}$$

$$K_{Ri} = K_{i3}\left(\frac{n_i}{n_e^2}\right)^* , \text{ for } i = 1,2, \tag{II-22}$$

where

$$\left(\frac{n_1}{n_2}\right)^* = \frac{g_1}{g_2} \exp\left(\varepsilon_{12}/kT_e\right) \quad , \tag{II-23}$$

$$\left(\frac{n_i}{n_e^2}\right)^* = \frac{1}{2}\left(\frac{h^2}{2\pi m_e kT_e}\right)^{3/2} \frac{g_i}{g_3} \exp\left(\varepsilon_{i3}/kT_e\right) \quad . \tag{II-24}$$

The deexcitation and the recombination rates given by eq. II-21 and II-22 respectively,are also used for the case where $T_t \neq T_e$, replacing T_t by T_e in the expression of K_{ij}. That is in agreement with the dependance of this type of nonelastic collision on the bulk electron energy.

II-3-3 *The tail balance equation*

The energy balance of the tail electrons is given by eq. II-6. The Coulomb terms P_C^{tb} and P_C^{bt} are given in Sec. II-3-1.

A further simplification is made in the terms P_E^t and P_{el}^t. In the plasma considered electron collisions with Ar atoms are dominant over other electron collisions involved in P_E^t and P_{el}^t for electron energies higher than ε_{12}. This is not the case for smaller ε_e. That follows from the comparison of the electron momentum cross sections for argon and cesium as it can be seen in Refs. 10 and 11. For the energy range $\varepsilon_{12} \leq \varepsilon_e \leq 3$ eV, the momentum transfer cross section of argon (10) can be represented by

$$\sigma_{Ar} = a'\varepsilon_e \quad . \tag{II-25}$$

where the fitting constant is $a = 7.428 \times 10^{-2}$ m^2/J. Then from eq. II-10 and eq. II-11 it follows that

$$P_E^t = \frac{2n_e e^2 E^2}{3a'n_{Ar}} \left(\frac{2}{\pi m_e (kT_t)^3}\right)^{\frac{1}{3}} \exp\left(-\frac{\varepsilon_{12}}{kT_t}\right), \tag{II-26}$$

22

$$P_{el}^t = 4 n_e n_{Ar} m_{Ar}^{-1} a' \left(\frac{2 m_e}{\pi k T_t} \right)^{\frac{1}{2}} \times$$

$$\times \left\{ \varepsilon_{12}^3 + 3 \varepsilon_{12}^2 k T_t + 6 \varepsilon_{12} (k T_t)^2 + 6 (k T_t)^3 \right\} \times$$

$$\times \exp \left(- \frac{\varepsilon_{12}}{k T_t} \right) \quad . \tag{II-27}$$

For the nonelastic collision terms in the tail energy balance the following approximated expressions can be used instead of the exact integrals given by eqs. II-12 and II-14:

$$P_{ij}^t = n_e n_i (\varepsilon_{ij} + 2 k T_t) K_{ij} \quad , \tag{II-28}$$

$$P_{ji}^t = n_e n_j (\varepsilon_{ij} + 2 k T_e) K_{ji} \quad . \tag{II-29}$$

where the K_{ij} and K_{ji} are given in Sec. II-3-2.

II-3-4 The bulk balance equation

Adding eq. II-6 to eq. II-7 yields

$$P_E^b + P_E^t = P_{el}^b + P_{el}^t + P_{Nel} \quad . \tag{II-30}$$

Here P_{Nel} is given by the nonelastic collision terms of eqs. II-6 and II-7. From eqs. II-12 - II-14 it follows

$$P_{Nel} = \sum_{\substack{i,j=1 \\ i<j}}^{3} n_e n_i \langle v_e \sigma_{ij} \varepsilon_{ij} \rangle^t -$$

$$- \sum_{\substack{i,j=1 \\ i<j}}^{3} n_e n_j \langle v_e \sigma_{ji} \varepsilon_{ij} \rangle^b \quad . \tag{II-31}$$

23

Hence

$$P_{Nel} = n_e \sum_{\substack{i,j=1 \\ i<j}}^{3} \varepsilon_{ij} \left(n_i K_{ij} - n_j K_{ji} \right) .$$ (II-32)

Using for the Joule heating terms $P_E^b + P_E^t$ and for the elastic collision losses terms $P_{el}^b + P_{el}^t$ standard expressions, eq. II-30 becomes

$$JE = 3k n_e n_e (T_e - T_g) \sum_i \frac{\nu_i}{m_i} + P_{Nel} .$$ (II-33)

Here ν_i is the momentum transfer collision frequency between an electron and a heavy particle of the species i, and m_i is the mass of the heavy particle.

For Ohm's law:

$$J = \sigma E ,$$ (II-34)

where J is the current density and σ the electrical conductivity:

$$\sigma = \frac{n_e e^2}{m_e \sum_i \nu_i} .$$ (II-35)

The heavy particle species contributing to the momentum transfer collisions are Ar neutrals, Cs neutrals, and singly ionized Cs atoms. Hence for Ar and Cs atoms

$$\nu_i = n_i \sigma_i \left(\frac{8kT_e}{\pi m_e} \right)^{\frac{1}{2}} .$$ (II-36)

The following expressions of the momentum transfer cross section are introduced for electron collisions with cesium and argon respectively:

$$\sigma_{Cs} = 5 \times 10^{-18} \ m^2 ,$$ (II-37)

$$\sigma_{Ar} = 0.28 \times 10^{-20} \left(\frac{T_e}{1000} - 0.54 \right) \ m^2 .$$ (II-38)

24

According to Ref. 9, the electron ion momentum transfer cross section is:

$$\sigma_{ei} = 5.85 \times 10^{-10} \, T_e^{-2} \, \ln\Lambda' \; m^2 \; .$$ (II-39)

where

$$\Lambda' = 1.24 \times 10^7 \left(\frac{T_e^3}{n_e} \right)^{\frac{1}{2}} \; .$$ (II-40)

Using eq. II-35 for σ, the influence of the non-Maxwellian electron distribution on the electrical conductivity is neglected. The same approximation is used in the expressions of the Joule heating and of the elastic collision losses. A discussion about this assumption will be given in Appendix B.

II-4 RADIATIVE TRANSITIONS

II-4-1 Resonance radiation

In the plasma under investigation the effective probability of radiative deexcitations to the ground state are considerably reduced by trapping of resonance radiation. Moreover, due to the splitting of the 6P level into the $6P_{3/2}$ and the $6P_{1/2}$ levels, the radiative transport for the two different lines has to be considered. In order to do that, the $6P_{1/2}$ and the $6P_{3/2}$ levels are assumed to be strongly coupled by electron collisions. As the energy level separation $\Delta\varepsilon$ is much smaller than the average electron energy $(\Delta\varepsilon = 0.06 \text{ eV})$, the ratio of the number densities in both states is assumed to follow from their statistical weights. Hence:

$$\frac{n_2(3/2)}{n_2(1/2)} = \frac{g_2(3/2)}{g_2(1/2)} \quad \text{,}$$ (II-41)

$$n_2(3/2) + n_2(1/2) = n_2 \quad \text{,}$$ (II-42)

where the subscripts 3/2 and 1/2 refer to the levels $6P_{3/2}$ and $6P_{1/2}$ respectively. The statistical weights are: $g_2(3/2) = 4$, $g_2(1/2) = 2$.

25

Then it follows:

$$n_2(1/2) = \frac{1}{3} n_2 \ , \ n_2(3/2) = \frac{2}{3} n_2 \ , \tag{II-43}$$

and

$$n_2 A_{21} \beta_{21} = \frac{n_2}{3} \{A_{21}(1/2)\beta_{21}(1/2) + 2A(3/2)\beta_{21}(3/2)\} \ . \tag{II-44}$$

The Einstein coefficient A_{21}, corresponding to the transition $j \rightarrow i$, is calculated from the absorption oscillator strenght f_{ji} and the radiation frequency ν_{ji} :

$$A_{ji} = \frac{g_i}{g_j} \ \frac{2\pi e^2}{\epsilon_o m_e c^3} \ \nu_{ji}^2 f_{ji} \ . \tag{II-45}$$

Here c is the velocity of light. Values of the optical oscillator strengths for cesium are available from several authors (12,13). The semiempirical values of the oscillator strengths given by Fabry are used in this study.

By solving the equation of radiative transfer the radiation escape parameter β_{ji} is calculated as:

$$\beta_{ji} = \alpha (\pi k_o d)^{-\frac{1}{2}} \ . \tag{II-46}$$

where d is the characteristic dimension of the plasma and k_o is the absorption coefficient at the center of the line. α is a coefficient which depends on the radiating atom distribution. For the case of Lorentz broadening and a nearly parabolic profile of the density of excited atoms, Holstein (14) gives: $\alpha = 1.150$ in an infinite slab of thickness d and $\alpha = 1.115$ in a cylinder of radius $r = d$.

The spectral profiles of the resonance lines emitted by the 6P atoms are dominated by collisional line broadening mechanisms: van der Waals broadening (foreign perturber) and resonance broadening (like perturber). At the plasma pressures investigated the influence of natural broadening, Doppler broadening and Stark broadening are negligible. A dispersion profile can be assumed to describe the line profile. Hence the absorption coefficient at the center of the line is:

$$k_o = \frac{e^2}{2\pi\varepsilon_o m_e c} \frac{f_{ji} n_j}{\Delta \nu} \quad , $$

$(II-47)$
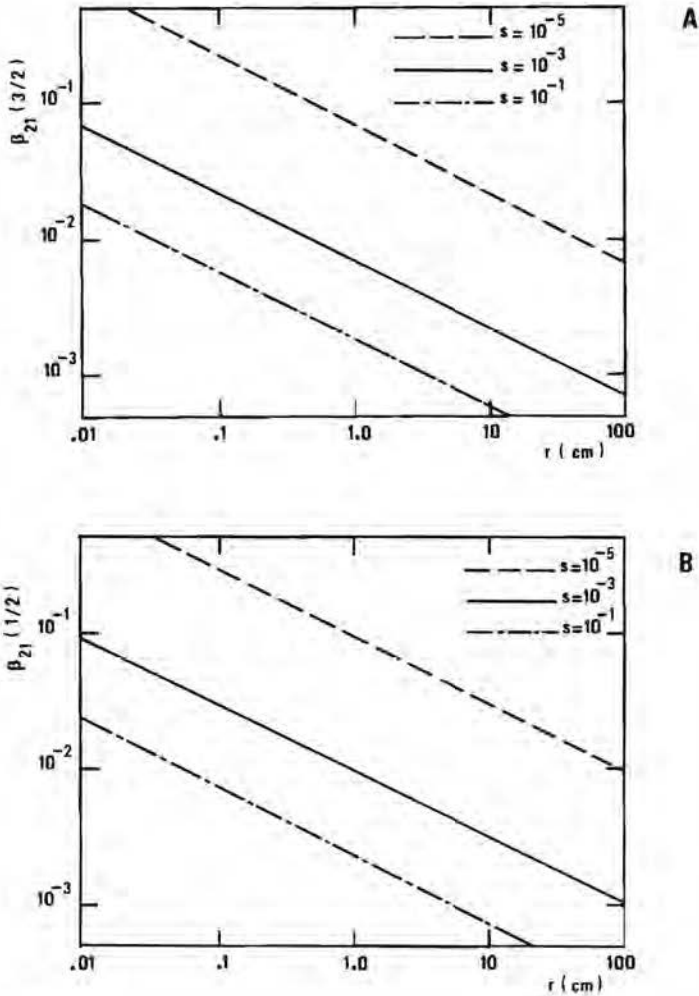
Figure II-3.

Radiation escape parameter as a function of the plasma dimension.
A cylindrical geometry is assmumed. β_{21} for the transition
$6P_{3/2} \rightarrow 6S_{1/2}$ is given in Fig. II-3-A. β_{21} for the transition
$6P_{1/2} \rightarrow 6S_{1/2}$ is given in Fig. II-3-B. In both figures the
plasma parameters are: $T_e \lesssim 2500$ K, $T_g = 1000$ K and $p_g = 1$ bar.

where $\Delta\nu$ is the half width of the spectral line. In the case under investigation the following relation holds:

$$\Delta\nu = \Delta\nu_R + \Delta\nu_W \quad . \tag{II-48}$$

The contributions of the resonance broadening and of the van der Waals broadening to the half width of the line, are given by the expressions (15):

$$\Delta\nu_R = \frac{3}{16\pi^2\varepsilon_0} \cdot \frac{e^2}{m_e c} \left(\frac{g_i}{g_j}\right)^{\frac{1}{3}} \lambda_{ji} f_{ji} n_{Cs} \quad . \tag{II-49}$$

$$\Delta\nu_W = 2.71 \left(\frac{C_6}{h}\right)^{2/5} \frac{8kT_g}{\pi} \left[\left(\frac{1}{m_{Ar}} + \frac{1}{m_{Cs}}\right)\right]^{3/10} n_{Ar} \quad . \tag{II-50}$$

In eq. II-49 λ_{ji} stands for the line wave length. In eq. II-50 C_6 stands for the van der Waals constant, as given by Mahan (16).

Calculated values of the radiation escape parameter for the transition $6P_{3/2} \rightarrow 6S_{1/2}$ and for the transition $6P_{1/2} \rightarrow 6S_{1/2}$ are given in Fig. II-3.

II-4-2 Radiative recombinations

For low electrons densities ($n_e \leq 10^{20}$ m^{-3}) two body recombinations of the kind $e + Cs^+ \rightarrow Cs^* + h\nu$ become more important than three body recombinations. The plasma is transparent to recombination radiation. The inverse process, photionization, is negligible. The rate integral for two body recombinations is given in terms of the corresponding cross section $\sigma_{\lambda j}$ by

$$A_{\lambda j} = \int_0^\infty v_e \sigma_{\lambda j} f^b(\varepsilon_e) d\varepsilon_e \quad . \tag{II-51}$$

By describing the radiative recombination cross section as

$$\sigma_{\lambda j} = \frac{\bar{\sigma}_{\lambda j}}{v_e^2} \, , \tag{II-52}$$

28

eq. II becomes

$$A_{\lambda j} = 2\bar{\sigma}_{\lambda j} \left(\frac{m_e}{2\pi k T_e} \right)^{\frac{1}{2}} \quad . \tag{II-53}$$

The value of the cross section for radiative recombination to the
6P level of cesium is taken from Norcross and Stone (17):
$\bar{\sigma}_{\lambda 2}$ = 2.79 × 10^{-14} m^4/sec^2. The value of the cross section for radiative
recombination to the ground state of cesium is calculated from photo-
ionization data (18): $\bar{\sigma}_{\lambda 2}$ = 1.77 × 10^{-16} m^4/sec^2.

The effect of non-Maxwellian electron energy distribution with
$T_t \neq T_e$ is not considered by eq. II-51 as the recombinations are do-
minated by bulk electrons.

II-5 INFLUENCE OF AMBIPOLAR DIFFUSION

For small plasma dimensions and low electron densities, the
ambipolar diffusion becomes an important loss of electrons from the
body of the plasma. As the density of the charged particles decreases
toward the boundary, diffusion of charged particles will be present.
The charged particles will recombine at the boundary and then return
to the plasma as neutral particles. As the plasma boundary is at low
temperature, the neutrals formed here by recombination, are considered
to be in the ground state. Hence in eq. II-2 the diffusion of n_2
particles is neglected (19). If the system is assumed to be in steady
state, it is $\dot{n}_1 = \dot{n}_2 = \dot{n}_e = 0$ in eq. II-1 through eq. II-3. From the
particle balance it follow that

$$D_a \nabla^2 n_e = - D_{Cs} \nabla^2 n_1 \quad . \tag{II-55}$$

For a characteristic dimension d the influence of ambipolar diffusion
is approximated by:

$$D_a \nabla^2 n_e = - \frac{D_a}{(d/2)^2} n_e \quad . \tag{II-56}$$

The following expression is used for the ambipolar diffusion
coefficients:

29

$$D_a = D_i (1 + \frac{T_e}{T_g}),$$ (II-57)

where D_i is the diffusion coefficient of the ions. D_i is related to the ion mobility μ_i by the Einstein relation:

$$D_i / \mu_i = kT_g / e \quad .$$ (II-57)

The value of μ_i for Cs ions in argon measured by Tyndal [20] is used. Further D_i is assumed to be proportional to $T_g^{2/3}$:

$$D_i = 5.18 \times 10^{-6} \left(\frac{T_g}{290} \right)^{2/3} \left(\frac{1}{p_g} \right) \quad \frac{m^2}{sec} \quad ,$$ (II-58)

where p_g is in bar and T_g in K.

II-6 RESULTS AND DISCUSSION

Calculations based upon the model described above, are carried out for a stationary discharge. In eqs. II-1 - II-3 the time and space derivatives are supposed to be equal to zero. The total number density n_{Cs} of the Cs atoms is assumed constant. Hence

$$n_1 + n_2 + n_e = n_{Cs} = s \, n_{Ar} \quad .$$ (II-59)

The seed ratio is defined as $s = n_{Cs}/n_{Ar}$. Then eqs. II-1,2,6,33,34 and 53 become a system of six algebraic equations with seven unknowns (n_1, n_2, n_e, T_e, T_t, E, J). Once one unknown is given, the system has a unique solution. In order to determine the coefficients of the equations an interactive method has been used. In this section the most important results will be presented and discussed.

The model describes the electron energy distribution using two parameters: the bulk temperature T_e and the tail temperature T_t. Fig. II-4 shows the behaviour of T_e as a function of T_t. For decreasing T_t the bulk temperature begins to deviate from T_t and reaches a minimum. For T_t below this critical value, the discharge can be self-sustained only for an increase of the bulk temperature. A lower bulk temperature can not balence the resonance radiation
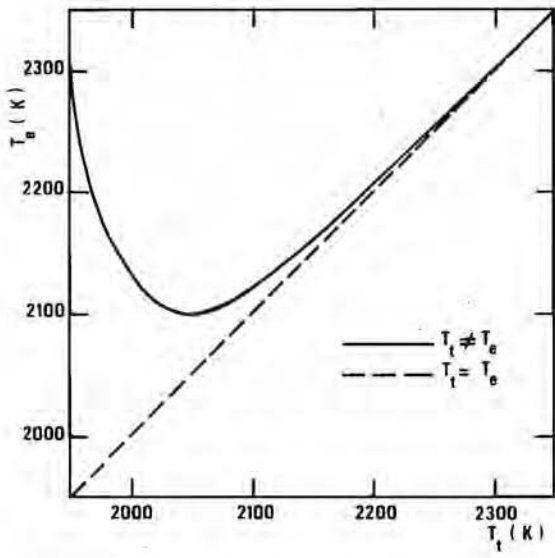
30

losses R $(R = P_{12}^t - P_{21}^t)$.

Figure II-4.
Bulk temperature as a function of the tail temperature for
$T_g = 1000$ K, $p_g = 1$ bar, $s = 10^{-3}$, $d = 1$ cm.

As it can be seen in Tab. II-1, when $T_t = T_e$, the Coulomb electron electron collision terms are much higher than the other terms in the electron energy balance which is reduced to the condition for Maxwellian electron distribution:

$$P_C^{tb} = P_C^{bt}. \tag{II-60}$$

With decreasing T_t, the number of ionization processes, dependent on T_t, decreases. That is followed by a decrease of n_e and of P_C^{bt} ($\propto n_e^2$). The excitation and ionization energy losses depend only linearly on n_e and reduce with a smaller rate. Among them the excitation term to the first excited level is dominant, and when $P_{12}^t \approx P_C^{tb}$ the condition for a Maxwellian distribution function fails. The electron energy in the tail is directly used for the excitation while the electron energy in the bulk has to be transferred to the tail before being used to excite

31

n_e	n_2	T_e	T_t	P_C^{bt}	P_C^{tb}	P_{12}^t	P_{21}^t	P_{23}^t	P_{13}^t	P_E^t	P_{el}^t	$R=n_2\beta_{21}A_{21}\varepsilon_{12}$
($10^{18} m^{-3}$)		(K)					($10^6 W\,m^{-3}sec^{-1}$)					
143	27.3	2500	2500	4290	4288	194	193	3.6×10^{-3}	3.4×10^{-4}	3.4×10^{-2}	4.8×10^{-1}	1.61
23.5	10.6	2204	2200	63.6	62.8	12.0	11.3	4.4×10^{-5}	4.5×10^{-6}	9.5×10^{-4}	3.2×10^{-2}	0.62
9.22	6.71	2120	2100	8.09	7.60	3.20	2.72	5.7×10^{-6}	6.5×10^{-7}	2.1×10^{-4}	8.8×10^{-3}	0.39
3.13	3.79	2110	2020	1.07	0.80	0.82	0.55	6.6×10^{-7}	9.8×10^{-8}	5.3×10^{-5}	2.3×10^{-3}	0.22
0.67	1.12	2405	1940	0.11	0.03	0.12	0.04	2.2×10^{-8}	7.7×10^{-9}	1.4×10^{-5}	3.4×10^{-4}	0.07

Table II-1.

Values of the main terms of the discharge model for: $T_g = 1000$ K, $p_g = 1$ bar, $s = 10^{-3}$ and $d = 1$ cm.
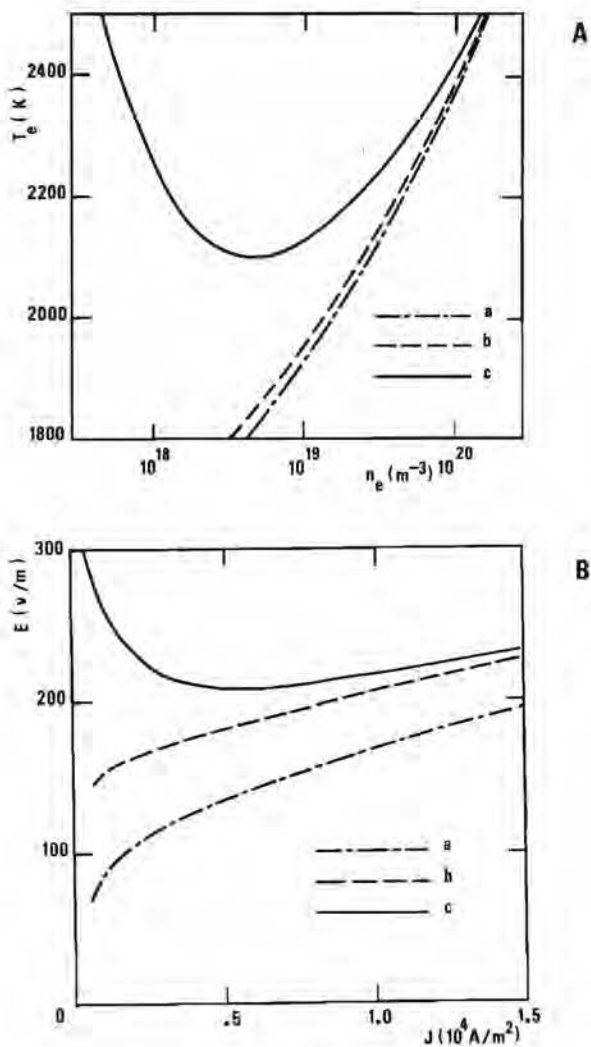
Figure II-5.
(A) Electron temperature as a function of the electron density,
and (B) electric field as a function of the current density for
$T_g = 1000$ K, $p_g = 1$ bar, $s = 10^{-3}$, $d = 1$ cm, and for: a – Saha
equilibrium; b – Maxwellian distribution with resonance radiation
losses; c – Non-Maxwellian electron distribution.

and ionize. The exciting collisions are then the cause of deviations
from a Maxwellian distribution of the electrons. As criterion for non-
Maxwellian electron energy distribution due to excitations, the
following expression can be used:

$$P_{12}^{t} \gtrsim P_{C}^{bt} \; . \tag{II-61}$$

In Fig. II-5 the electron temperature as a function of the elec-
tron density and the electric field as a function of the current den-
sity for the same plasma conditions of Fig. II-4, are shown.
In Fig. II-5A the behaviour of T_e against n_e given by the model, is
compared to the results of a model where the electron distribution
is assumed to be Maxwellian and where the energy losses are due to
elastic collisions and to radiation, and to the results of a model
where the Saha equilibrium is assumed. The two electron group model
gives a minimum value of T_e which corresponds to a critical electron
density n_{ec} whereas for the last two models considered, the relation
$n_e - T_e$ is represented by a monotonic increasing function. Above n_{ec},
the two group model indicates a nearly Maxwellian function: for
$n_e \lesssim n_{ec}$ a strong deviation from a Maxwellian function arises. In
Fig. II-5-B the behaviour of the electric field E against the current
density J is given for the same case. Following the Maxwellian and
the Saha model one value of the current density corresponds to one value
of the electric field. The two electron group model gives a minimum
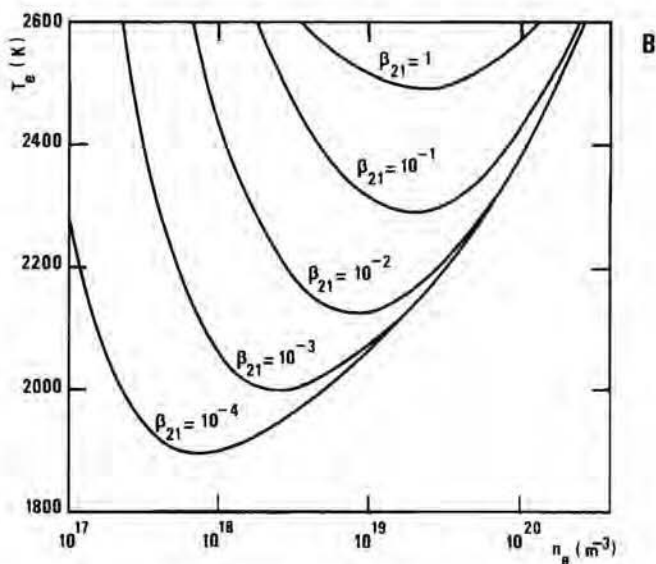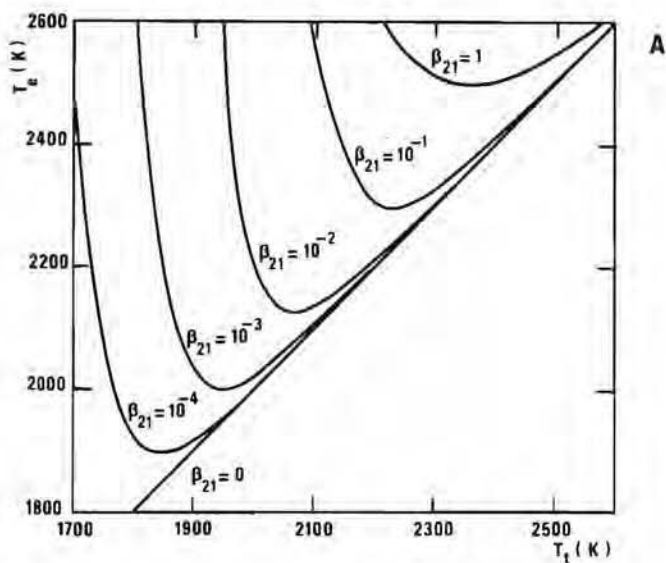value of E below which the discharge can not be self-sustained.

Figure II-6.

Departure from the Maxwellian electron distribution for several
values of the radiation escape parameter and for $T_g = 1000$ K,
$p_g = 1$ bar, $s = 10^{-3}$.

The excitation energy loss P^t_{12} is not balanced by the deexcitation energy gain P^t_{21} due to the radiation. As the resonance radiation term grows, the difference $P^t_{12} - P^t_{21}$ becomes larger. Then the excitation energy has to be supplied in a larger amount by the tail electron energy and the deviation from the Maxwellian equilibrium is enhanced. The resonance radiation term depends on the escape parameter. The dependence of the electron distribution on the escape parameter is shown in Fig. II-6. In this case the escape parameter is supposed constant and equal for both resonance lines. The resonance radiation term then becomes:

$$n_2 \beta_{21} A_{21} = \frac{n_2 \beta_{21}}{3} \{A_{21}(1/2) + 2A_{21}(3/2)\}.$$

As can be seen in the figure, for increasing β_{21}, the critical values of T_t (Fig. II-6-A) and n_e (Fig. II-6-B) increase.

As stated before, the non-Maxwellian electron distribution is caused by the excitations to the first excited level of the alkali
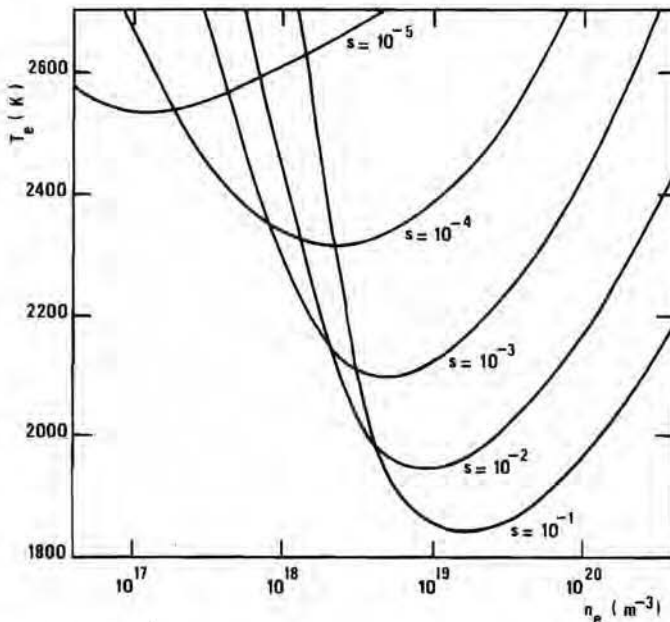

Figure II-7.
Electron temperature as a function of the electron density for several values of the seed fraction assuming: $T_g = 1000$ K, $p_g = 1$ bar and $d = 1$ cm.

atom. The excitation energy term P_{12}^t depends on n_1. Hence the establishment of the non-Maxwellian regime depends on the cesium density. In Fig. II-7 the behaviour of T_e as a function of n_e for different values of the seed fraction $s = n_{Cs}/n_{Ar}$ is shown. With increasing s, n_{ec} increases as can be expected. The corresponding value of T_e decreases. In Fig. II-8 the electric field as a function of the current density is plotted for different values of s.
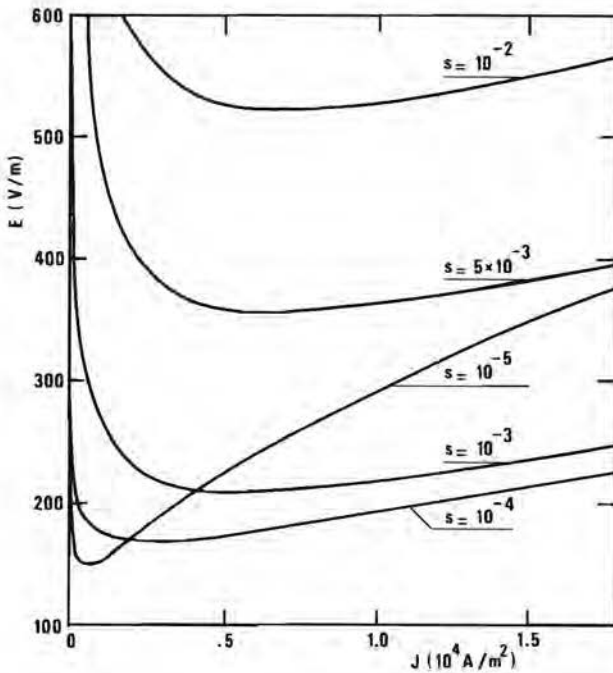

Figure II-8.
Electric field as a function of the electron density for several values of the seed fraction assuming: T_g = 1000 K, p_g = 1 bar and d = 1 cm.

The influence of the gas temperature and of the gas pressure on the electron distribution is shown in Fig. II-9. Here C_d is defined as a ratio between the critical value of the electron density for the actual T_g or p_g, and n_{ec} of a reference situation. In both cases the reference situation is defined by T_g = 1000 K and p_g = 1 bar and by $n_{Cs} = 10^{22}$ m^{-3}.
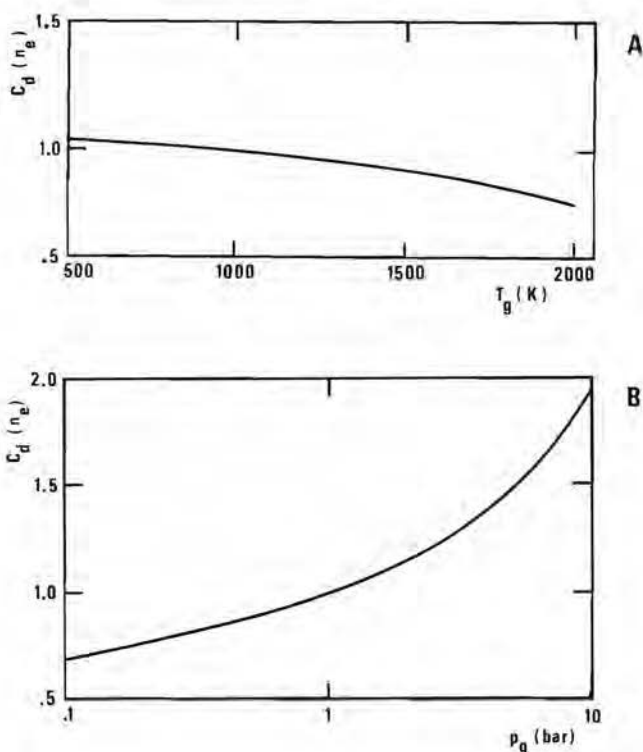
Figure II-9.
A) Correction factor of the critical electron density for gas
temperature variations. B) Correction factor of the critical
electron density for gas pressure variations.

The influence of the ambipolar diffusion is calculated following
the method described in Sec. II-6. In Fig. II-10 the results of the
model which includes the effects of ambipolar diffusion are compared
to the results of the model where ambipolar diffusion is neglected.
Due to diffusion, charged particles will be lost from the plasma
without the relative gain of the recombination energy. A deviation
from the Maxwellian distribution takes place for higher values of
the electron density and of the current density. In the figure the
curve b is terminated at $n_e = 2.6 \times 10^{18} \, m^{-3}$. Here the calculations
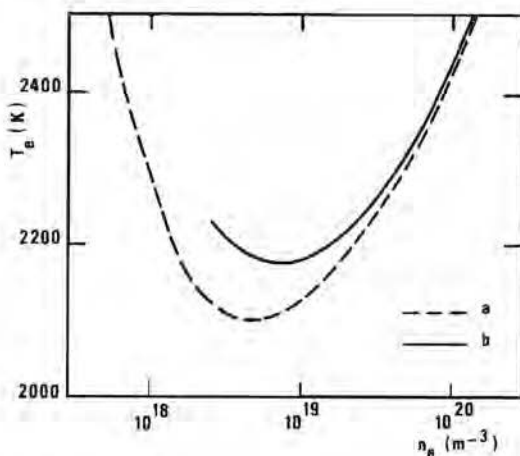
Figure II-10.
Comparison of the model results when the ambipolar diffusion
is neglected (a) and when it is taken into account (b).

stop due to numerical instabilities. In Fig. II-11 the influence of
the ambipolar diffusion as a function of the radius r of the discharge
is shown. $C_d(n_e)$ is defined as the ratio between the actual n_{ec} at

Figure II-11.
Correction factor for the ambipolar diffusion of the critical
electron density $C_d(n_e)$, and of the critical current density
$C_d(J)$.

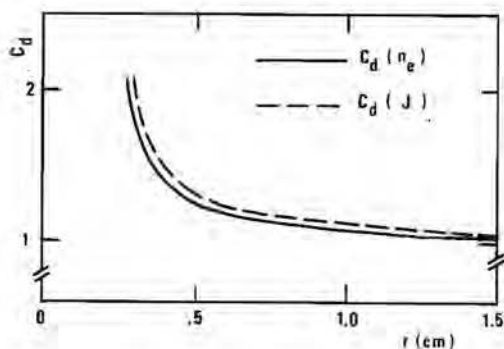the given r, and n_{ec} for the model which neglects the ambipolar diffusion. Similarly $C_d(J)$ is defined as the ratio between the actual value of the critical current density J_c (current density corresponding to the minimal value of the electric field) at the given r and J_c for the model which neglects the ambipolar diffusion. The calculations are made for $s = 10^{-3}$, $T_g = 1000$ K and $p_g = 1$ bar.

II-7 CONCLUSIONS

For the stationary discharge investigated, deviations from the Maxwellian electron energy distribution take place for electron densities below a critical density which is generally between 10^{18} and 10^{19} particles per cubic meter. Below this critical value of the electron density, the electron distribution has a strongly depleted tail. The non-elastic collision losses for the excitations to the 6P level of cesium, are the main cause of deviations from a Maxwellian distribution. The excitation losses are not balanced either by deexcitations due to resonance radiations or by thermalization due to electron electron collisions, therefore excitation energy has to be supplied by high energetic electrons. Hence the following can be stated:

a. An increase of the radiation losses due to an increase of the escape parameter, will cause an increased critical electron density for deviations from the Maxwellian distribution.

b. An increase of the density of cesium will cause a larger excitation loss term and consequently a higher critical electron density.

c. Ambipolar diffusion is the cause of a loss of electrons without gain of recombination energy. Therefore ambipolar diffusion is a cause of a higher critical electron density.

d. For decreasing electron density below its critical value, the tail of the electron distribution becomes more and more depleted. In consequence of that, the discharge has to be sustained by an increasing electric field as the current density decreases.

Appendix A

The normalization condition requires that

$$\int_0^\infty f(\varepsilon_e)d\varepsilon_e = 1,$$ (II-A-1)

where $f(\varepsilon_e)$ is the electron distribution function. When $f(\varepsilon_e)$ is given by eqs. II-4 and II-5, eq. II-A-1 becomes

$$S \int_0^{\varepsilon_{12}} f^b(\varepsilon_e)d\varepsilon_e + \int_{\varepsilon_{12}}^\infty f^t(\varepsilon_e)d\varepsilon_e = 1 \quad .$$ (II-A-2)

Here S is a correction factor equal to 1 when $f^b(\varepsilon_e) = f^t(\varepsilon_e)$.
In general S can be defined as follows:

$$S = \frac{\int_0^\infty f^b(\varepsilon_e)d\varepsilon_e - \int_{\varepsilon_{12}}^\infty f^t(\varepsilon_e)d\varepsilon_e}{\int_0^{\varepsilon_{12}} f^b(\varepsilon_e)d\varepsilon_e} \quad .$$ (II-A-3)

In the case investigated, the average kinetic energy of the electrons is sufficiently small compared to ε_{12} and the number of electrons in the tail is small too. Hence the factor S can be taken equal to 1 with a good approximation. For example if $T_e = 2500$ K and $T_t = 1900$ K (see Tab. II-1), eq. II-A-3 gives S = 1.0035.

Appendix B

In the Chapman-Enskog approximation the electrical conductivity
is expressed by:

$$\sigma = \frac{n_e e^2}{3kT} \int_0^\infty \frac{v_e}{\sum_i n_i \sigma_i} f(\varepsilon_e) d\varepsilon_e \quad . \tag{II-B-1}$$

where $f(\varepsilon_e)$ is a Maxwellian function with T as temperature. Hence the
contribution to σ of the tail electrons is given by:

$$\sigma^t = \frac{n_e e^2}{3kT_t} < \frac{v_e}{\sum_i n_i \sigma_i} >^t . \tag{II-B-2}$$

With the assumption made in Sec. II-3-3, the momentum transfer cross
section of argon is given by eq. II-25 and the momentum transfer cross
section of cesium is neglected.
Eq. II-B-2 then becomes:

$$\sigma^t = \frac{2}{3} \frac{n_e e^2}{a n_{Ar}} \left(\frac{2}{\pi m_e (kT_t)^3} \right)^{1/2} \exp \left(-\frac{\varepsilon_{12}}{kT_t} \right) \quad . \tag{II-B-3}$$

By eq. II-35 the contribution to the electrical conductivity of
the tail electrons is calculated as if the tail electron temperature
were T_e instead of T_t. Then an overestimation of

$$\Delta\sigma^t = \sigma^t(T_e) - \sigma^t \tag{II-B-4}$$

is made. In eq. II-B-4 σ^t and $\sigma^t(T_e)$ are given by eq. II-B-3 with T_t
and T_e respectively. In Tab. II-2 the values of σ calculated by eq.
II-35, σ^t and $\Delta\sigma^t$ are listed for the case of Tab. II-1.

The same overestimation is made when eq. II-30 is replaced by
eq. II-33. The error introduced by the Joule heating term $JE = \sigma E^2$

n_e $(10^{18} m^{-3})$	σ	σ^t	$\Delta\sigma^t$
		(mho m^{-1})	
143	79.1	7.7×10^{-1}	4.4×10^{-4}
23.5	21.4	6.2×10^{-2}	7.8×10^{-4}
9.22	9.54	1.8×10^{-2}	1.1×10^{-3}
3.13	3.61	5.1×10^{-3}	1.7×10^{-3}
0.67	0.64	7.8×10^{-4}	2.2×10^{-3}

Table II-2.
Comparison of the electrical conductivity given by eq. II-31 and the contribution of the tail electrons to the electrical conductivity for the plasma conditions of Tab. II-1.

is given by the error in σ discussed above. The error introduced by the elastic collision term is expressed by

$$\Delta P_{el}^t = P_{el}^t - P_{el}^t (T_e).$$ (II-B-5)

where P_{el}^t and $P^t (T_e)$ are given by eq. II-27 for T_t and T_e respectively. In Tab. II-3 the values of P_{el}^t and ΔP_{el}^t are compared to the

n_e $(10^{18} m^{-3})$	P_{el}	P_{el}^t	ΔP_{el}^t
	$(10^3 W\ m^{-3} sec^{-1})$		
143	3537	480	0.35
23.5	329	32.1	0.50
9.22	109	8.81	0.68
3.13	37.7	2.32	0.96
0.67	11.7	0.34	1.40

Table II-3.
Comparison of the elastic collision loss term given by the right hand side of eq. II-29 and the contribution of the tail electrons to the elastic losses for the plasma conditions of Tab. II-1.

total elastic loss term P_{el} given by the first term of the right
hand side of eq. II-33, for the case of Tab. II-1.

REFERENCES

1. VRIENS, L., "Energy balance in low-pressure gas discharges",
   J. Appl. Phys., Vol. 44, p. 3980, (1973).
2. VRIENS, L., "Two- and three-electron group models for low-pressure
   gas discharges", J. Appl. Phys., Vol. 45, p. 1191, (1974).
3. MORGAN, W.L., and VRIENS, L., "Two-electron-group model and
   Boltzmann calculations for low-pressure gas discharges", J. Appl.
   Phys., Vol. 51, p. 5300, (1980).
4. SHKAROFSKY, I.P., JOHNSTON, T.W., BRACHYNSKI, M.P., "The Particles
   Kinetics of Plasmas", Addison-Wesley, Reading, Mass., (1966);
   CHAPMAN, S., and COWLING, T.G., "The Mathematical Theory of Non-
   Uniform Gases", Third Edition, Univ. Press, Cambridge, (1970).
5. VRIENS, L. and LIGTHART, F.A.S., "Energy balance and Coulomb
   relaxation in low pressure gas discharges", Philips Res. Repts.,
   Vol. 32, p. 1, (1977);
   VRIENS, L., "Energy loss of charged particles in a plasma", Phys.
   Rev., Vol. 8, no. 1, p. 332, (1973).
6. ZAPESOCHNYI, I.P., and SHIMON, L.L., "Effective excitation cross
   section of alkali-metal atoms colliding with slow electrons. IV .
   Cesium." Opt. Spectrosc., Vol. 20, p. 421, (1966), "V. Resonance
   levels", Opt. Spectrosc., Vol. 21, p. 155, (1966);
   ZAPESOCHNYI, I.P., "Absolute cross section for the excitation of
   the levels of alkali metal atoms by low-energy electrons", High
   Temp., Vol. 5, p. 6, (1967);
   CHEN, S.T., and GALLAGHER A.C., "Electron excitation of the
   resonance lines of the alkali-metal atoms", Phys. Rev. A., Vol. 17,
   p. 551, (1978);
   KORCHEVOI, Yw.P., LUKASHENKO, V.I., LUKASHENKO, S.N., and KHIL'KO
   I.N., "Experimental determination of the effective electron-ioniza-
   tion cross sections of potassium, rubidium and cesium atoms excited
   to the first resonance level", High Temp., Vol. 15, p. 7, (1977).
7. NYGAARD, K.J., "Electron-impact ionization cross section in cesium",
   J. Chem. Phys., Vol. 49, p. 1995, (1968);
   ZAPESOCHNYI, I.P., and ALEKSAKHIN, I.S., "Ionization of alkali

metal atoms by slow electrons", Sov. Phys. JETP, Vol. 28, p. 41,
(1969).

8. VAN TONGEREN, H., "Positive column of Cs-Ar low-pressure discharge",
   J. Appl. Phys., Vol. 45, p. 89, (1974);
   VAN TONGEREN, H., "Positive Column of Cesium- and Sodium-noble-
   gas discharges", Ph. D. Thesis, Eindhoven University of Technology,
   Eindhoven, (1975).

9. MITCHNER, M., and KRUGER, C.H., "Partially Ionized Gases", John
   Wiley and Sons, New York, (1973).

10. STEFANOV, B., "Electron momentum-transfer cross section in cesium:
    Fit to the experimental data", Phys. Rev. A, Vol. 22, p. 427, (1980).

11. Mc. DOWELL, M.R.C., "A phase shift analysis of electron-atom
    scattering.IV Scattering of slow electrons by neon and argon",
    J. Phys. B, Vol. 4, p. 1649, (1971);
    GOLDEN, D.E., "Comparison of low-energy total and momentum-transfer
    scattering cross section for electrons of Helium and Argon", Phys.
    Rev., Vol. 151, p. 48, (1966).

12. THORNE, A.P., "Spectrophysics", Chapman and Hall, London, (1974);
    SOBELMAN, I.I., "Atomic Spectra and Radiative Transitions",
    Springer-Verlag, Berlin, (1979);
    GRIEM, H.R., "Plasma Spectroscopy", Mc Graw-Hill, New York, (1964).

13. STONE, M.P., "Cesium oscillator strengths", Phys. Rev., Vol. 127,
    p. 1151, (1962);
    FABRY, M., "Theoretical and experimental determination of cesium
    oscillator strengths", J.Q.S.R.T., Vol. 16, p. 127, (1976);
    LINDGARD, A., and NIELSEN, S.E., "Transitions probabilities for
    the alkali isoelectronic sequences Li I, Na I, K I, Rb I, Cs I,
    Fr I.", Atomic Data and Nuclear Data Tables, Vol. 19, p. 533, (1977).

14. BIBERMAN, L.M., "Approximate method of considering the resonance
    radiation diffusion", Dokl. Akad. Nauk. SSSR (Sov. Phys.-Dokl.),
    Vol. 49, p. 659 (1948); "Radiative transfer in spectral lines",
    Pure Appl. Chem., Vol. 13, p. 393, (1966);
    HOLSTEIN, T., "Imprisonment of resonance radiation in gases",
    Phys. Rev., Vol. 72, p. 1212, (1947); "Imprisonment of resonance
    radiation in gases II" Phys. Rev., Vol. 83, p. 1159, (1951);
    LUTZ, M.A., "Radiation and its effects on the nonequilibrium
    properties of a seeded plasma", AIAA J., Vol. 5, p. 1416, (1967);
    SOLBES, A., "Radiation operator in nonequilibrium plasmas",

AIAA J., Vol. 6, p. 737, (1968);

HIRAMOTO, T., "Rates of total and local radiative energy losses in nonequilibrium plasmas", J. Phys. Soc. Jap., Vol. 26, p. 785, (1969).

15. HINDEMARSH, W.R., and FARR, J.M., "Collision broadening of spectral lines by neutral atoms", Progr. in Quant. Elect., Vol. 2, p. 141, (1972), and references herein.

16. MAHAN, G.D., "Van der Waals constant between alkali and noble-gas atoms. II. Alkali atoms in excited states", J. Chem. Phys., Vol. 50, p. 2755, (1969).

17. NORCROSS, D.W., and STONE, P.M., "Radiative recombination in cesium", J.Q.S.R.T., Vol. 6, p. 277, (1966).

18. MARR, G.V., "Photoionization Processes in Gases", Academic Press, New York, (1967).

19. NUMANO, M., CUSSENOT, J.R., FABRY, M. and FELDEN, M., "A theoretical study of the influence of ambipolar diffusion on the population distribution of excited states in a plasma", J.Q.S.R.T., Vol. 15, p. 1007, (1975).

20. TYNDALL, A.H., "The Mobility of Positive Ions in Gases", Cambridge U.P., Cambridge, (1938).

21. BORGHI, C.A., VEEFKIND, A., "Theoretical model for a low current discharge in an MHD generator", Symp. SPIG-80, p. 192, Dubrownik, Yugoslavia, (1980).

IONIZATION RELAXATION PROCESSES

III-1 INTRODUCTION

In this chapter the effect of a non-Maxwellian electron energy distribution on the ionization process will be analyzed and applied to situations occurring at the inlet of MHD generators. Because of the importance of stepwise ionization processes [1], the three level model of the previous chapter can no longer be used for the Cs atom. Besides the ionization process, also the recombination process will be discussed. This will be done on behalf of the interpretation of the afterglow experiments to be described in the next chapter. The theoretical model is developed with J.M. Wetzer [2]. It includes radiative transitions. The influence of radiation on the ionization and recombination of the plasma, will be discussed. The two electron group model is used to approximate the electron distribution function. For the calculations of this chapter, an ionizing plasma (where excitation to the first excited state represents the principal energy loss of the electrons) is represented by an electron distribution with a depleted tail ($T_t < T_e$). A recombining plasma (where deexcitation from the first excited state represents the principal energy gain of electrons, is represented by an electron distribution with an overpopulated tail ($T_t > T_e$). First the influence of radiative transitions is considered when assuming a Maxwellian electron energy distribution. Then the effect of a deviation from the Maxwellian electron energy distribution is determined, including the radiative transitions.

III-2 THEORETICAL MODEL

III-2-1 Basic assumptions

In the model adopted in this chapter only Cs atoms are supposed to be excited and to be ionized while the noble gas will act only as

a buffer gas, which implies that all Ar atoms are in the ground state.
Further, it is assumed that the time required for the electron energy
distribution to relax to its final condition, is short compared to the
ionization relaxation time. Consequently the final electron energy dis-
tribution is assumed to be established at t = 0 and maintained constant
in time. The initial population of excited states and electron density
are obtained from the stationary solution of the model for a given
initial electron energy distribution (at t < 0). When a Maxwellian
electron energy distribution is assumed and the radiative transitions
are neglected, the values of the population density and electron den-
sity given by the stationary solution of the model, are equal to the
values given by the Saha relation.

III-2-2 Atomic model

An atomic model of cesium having 10 bound states is used. Each
state is characterized by its principal quantum number and orbital
momentum (see Table 1). Energy levels higher than the 10th (7D, $\varepsilon_{1,10}$ =

i	State	Energy level ε_{1i} (eV)	Degeneracy g_i
1	6S	0.00	2
2	6P	1.43	6
3	5D	1.80	10
4	7S	2.30	2
5	7P	2.71	6
6	6D	2.80	10
7	8S	3.01	2
8	4F	3.03	14
9	8P	3.19	6
10	7D	3.23	10
11	ion	3.89	1

Table III-1.
Atomic model for cesium with level energy ε_{1i} and degeneracy g.

3.23 eV) are assumed to be in instantaneous Saha equilibrium with the electrons.

The collisional processes taken into account are inelastic electron atom collisions as excitation, deexcitation, ionization and three body recombination. Because of the lack of experimental values of cross sections for electron induced excitation or ionization from intermediate levels of the Cs atom, the formulae derived by Gryzinski (1965) on the basis of a semi-classical model, are used[3]. According to Gryzinski's theory the cross section $\sigma_i(\varepsilon_e, \Delta\varepsilon)$ for loss of energy larger than or equal to $\Delta\varepsilon$ by one incoming electron of energy ε_e colliding with a bound electron in the i-th level, is given by:

$$\sigma_i(\varepsilon_e, \Delta\varepsilon) = 4\pi a_o^2 \left(\frac{R}{\Delta\varepsilon}\right)^2 \xi_i g(u,v),$$ (III.1)

where

$$g(u,v) = \frac{u-1}{u^2} \left(\frac{u}{u+v}\right)^{3/2} \left(1 - \frac{1}{u}\right)^{\frac{v}{v+1}} \left\{ 1 + \frac{2v}{3}\left(1 - \frac{1}{2u}\right) \times \right.$$

$$\left. \times \ln\left[2.718 + \left(\frac{u-1}{v}\right)^{1/2}\right] \right\}.$$ (III.2)

Here $a_o = 5.29 \times 10^{-11}$ m is the radius of the first Bohr orbit for hydrogen, $R = 13.6$ eV is Rydberg's constant. ξ_i is the number of equivalent electrons in the i-th level, $u = \varepsilon_e/\Delta\varepsilon$ and $v = \varepsilon_{i\lambda}/\Delta\varepsilon$ where $\varepsilon_{i\lambda}$ is the ionization energy for the ith level. Excitation from level i to level j is obtained when the minimum energy loss is larger than the excitation energy ε_{ij} but smaller than the excitation energy of the next level, $\varepsilon_{i,j+1}$. Hence

$$\sigma_{ij}(\varepsilon_e) = \sigma_i(\varepsilon_e, \varepsilon_{ij}) - \sigma_i(\varepsilon_e, \varepsilon_{i,j+1}).$$ (III.3)

Similarly the cross section for ionization from level i is:

$$\sigma_{i\lambda}(\varepsilon_e) = \sigma_i(\varepsilon_e, \varepsilon_{i\lambda}).$$ (III.4)

The dominating radiative processes are 6P → 6S resonance radiation and radiative recombination into the levels 6P and 5D. Other radiative transitions are taken into account but appear to have a negligible

effect on populations and electron density. Oscillator strengths are taken from Fabry (4), cross sections for radiative recombination from Norcross and Stone (5).

III-2-3 Rate integrals

The rate integrals for excitation, deexcitation, ionization and recombination are calculated for collisions with electrons having an energy distribution as defined in Sec. II-3-1. The excitation rate integral K_{ij} is defined in terms of the excitation cross section σ_{ij} by:

$$K_{ij} = \int_{\varepsilon_{ij}}^{\infty} f(\varepsilon_e)\sigma_{ij}(\varepsilon_e)v_e(\varepsilon_e)d\varepsilon_e, \qquad (III-5)$$

where $f(\varepsilon_e)$ is the electron distribution function and v_e the electron velocity. Using the excitation cross section from the previous section, eq. III-5 gives:

$$K_{ij} = K_i(\varepsilon_{i,j}) - K_i(\varepsilon_{i,j+1}), \qquad (III-6)$$

where $K_i(\varepsilon_{i,j})$ is defined as:

$$K_i(\varepsilon_{i,j}) = \int_{\varepsilon_{i,j}}^{\infty} f(\varepsilon_e)\sigma(\varepsilon_e,\varepsilon_{ij})v_e(\varepsilon_e)d\varepsilon_e. \qquad (III-7)$$

When the distribution function is given by eqs. II-3 and II-4, two cases are distinguishable for the calculation of $K_i(\varepsilon_{ij})$.
Case a: $\varepsilon_{ij} < \varepsilon_{12}$, then

$$K_i(\varepsilon_{ij}) = \int_{\varepsilon_{ij}}^{\varepsilon_{12}} f^b(\varepsilon_e)\sigma_i(\varepsilon_e,\varepsilon_{ij})v_e(\varepsilon_e)d\varepsilon_e +$$

$$+ \int_{\varepsilon_{12}}^{\infty} f^t(\varepsilon_e)\sigma_i(\varepsilon_e,\varepsilon_{ij})v_e(\varepsilon_e)d\varepsilon_e. \qquad (III-8)$$

Case b: $\varepsilon_{12} \leq \varepsilon_{ij}$, then

$$K_i(\varepsilon_{ij}) = \int_{\varepsilon_{ij}}^{\infty} f^t(\varepsilon_e)\sigma_i(\varepsilon_e,\varepsilon_{ij})v_e(\varepsilon_e)d\varepsilon_e. \qquad (III-9)$$

The ionization rate integral is

$$K_{i\lambda} = K_i(\varepsilon_{i\lambda}), \qquad (III-10)$$

and $K_i(\varepsilon_{i\lambda})$ is expressed by eqs. III-8 and III-9 where ε_{ij} is replaced by $\varepsilon_{i\lambda}$.

The deexcitation and recombination rates are derived from detailed balancing as

$$K_{ji} = K_{ij}\left(\frac{n_i}{n_j}\right)^*, \qquad (III-11)$$

and

$$K_{Ri} = K_{i\lambda}\left(\frac{n_i}{n_e^2}\right)^*, \qquad (III-12)$$

where

$$\left(\frac{n_i}{n_j}\right)^* = \frac{g_i}{g_j} \exp(\varepsilon_{ij}/kT_e), \qquad (III-13)$$

and

$$\left(\frac{n_i}{n_e^2}\right)^* = \frac{1}{2}\left(\frac{h^2}{2\pi m_e kT_e}\right)^{3/2} g_i \exp(\varepsilon_{i\lambda}/kT_e). \qquad (III-14)$$

Furthermore in eqs. III-11 and III-12, K_{ij} and $K_{i\lambda}$ are calculated for a Maxwellian distribution function at the bulk temperature T_e (i.e. in eqs. III-8 and III-9 $f^t(\varepsilon_e)$ is replaced by $f^b(\varepsilon_e)$). The effect of the non-Maxwellian distribution is neglected for the deexcitation and the recombination collisions as these processes are dominated by the bulk electrons. In fact their energy threshold is zero and the thermal energy of the electrons is sufficiently small compared to ε_{12}.

In a similar way as described for excitation and ionization pro-

cesses, the rate integral for radiative recombination to level i, $A_{\lambda i}$ is calculated from

$$A_{\lambda i} = \int_0^\infty f(\varepsilon_e)\sigma_{\lambda i}(\varepsilon_e)v_e(\varepsilon_e)d\varepsilon_e. \tag{III-15}$$

III-2-4 Time dependent continuity equations

In general the continuity equation for atoms in state i can be written as

$$\frac{\partial n_i}{\partial t} = \left(\frac{\partial n_i}{\partial t}\right)_{coll.rad.} + \vec{\nabla}\cdot(n_i\vec{v}_i) \tag{III-16}$$

In our model diffusive effects are not taken into account. Then the righthand side of eq. III-16 reduces to collisional and radiative terms:

$$\frac{\partial n_i}{\partial t} = \left(\frac{\partial n_i}{\partial t}\right)_{coll.rad.} = n_e\left\{\sum_{j\neq i} n_j K_{ji} - n_i \sum_{j\neq i} K_{ij} - \right.$$
$$\left. - n_i K_{i\lambda} + n_e^2 K_{Ri} + n_e A'_{\lambda i}\right\} +$$
$$+ \sum_{j>i} n_j A'_{ji} - n_i \sum_{j>i} A'_{ij} , \tag{III-17}$$

where charge neutrality is assumed.

$A'_{\lambda i}$ is the net rate integral for radiative recombination and A'_{ij} is the net emission coefficient that takes into account the corresponding absorption processes. Using the radiation escape factors $\beta_{\lambda i}$ and β_{ij}, $A'_{\lambda i}$ and A'_{ij} are defined as follows

$$A'_{\lambda i} = A_{\lambda i}\beta_{\lambda i}, \tag{III-18}$$
$$A'_{ij} = A_{ij}\beta_{ij}. \tag{III-19}$$

The plasma is considered optically thin to recombination radiation thus $\beta_{\lambda 1} = 1$.

Using Holstein's theory (6) β_{21} is calculated for the plasma considered, yielding values in the order of 0.01 (see Chap. II). All other radiative transitions appear to have a negligible effect even in case of complete radiation escape ($\beta=1$).

The assumption of Saha equilibrium for levels higher than 70 is realised by adjusting $K_{i\lambda}$ and K_{Ri}. According to Ref. 7, these rate integrals should then be replaced by $K'_{i\lambda}$ and K'_{Ri} as follows:

$$K'_{i\lambda} = K_{i\lambda} + \sum_{j=n}^{\infty} K_{ij} \qquad (III-20)$$

$$K'_{Ri} = (n_i/n_e^2)^* K'_{i\lambda} \qquad (III-21)$$

where n is the number of levels taken into account. The converging character of the summation leads to a value for $K'_{i\lambda}$ which is in good agreement with the rate integral $K_{i\lambda}$ obtained when using $\varepsilon_{e,n+1}$ (=3.33 eV) as effective ionization energy. It should be noted however that this effective ionization energy is used only for evaluating $K'_{i\lambda}$, and that for all other processes involving the ionization energy the real value is used.

The resulting set of stiff differential equations is numerically solved with a Curtiss-Hirschfelder method (8), while n_e is simultaneously calculated from

$$n_e = n_{Cs} - \sum_{i}^{n} n_i . \qquad (III-22)$$

III-3 RESULTS AND DISCUSSION

III-3-1 Conditions

The development of the electron temperature is simulated by a step function at t = o. Moreover, when the influence of a non-Maxwellian distribution is considered, the electron distribution is assumed to have a discontinuity at energy ε_{12}. The behaviour in time of the electron energy distribution is given by two step functions of the bulk and tail temperature as follows:

$$T_e = T_{eo} \, , \, T_t = T_{to} \text{ for } t < o \, , \qquad\qquad (III\text{-}23.a)$$

$$T_e = T_{e\infty} \, , \, T_t = T_{t\infty} \text{ for } t \geq o \, . \qquad\qquad (III\text{-}23.b)$$

The initial conditions are given by eq. III-23.a. The values of T_{eo} and of T_{to} determine the stationary solution of the model from which the electron density $n_e(o)$ and the population density $n_i(o)$ are derived. The rate integrals in the time dependent equations (eq. III-17), are calculated from the values of $T_{e\infty}$ and $T_{t\infty}$ given by the final conditions (eq. III-23.b).

The electron density and the excited state densities are calculated for three different sets of conditions:

1) Radiation is neglected.

   The electron distribution function is Maxwellian.

   - Initial conditions (t<o): $T_e = T_t = T_{eo}$.
   - Final conditions   (t≥o): $T_e = T_t = T_{e\infty}$.

2) Radiation is taken into account.

   The electron distribution function is Maxwellian.

   - Initial conditions: $T_e = T_t = T_{eo}$.
   - Final conditions : $T_e = T_t = T_{e\infty}$.

3) Radiation is taken into account.

   The electron distribution function is non-Maxwellian.

   With regard to the electron distribution three different possibili-

   ties are considered:

   a) Initial conditions: $T_e = T_{eo}, \, T_t = T_{to}$.
      Final conditions : $T_e = T_t = T_{e\infty}$.
   b) Initial conditions: $T_e = T_t = T_{eo}$.
      Final conditions : $T_e = T_{e\infty}, \, T_t = T_{t\infty}$.
   c) Initial conditions: $T_e = T_{eo}, \, T_t = T_{to}$.
      Final conditions : $T_e = T_{e\infty}, \, T_t = T_{t\infty}$.

When a non-Maxwellian electron distribution function is considered, the ionizing plasma case is distinguished from the recombining plasma case. For ionizing plasmas T_t is assumed to be smaller than T_e due to the excitation losses (see Chap. II). For recombining plasma T_t is assumed to be larger than T_e as the deexcitations and the recombinations, as far as not balanced by the excitations and the ionizations, cause extra

population of the tail of the electron distribution function.

The results of the calculations are plotted for normalized values of the electron density $\tilde{n}_e$ and of the population density $\tilde{n}_i$ defined as

$$\tilde{n}_K = \frac{n_K(t) - n_K(o)}{n_K(\infty) - n_K(o)} , \tag{III-24}$$

where $K = e, 1, 2 \ldots n$ and $n_K(\infty)$ stands for the stationary solution of the model at $T_e = T_{e\infty}$ and $T_t = T_{t\infty}$.
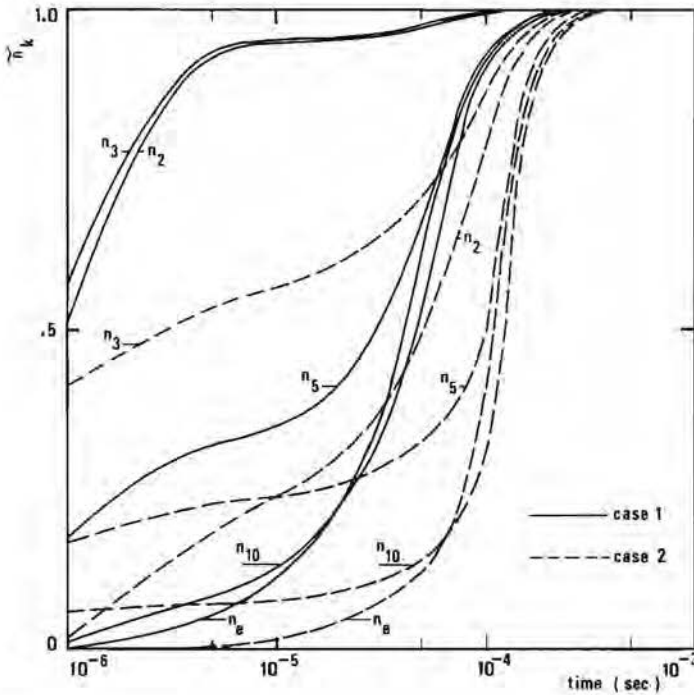
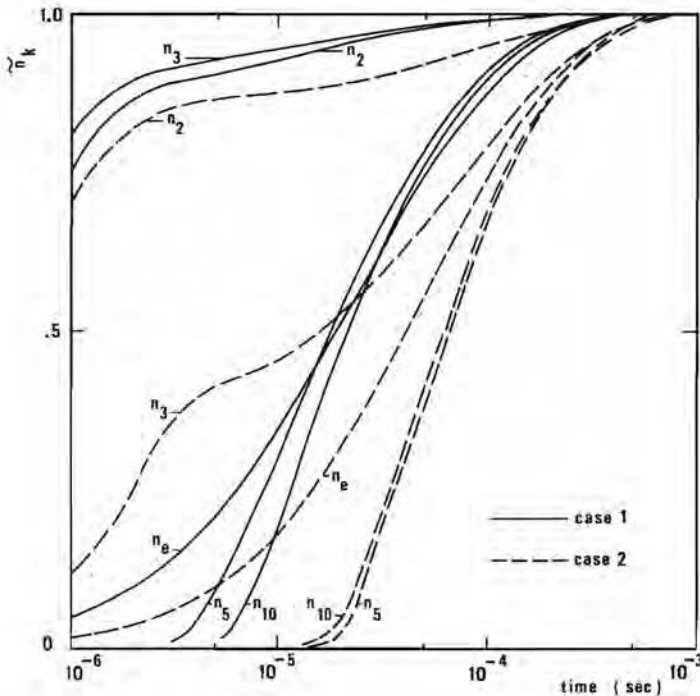### III-3-2 *Influence of radiation and distribution function*

Figure III-1-A.
Development in time of reduced densities in case of a Maxwellian distribution function, $n_{Cs} = 7.2 \times 10^{21} \ m^{-3}$.   Ionizing plasma, $T_{eo} = T_{to} = 2100 \ K$, $T_{e\infty} = T_{t\infty} = 2300 \ K$. Case 1. No radiation included. Case 2. Radiation included.

In Fig. III-1-A a comparison is presented of the results of the model where radiation is neglected (case 1), with the results of the model which takes radiation into account (case 2). A temperature step from $T_{eo} = 2100$ K to $T_{e\infty} = 2300$ K is taken. When radiation is neglected $\tilde{n}_2$ and $\tilde{n}_3$ reach quickly their final values. The development becomes slower for the higher energy levels. The electron density develops in the same way as the populations of the high levels $(\tilde{n}_e(t) \sim \tilde{n}_i(t)$, $i = 8, 9, 10)$.

In case resonance radiation is included a slower increase of $\tilde{n}_2(t)$ due to a continous loss of particles from level 2, is observed. As a consequence the characteristic relaxation times for all levels become longer. In Fig. III-1-B a comparaison of the same models for a re-

Figure III-1-B.
Development in time of reduced densities in case of a Maxwellian distribution function, $n_{Cs} = 7.2 \times 10^{21}$ m^{-3} . Recombining plasma, $T_{eo} = T_{to} = 2300$ K, $T_{eo} = T_{t\infty} = 2100$ K. Case 1. No radiation included. Case 2. Radiation included.

combining plasma with T_{eo} = 2300 K and $T_{e\infty}$ ≈ 2100 K is given. Non-
normalized results of the model that includes radiation, yield a lar-
ger difference between the initial and the final values of the elec-
tron and population densities. As a consequence the whole relaxation
process is retarded in comparison with the results given by the model
which neglects radiation. The development of $\tilde{n}_2(t)$ only remains appre-
ciably fast due to resonance radiation.

In Fig. III-2-A a comparison of the results of the model inclu-
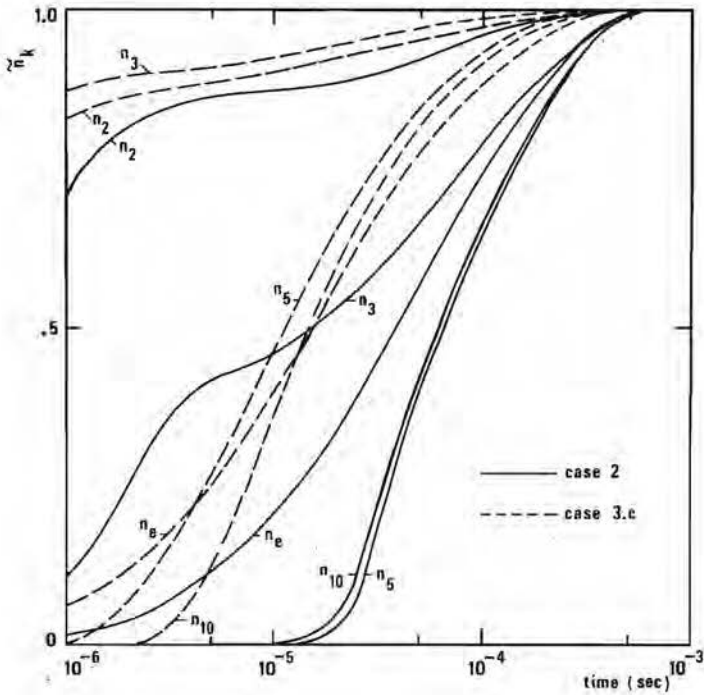ding radiation with and without deviations from a Maxwellian distribution
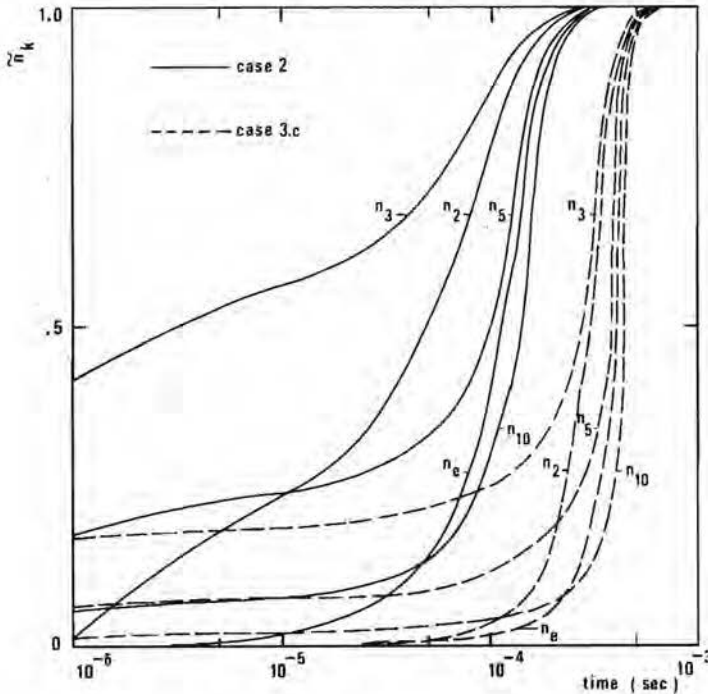
Figure III-2-A.

Development in time of reduced densities, radiation included,
with Maxwellian (case 2) and non-Maxwellian (case 3c) distribu-
tion function, n_{Cs} = 7.2×10^{21} m^{-3}. Ionizing plasma.
Case 2: $T_{eo} = T_{to}$ = 2100 K, $T_{e\infty} = T_{t\infty}$ = 2300 K.
Case 3c: T_{eo} = 2100 K, T_{to} = 2000 K, $T_{e\infty}$ = 2300 K, $T_{t\infty}$ = 2200 K.

is shown (case 2 and 3 respectively). For case 2: $T_{eo} = T_{to} = 2100$ K, $T_{e\infty} = T_{t\infty} = 2300$ K. For case 3: $T_{eo} = 2100$ K, $T_{to} = 2000$ K, $T_{e\infty} = 2300$ K and $T_{t\infty} = 2200$ K. When an electron energy distribution with a depleated tail is considered, the difference between initial and final densities increases and the values of the rate integrals for excitation between levels with a large energy gap decrease. As a result, the relaxation process is retarded. The decreased values of K_{12} and K_{13} cause a further depressed time development of $\tilde{n}_2(t)$ and $\tilde{n}_3(t)$ which gets closer to the development of the other population densities and of the electron density. A comparison between results of the two models of case 2 and

Figure III-2-B.
Development in time of reduced densities, radiation included, with Maxwellian (case 2) and non-Maxwellian (case 3c) distribution function, $n_{Cs} = 7.2 \times 10^{21}$ m^{-3}.   Recombining plasma.
Case 2 : $T_{eo} = T_{to} = 2300$ K, $T_{e\infty} = T_{t\infty} = 2100$ K.
Case 3c: $T_{eo} = 2300$ K, $T_{to} = 2400$ K, $T_{e\infty} = 2100$ K, $T_{t\infty} = 2200$ K.

case 3 for a recombining plasma are presented in Fig. III-2-B. For the
first one: $T_{eo} = T_{to} = 2300$ K, $T_{e\infty} = T_{t\infty} = 2100$ K. For the second one:
$T_{eo} = 2300$ K, $T_{to} = 2400$ K, $T_{e\infty} = 2100$ K, $T_{t\infty} = 2200$ K. In the non-Max-
wellian case $T_t > T_e$. As a consequence $\tilde{n}_2$, $\tilde{n}_3$ and then $\tilde{n}_2$ develop faster.

The time dependences of the electron density for the cases of
Figs. III-1 and III-2 and for the three different possibilities in
which the non-Maxwellian case is divided (see case 3 at the beginning of
this section) are plotted in Fig. III-3. The ionizing case is shown
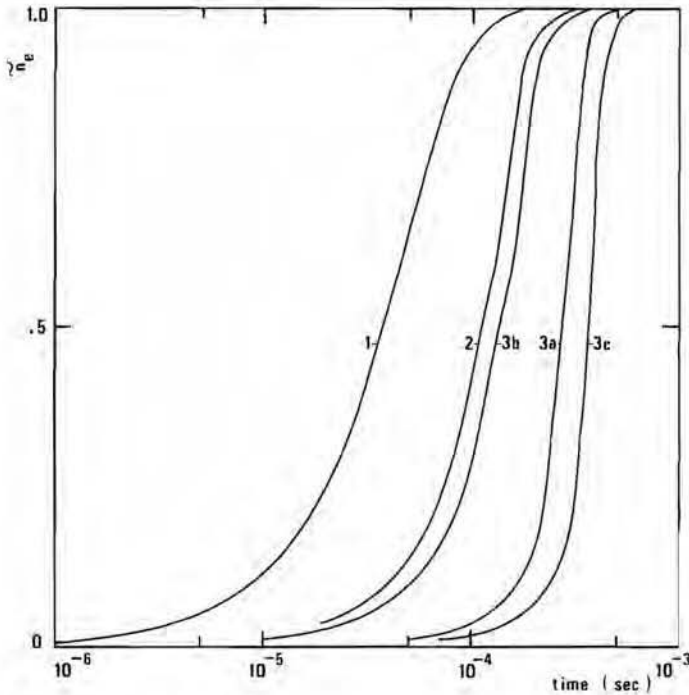
Figure III-3-A.

Development in time of reduced electron density, $n_{Cs} = 7.2 \times 10^{21} m^{-3}$. Case 1, no radiation included. Cases 2 and 3, radiation included. Ionizing plasma, $T_{eo} = 2100$ K, $T_{e\infty} = 2300$ K.

Case 1 and 2: $T_t = T_e$.

Case 3a: $T_{to} = 2000$ K $T_{t\infty} = 2300$ K

"   3b: $T_{to} = 2100$ K $T_{t\infty} = 2200$ K

"   3c: $T_{to} = 2000$ K $T_{t\infty} = 2200$ K

in Fig. III-3-A. The recombining case is shown in Fig. III-3-B.
Comparing the resulting $n_e(t)$ for a non-Maxwellian initial condition
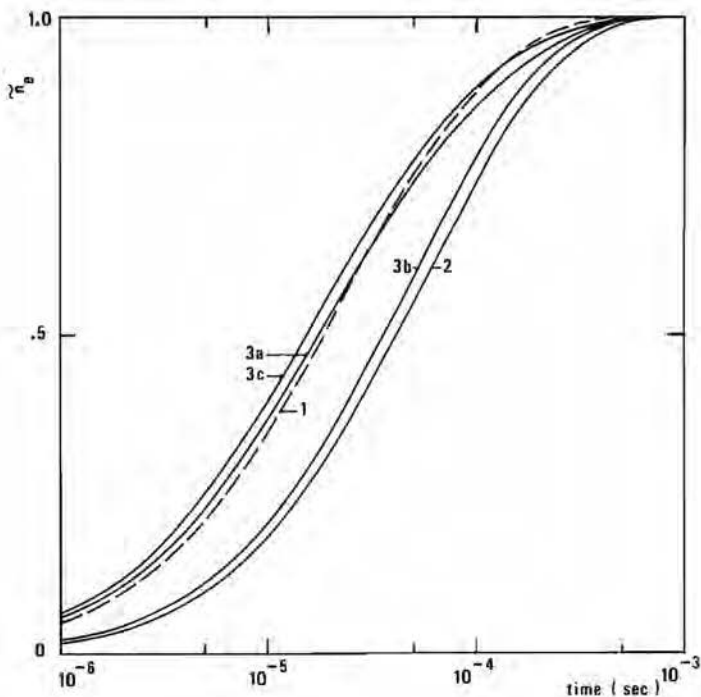and for a non-Maxwellian final condition, it can be noted that the

Figure III-3-B.

Development in time of reduced electron density, $n_{Cs} = 7.2 \times 10^{21} m^{-3}$. Case 1, no radiation included. Cases 2 and 3, radiation included. Recombining plasma, $T_{eo} = 2300$ K, $T_{e\infty} = 2100$ K.

Case 1 and 2: $T_t = T_e$.

Case 3a: $T_{to} = 2400$ K $T_{t\infty} = 2100$ K

"   3b: $T_{to} = 2300$ K $T_{t\infty} = 2200$ K

"   3c: $T_{to} = 2400$ K $T_{t\infty} = 2200$ K

former shows a more pronounced deviation from the Maxwellian case.

In Fig. III-4 the values of the characteristic time for the
electron density relaxation as function of the seed fraction s are
plotted for different conditions. The argon density is $n_{Ar} = 7.2 \times 10^{24} m^{-3}$, corresponding to a gas pressure of 1 bar at a gas temperature
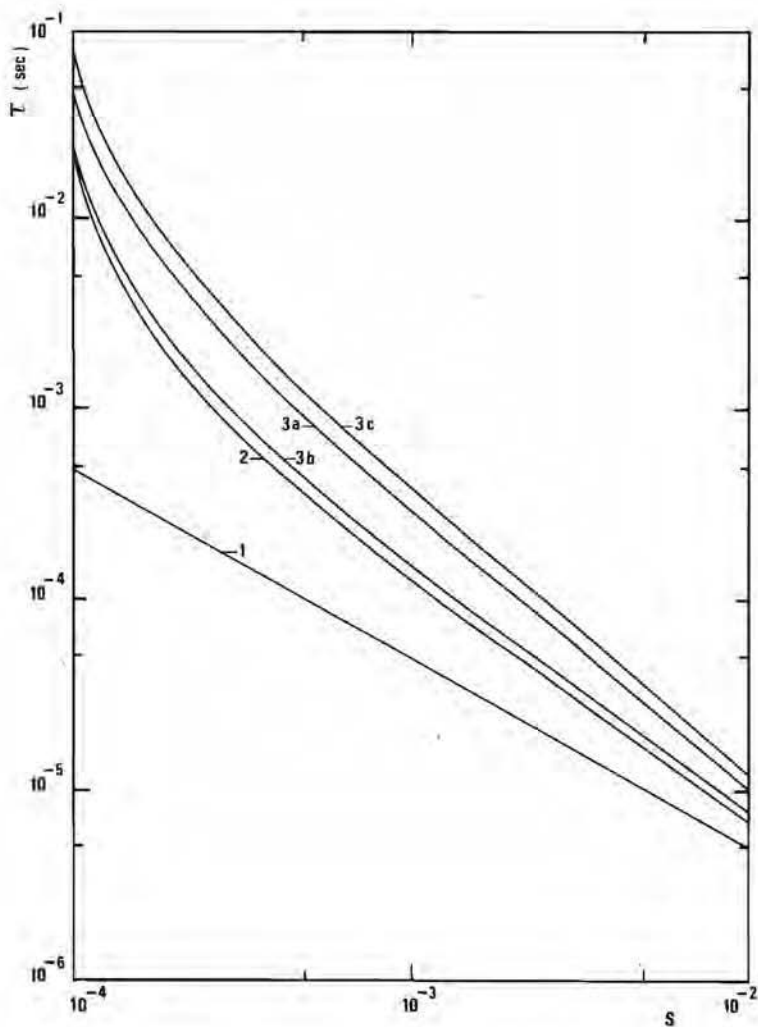
Figure III-4-A.

Relaxation time for an ionizing plasma ($f=1-e^{-1}$) as a function of seed ratio. Different cases like in Fig. III-3-A, $n_{Ar} = 7.2 \times 10^{24}$ m^{-3}.

of 1000 K. The characteristic time τ for the relaxation of the electron density is defined by the following expression:

$$\tilde{n}_e(\tau) = f \tag{III-25}$$

In the ionizing plasma case (Fig. III-4-A) f is taken as $1-e^{-1} = 0.632$. For decreasing seed fraction, τ increases. This effect becomes more
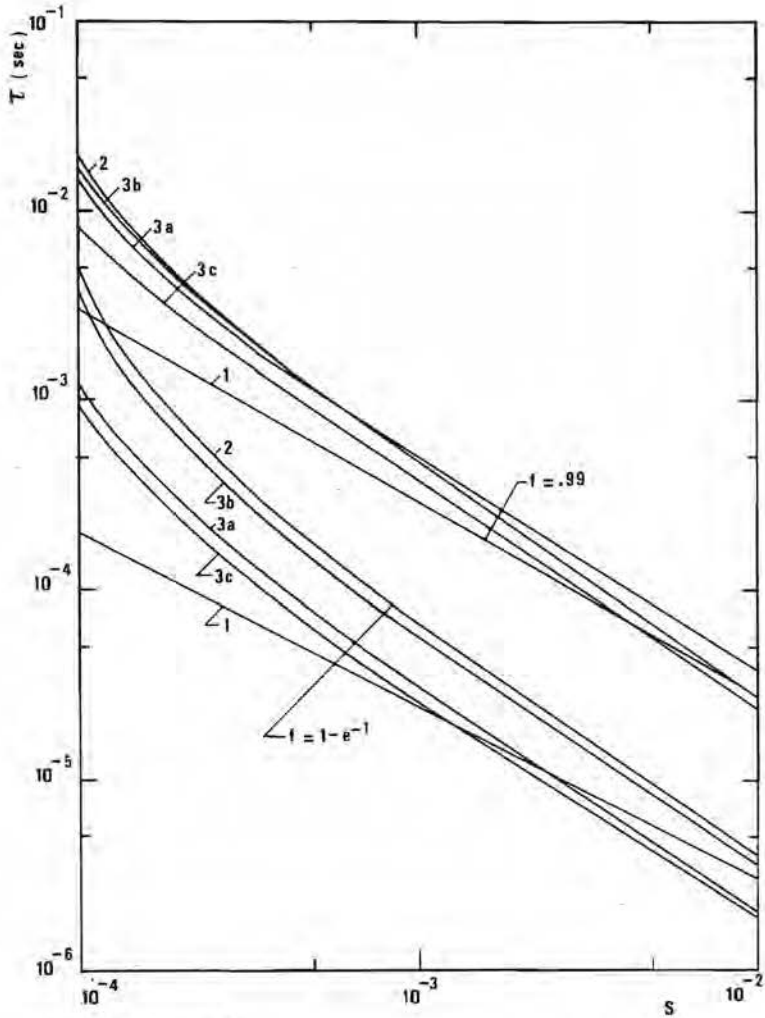

Figure III-4-B.

Relaxation time for a recombining plasma (early relaxation:
$f = 1 - e^{-1}$; *late relaxation: f=0.99) as a function of seed ratio.*
Different cases like in Fig. III-3-B,
$n_{Ar} = 7.2 \times 10^{24} \ m^{-3}$.

pronounced at low seed fraction when the model includes radiation or a non-Maxwellian distribution. For a recombining plasma two characte-

ristic times are defined. One is connected with the early relaxation of $\tilde{n}_e(t)$ and is defined by eq. III-25 for $f = 0.632$. The other one is defined by eq. III-25 for $f = 0.99$ and accounts for the late relaxation of $\tilde{n}_e(t)$. The dependence on seed ratio of the characteristic time for early and late relaxation of a recombining plasma is shown in Fig.III-4-B.

The influence of the temperature step on the characteristic time is shown in Fig. III-5. Fig. III-5-A shows examples of ionizing plasmas ($T_{eo} = 2100$ K, $T_{e\infty} = T_{eo} + \Delta T$). In the non-Maxwellian case only the ini-
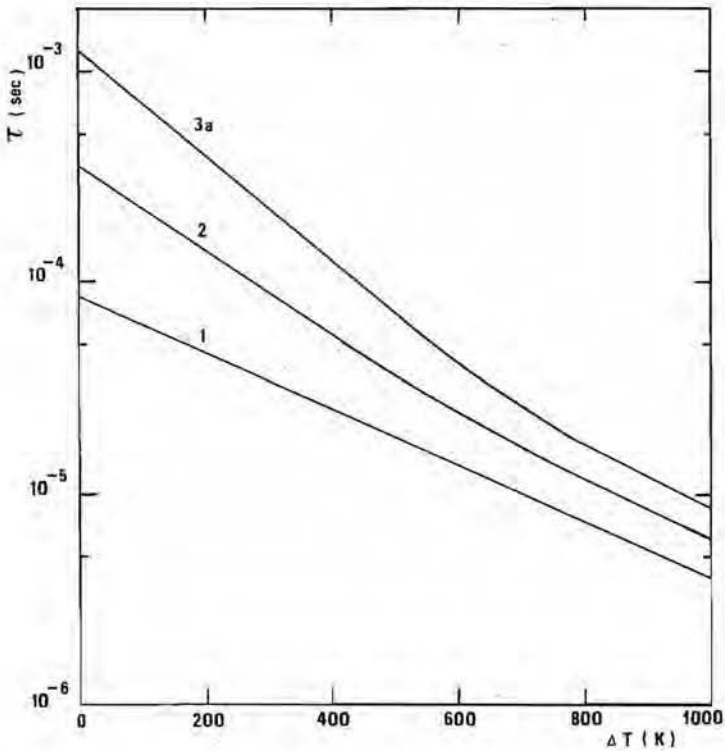
Figure III-5-A.
Relaxation time as a function of temperature step $n_{Cs} = 7.2 \times 10^{21} m^{-3}$. Case 1: no radiation included. Case 2 and 3a, radiation included; $T_{e\infty} = T_{t\infty}$. Ionizing plasma ($f=1-e^{-1}$), $T_{eo} = 2100$ K, $T_{e\infty} = T_{eo} + \Delta T$. Case 1 and 2: $T_{to} = T_{eo}$, case 3a: $T_{to} = 2000$ K.

tial condition is assumed non-Maxwellian with $T_{eo} = 2100$ K, $T_{to} = 2000$ K,

whereas $T_{e\infty} = T_{t\infty} = T_{eo} + \Delta T$. The characteristic time decreases for increasing values of ΔT. Fig. III-5-B shows examples of recombining plasmas (T_{eo} = 2300 K, $T_{e\infty} = T_{eo} - \Delta T$). In the non-Maxwellian case T_{eo} = 2300 K,
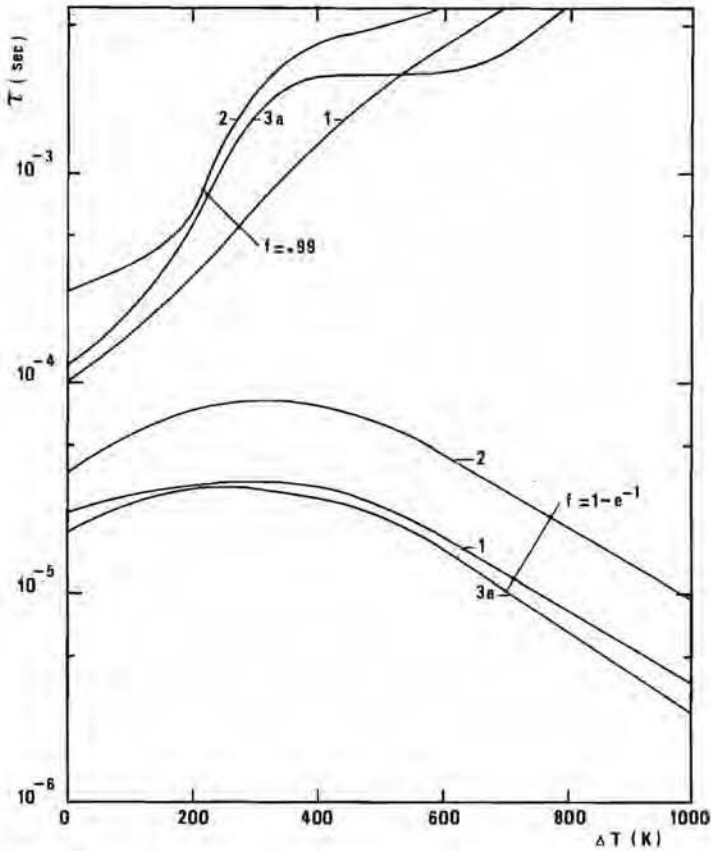

Figure III-5-B.

Relaxation time as a function of temperature step n_{Cs} = 7.2 ×
10^{21} m^{-3}. Case 1, no radiation included. Case 2 and 3, radiation
included; $T_{e\infty} = T_{t\infty}$. Recombining plasma, T_{eo} = 2300 K.
$f = 1-e^{-1}$, early relaxation
$f = 0.99$, late relaxation
$T_{e\infty} = T_{eo} - \Delta T$.
Case 1 and 2: $T_{to} = T_{eo}$, case 3a: T_{to} = 2400 K.

T_{to} = 2400 K, $T_{e\infty} = T_{t\infty}$, $T_{eo} - \Delta T$. The characteristic time for the

early relaxation decreases for increasing ΔT whereas the characteristic time for the late relaxation increases for increasing ΔT.

III-4 CONCLUSIONS

The ionization and the recombination of cesium as a response to step-wise electron temperature changes, have been analyzed. The effects of radiation and deviations from the Maxwellian shape of the electron distribution on the relaxation processes have been determined.

Both radiative transitions and a non-Maxwellian electron energy distribution affect the ionization and recombination of the plasma. Radiation causes lower densities of electrons and of excited atoms in the initial and in the final state as well as an enhancement of deexcitation. The combined effect consists of an increase of the ionization relaxation time. For the conditions considered the recombination relaxation time also increases because the effect of lower final values predominate the enhanced deexcitation. The effect of radiation is more pronounced at low seed ratio.

A non-Maxwellian energy distribution has its influence on n_e and n_i in the initial and in the final state as well as on the rate integrals. The latter has a minor effect on the relaxation behaviour. For ionization processes the relaxation time increases in case of a non-Maxwellian distribution mainly because the depleted tail causes lower initial values. For recombination processes, when the tail of the energy distribution is overpopulated, the relaxation time is shorter.

The relaxation time appears to be strongly dependent on the seed ratio and on the temperature step in all cases considered.

REFERENCES

1. TAKESHITA, T., GROSSMAN, L.M., "Excitation and ionization processes in nonequilibrium MHD plasmas", Proc. of the 4th Int. Symp. on MHD, Vol. 1, p. 191, Warsaw, (1968);
   BERTOLINI, E., TOSCHI, R., Mc NAB, I.R., "Relaxation phenomena in MPD generators", Proc. of the 3rd Int. Symp. on MHD, Vol. 1, p. 533, Salzburg,(1966);

ZAUDERER, B., "Experimental study of the relaxation processes and
the magnitude of non-thermal ionization in an MHD generator", Proc.
of the 3rd Int. Symp. on MHD, Vol. 1, p. 239, Salzburg (1966);
BLOM, J.H. HOUBEN, J.W.M.A., "Relaxation length calculations in
Ar-Cs mixtures for one- and two-dimensional pre-ionizer geometries",
Proc. of the 5th Int. Conf. on MHD El. Power Gen. , Munich, (1971).

2. BORGHI, C.A., VEEFKIND, A., WETZER, J.M., "Effect of radiation and
non-Maxwellian electron distribution on relaxation processes in an
atmospheric cesium seeded argon plasma", EUT Report 82-E-124, Eind-
hoven University of Technology, Eindhoven, (1982).

3. GRYZINSKI, M., "Classic theory of atomic collisions. I. Theory of
inelastic collisions", Phys. Rev., Vol. 138, no. 2A, p. A336, (1965).

4. FABRY, M., "Theoretical and experimental determinations of cesium
oscillator strengths", J.Q.S.R.T., Vol. 16, p. 127, (1976).

5. NORCROSS, D.W., STONE, P.M., "Radiative recombination in cesium",
J.Q.S.R.T., Vol. 6, p. 277, (1966).

6. HOLSTEIN, T., "Imprisonment of Resonance radiation in Gases. II.",
Phys. Rev., Vol. 83, p. 1159, (1951).

7. BATES, D.R., KINGSTON, A.E., Mc WHIRTER, R.W.P., "Recombination
between electrons and atomic ions. I. Optically thin plasmas",
Proc. Roy. Soc., Vol. 267A, p. 297 (1962); "II Optically thick
plasmas", Proc. Roy. Soc., Vol. 270A., p. 155, (1962).

8. GEAR, C.W., "Numerical initial value problems in ordinary differential
equations", Prentice Hall, Engl. Clitts N.J., (1971).

DISCHARGE EXPERIMENTS

IV-1 INTRODUCTION

In this chapter a gas discharge experiment is described. The aim is to obtain information on the behaviour of the discharge in the ionization relaxation region of a noble gas MHD generator where detailed measurements ar difficult to perform. In part of this region the electron density is lower than 10^{19} m^{-3}.

In the discharge experiment two conditions are investigated: a stationary state arc discharge and its afterglow. Values of the electron density down to 10^{20} m^{-3} are obtained under the stationary conditions. Lower electron densities are realized during the afterglow.

The experiments are carried out in a glass tube filled with cesium seeded argon gas. The filling pressure at room temperature is 200 torr. This corresponds to an argon density of 6.6×10^{24} m^{-3}. During the experiments the tube is kept at a temperature of 520 K. Then the cesium density is 7×10^{21} m^{-3}.

Current densities and electric fields are determined during the stationary discharge. From continuum recombination radiation intensities the electron temperature and the electron density are calculated. The population densities of several levels of cesium are obtained from the emission of line radiation. The afterglow measurements provide information on the characteristic times involved in the decay of the plasma. It is important to know which processes determine the time constants involved and hence dominate the plasma behaviour.

IV-2 EXPERIMENTAL SET UP

The discharge is produced in a pyrex glass tube with a diameter of 1 cm (see Fig. IV-1). The electrodes are placed on the axis of the tube. The cathode is a standard L-type cathode with the possibility
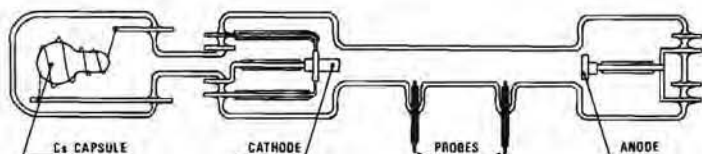
Cs CAPSULE   CATHODE   PROBES   ANODE

Figure IV-1.
Construction of the discharge tube.

to be heated by a hot filament. The anode is of molybdenum. The elec-
trode distance is 8 cm. Two electrical probes are mounted flush to the
wall at a distance of 2.5 and 5.5 cm from the cathode. After evacuation
at 10^{-6} Torr with outgassing of the electrodes for several hours, the
tube is filled with argon at a density $n_{Ar} = 6.6 \times 10^{24}$ m^{-3}. Then the
cesium capsule is broken by a hot filament and cesium vapour is mixed
into the argon atmosphere. In operating conditions the partial pressure
of cesium is assumed to be equal to the saturation pressure corresponding
to the temperature of the wall of the tube T_w and is given by the
following expression (1):

$$\log_{10} P_{Cs} = \frac{4530}{T_w} - 0.91 \log_{10} T_w + 12.05. \qquad (IV-1)$$

The constant temperature T_w is obtained by means of a thermostat in
which the discharge tube is placed. In order to obtain homogeneous
conditions, the temperature of the thermostat is set at T_w two hours
before the experiment.

The electrical circuit of the discharge is shown in Fig. IV-2.
In this figure G_1 and G_2 are two power supplies of 400 and 50 V res-
pectively. R_h, R_1 and R_i are resistors of 1250, 10 and 1 Ω. T is an
S.C.R. thyristor. G_1 is only used to start the discharge. After ignition
the switch S_1 is opened. The discharge power is supplied by G_2 and
stabilized by R_1. The discharge current is measured by the voltage
drop over R_i. The thyristor T is employed during the afterglow ex-
periments. After applying a triggering signal to the gate TS, the
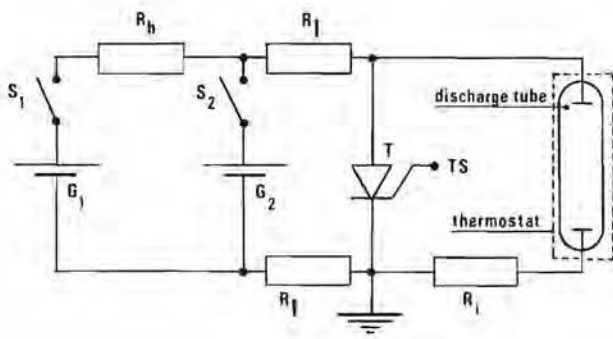discharge current will no longer pass through the tube and the after-

Figure IV-2.
Simplified electrical circuit diagram for the discharge experiments.

glow is initiated. As shown in Fig. IV-3, the discharge current drops from 2 A to 0.07 A in a time of about 3 µsec and then decreases slowly to zero in typically 10 msec.
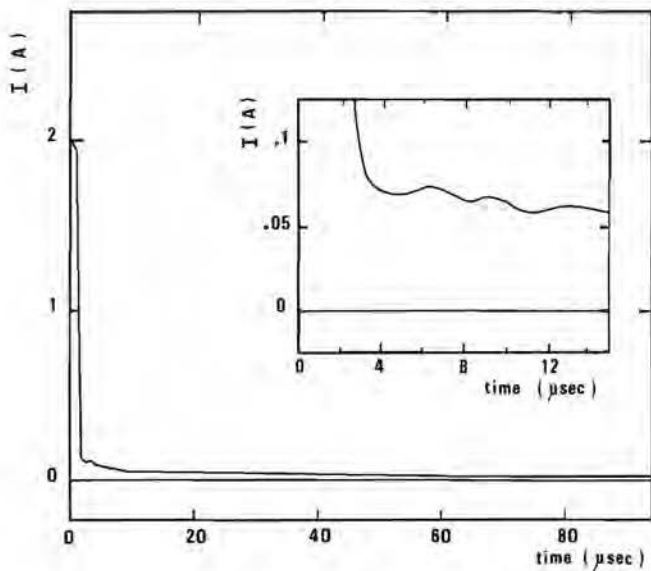

Figure IV-3.
Current decay after short circuiting of the voltage across the discharge at t=o.

Electrical measurements are carried out during the stationary discharge. The electric field is derived from the voltage difference between the probes. The voltage difference between the electrodes and the discharge current are measured.

Continuum and line radiation intensities are measured both during the stationary discharge and during the afterglow. In Fig. IV-4 the
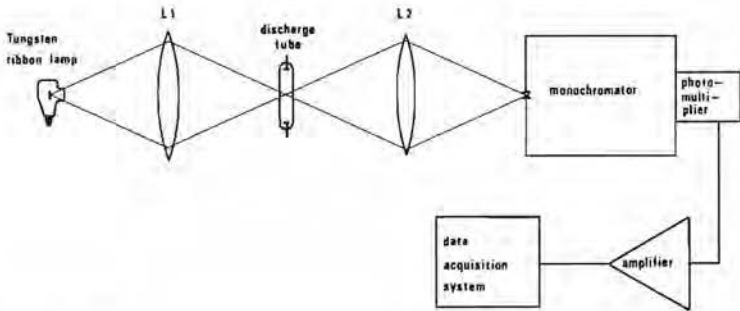
Figure IV-4.
Sketch of the experimental equipment for the spectroscopical
measurements.

detection system for the radiation measurements is shown. The system is calibrated by means of a standard tungsten ribbon lamp. The light coming from the discharge tube is focused by the lens L_2 on the slit of a monochromator. The characteristic time of the detection system is 1 µsec. For the stationary discharge measurements a 0.5 m monochromator can be coupled to two photomultipliers: one with a bialkali and one with a S-20 photocathode for low and high wave length respectively. In order to increase the sensivity of the system during the afterglow, the radiation is measured with a 0.25 m monochromator coupled to a gallium-arsenide photocathode. The resolution of the 0.5 m monochromator is 3.2 Å. The resolution of the 0.25 m monochromator is 4.8 Å. During the afterglow the photomultiplier is connected to the acquisition system through an emitter follower amplifier. The accuracy of the detection system is determined by the photoelectron statistical noise of the photomultipliers and by the calibration of the system.

Intensities of continuum recombination radiation and of line
radiation are measured.

The experimental values of the radiation intensities are corrected
for the transmission of the tube. During the operation time of the
discharge tube, a thin cesium layer is deposited on the walls of the
discharge tube and affects its transmissivity. The transmission coeffi-
cient $a(\lambda)$ decreases with the operation time. $a(\lambda)$ is defined by the
following expression:

$$a(\lambda) = \left\{ \left| \frac{I_w(\lambda)}{I'_w(\lambda)} \right| \right\}^{\frac{1}{2}} \tag{IV-2}$$
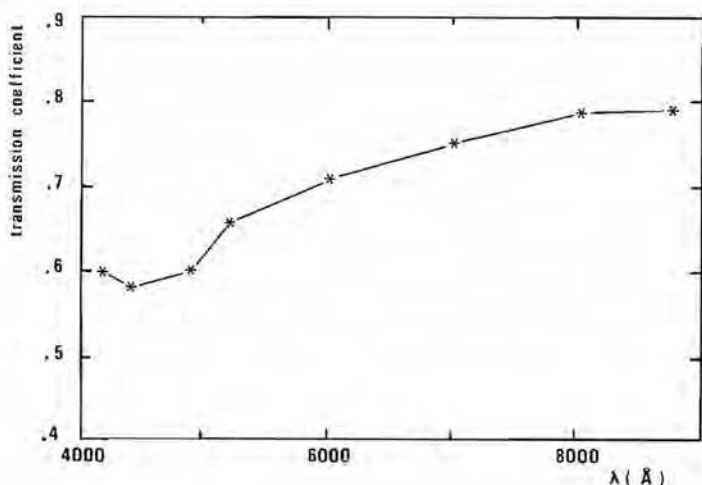
Figure IV-5.
Transmission coefficient of the tube walls after five hours of
operation of the discharge tube.

The intensity $I_w(\nu)$ and $I'_w(\nu)$, coming from the tungsten lamp, are
measured respectively with and without the discharge tube on the axis
of the optical system. A typical plot of $a(\lambda)$ measured after five hours
of operation of the discharge tube, is shown in Fig. IV-5.

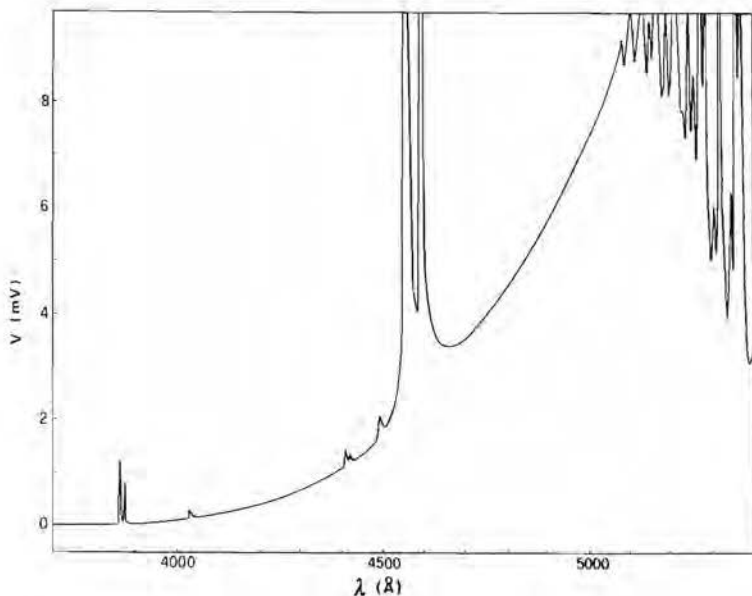The electron temperature and the electron number density are

Figure IV-6.

The continuum of recombination radiation emitted by the Ar-Cs discharge.

derived from the intensity of the continuum recombination radiation
(2,3). The spectrum of the continuum radiation detected from the
stationary discharge between 3700 and 5300 $\overset{\text{o}}{\text{A}}$ is shown in Fig. IV-6.
The continuum radiation in this interval is mainly due to recombination
of Cs$^+$ ions with electrons having a kinetic energy in the range 0 ÷ 0.89 eV,
yielding neutral cesium in the 6P state. Hence the radiation spectrum
follows from the electron energy distribution. In deriving T_e the
assumption of Maxwellian electron distribution is made. As deviations
from the Maxwellian shape are possible for $\varepsilon_e \geq 1.432$ eV, the value
of T_e obtained from the measurements, refers to the bulk electrons.

The population densities of the emitting atoms are derived from
the line intensities of non-absorbed lines. If the populations of
Cs levels are in Boltzmann equilibrium, their values are determined by
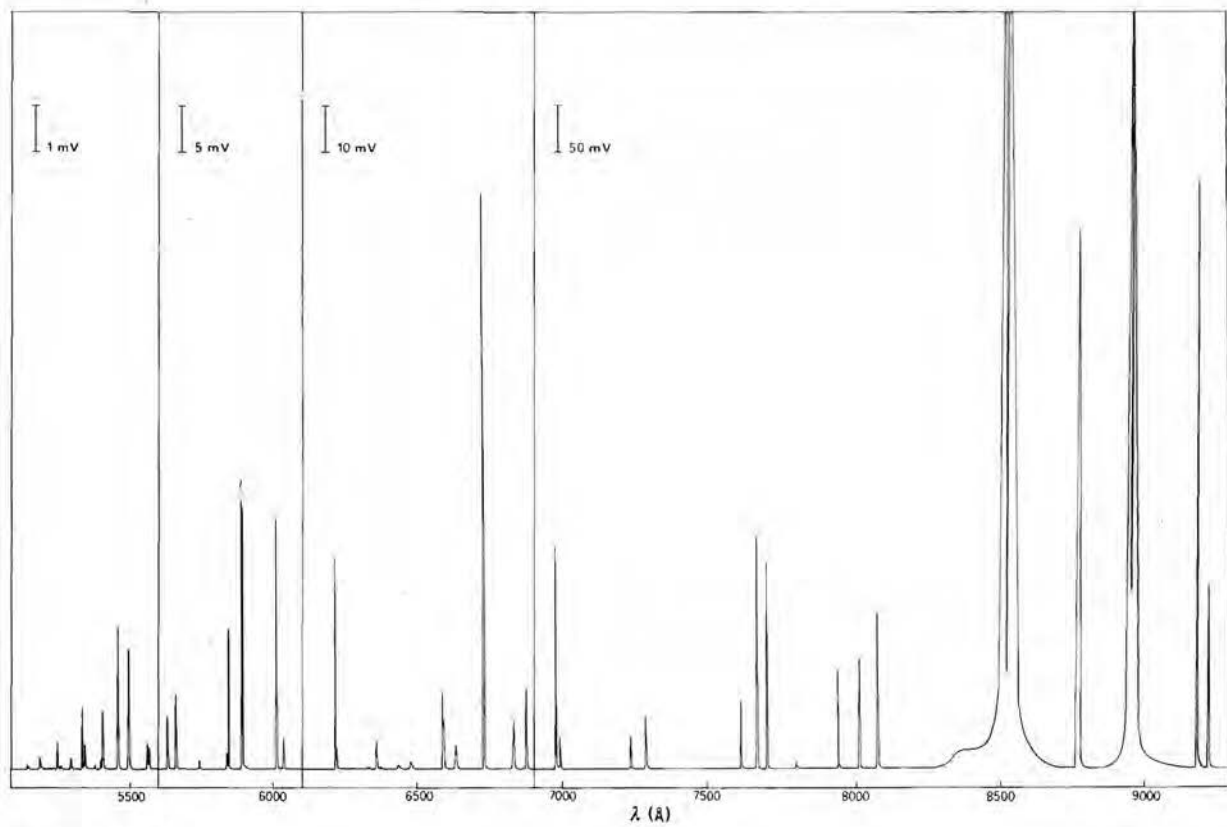the population temperature T_p.

Figure IV-7.
Discrete spectrum of the Ar-Cs discharge.

The discrete spectrum due to spontaneous emission of excited Cs atoms is shown in Fig. IV-7.

During the afterglow, lines for which the plasma is optically thick are also measured. Assuming that the line profile of the considered line does not vary during the afterglow, the relative variation $n_j(t)/n_j(o)$ of the population density of the j-state of cesium ($n_j(o)$ is the population density before the afterglow) is derived. The assumption of constant line profile during the afterglow holds for pressure broadened lines where the half width depends on the gas density and on the gas temperature, but not for lines dominated by stark broadening where the half width depends on the electron density.

The space profile of the discharge is obtained by means of Abel's inversion techniques (Lochte-Holtgreven, Ref. 4). A scan over the discharge radius is done by detecting the light intensity each 0.5 mm. The image of the slit of the detector covers 0.15 mm of the plasma.

The discharge diameter is estimated using a photographic technique. By using this method the discharge is assumed to be contracted in a homogeneous cylinder. The diameter of the cylinder is then determined.

IV-4 THE STATIONARY DISCHARGE

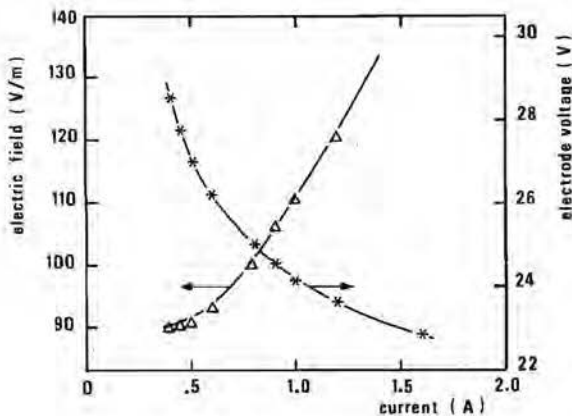The stationary discharge experiments (5) are done for T_w = 520 K.

Figure IV-8.
Electric field and electrode voltage at several values of the discharge current.

and for currents between 0.2 and 3 A. In Fig. IV-8 the measured electric
field and the voltage difference between the electrodes are shown. The
electric field decreases with decreasing current whereas the voltage
difference between the electrodes increases as the current decreases
showing a dominant influence of the electrodes on the current voltage
characteristic. Using the photographic technique the discharge diameter
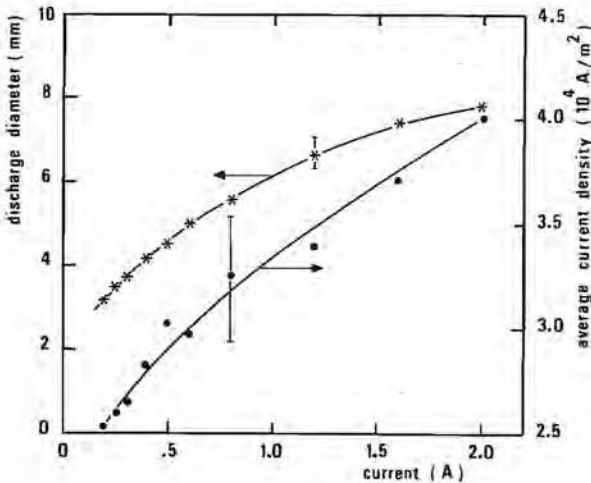is estimated and the current density is derived (Fig. IV-9). A con-

Figure IV-9.
Discharge diameter and current density as a function of the
discharge current.

traction of the discharge appears for low values of the current and
below 0.2 A an abrupt extinction of the discharge occurs.

The values of the electron temperature and of the electron density
are measured using the procedure presented in Sec. IV-3. The results
of these measurements are shown in Fig. IV-10. The maximum error in
the electron temperature is 8%. The error in n_e is determined by the
error in T_e, the error in the absolute intensity measurement and the
error in the discharge diameter. Assuming the total cesium density
$n_{Cs} = 7 \times 10^{21} \ m^{-3}$, as is given by eq. IV-1, the value of n_e calculated
from the experimental value of T_e by means of Saha's relation (eq. II-24)
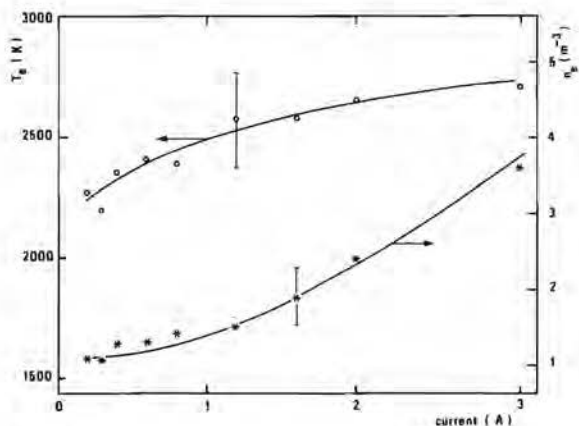agrees with the experimental value of n_e within the experimental error.

Figure IV-10.
Electron temperature and electron density as a function of the
the discharge current.

At two values of the current ($I = 2\,A$ and $I = 0.3\,A$), the line
intensities of the diffuse series corresponding to the transitions
$pD_{3/2} \rightarrow 6P_{1/2}$ ($p = 6 \div 12$), are measured. The measured intensities
are corrected for the line broadening (the method used is given in
Ref. 4 by Huddlestone, pag. 311). The values n_p of the population
densities of the $pD_{3/2}$ energy levels of cesium are then derived. In Fig.
IV-11 the values of n_p are plotted against the excitation energy ε_{1p}
of the $pD_{3/2}$ state. The experimental error due to the error made in
determining the absolute intensity, to the error in the discharge
diameter and to the uncertainity of the Einstein coefficient is es-
timated to be less than 10%. The statistical noise can be reduced even
for the lines with the lowest intensity because of the long time
available for the measurement. For the transitions from the high state,
($p = 10$, 11 and 12) the correction for the line broadening cannot be
neglected when deriving the population densities. For the discharge
of $2\,A$ the half width of the line corresponding to the transition
$12D_{3/2} \rightarrow 6P_{1/2}$ is $1.3\,\overset{\circ}{A}$ and a correction factor of 1.86 for measured
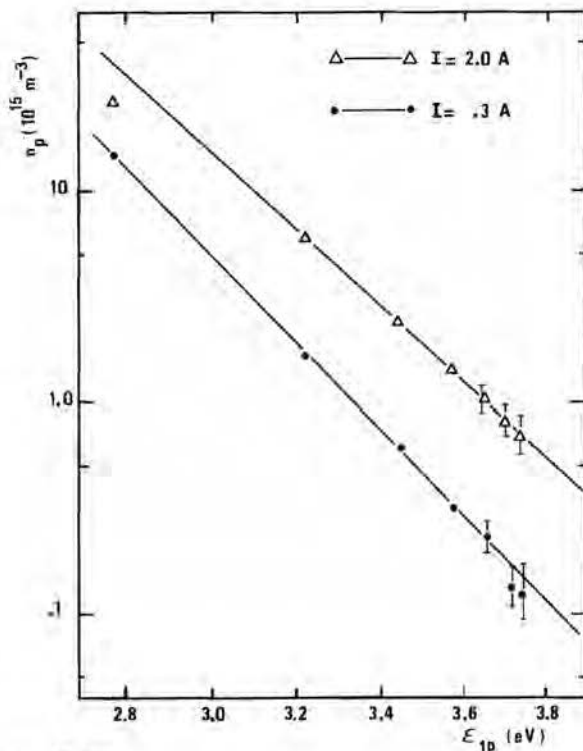line intensity is calculated.

Figure IV-11.

Boltzmann plot for:

a. $I = 2$ A: $T_p = 2640$ K;   b. $I = 0.3$ A: $T_p = 2420$ K.

T_e = 2670 ± 210 K	continuum intensity measur.	
n_e = (2.4 ± 0.3) × 10^{20} m-3	"	
T_p = 2640 ± 100 K	line intensity measur.	
n_{7D} = (6.3 ± 0.5) × 10^{15} m^{-3}	"	
n_{Cs} = 7 × 10^{21} m^{-3}	cal. from eq.IV-1	
n_e^* = (3.2 ± 2) × 10^{20} m^{-3}	cal. from eq. II-24, T_e and n_{Cs}	
n_{7D}^* = (5.8 ± 1.6) × 10^{15} m^{-3}	cal. from eq. III-14, T_e and n_e	

Table IV-1.

Comparison of experimental and theoretical values of the electron density and the population of the 7D state (n_e, n_{7D}, n_e^* and n_{7D}^* respectively) for the stationary discharge at $I = 2$ A. The theoretical values are obtained from Saha's relation at the measured value of T_e.

The population temperature is then determined (Sec. IV-3). The population temperature T_p is equal to the electron temperature and the population densities of these levels are in Saha equilibrium with the electron density (Tab. IV-1). The highest population density in Fig. IV-11, corresponding to the transition $6D_{3/2} \rightarrow 6P_{1/2}$ seems to be over-estimated by T_p. This is due to absorption of the line (compare Ref. 6). For the case of I = 0.3 A the discharge diameter and the electron density are smaller and the line, which is stark broadened, is less absorbed.
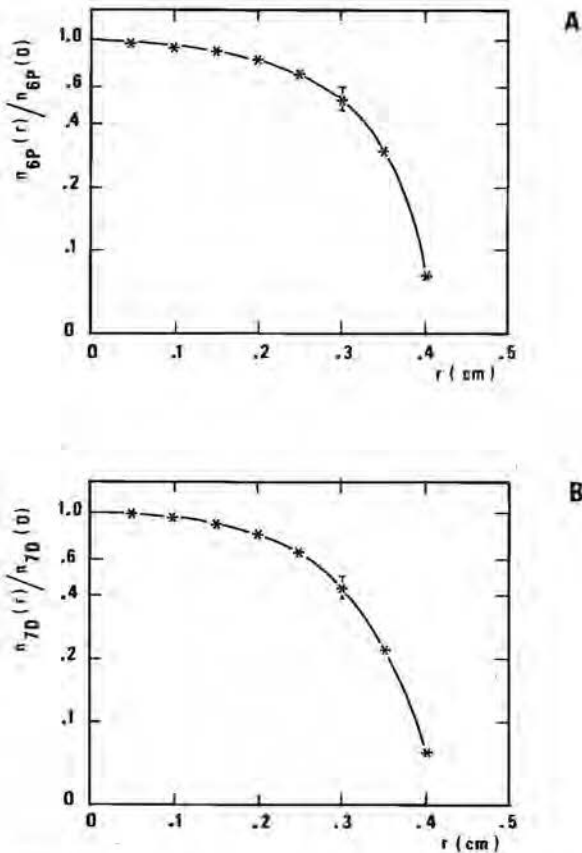
A

$n_{6P}(r)/n_{6P}(0)$

1.0
.6
.4
.2
.1
0

0   .1   .2   .3   .4   .5
r (cm)

B

$n_{7D}(r)/n_{7D}(0)$

1.0
.6
.4
.2
.1
0

0   .1   .2   .3   .4   .5
r (cm)

Figure IV-12.
Radial dependence of the population density of:
A. $6P_{3/2}$ level of cesium, B. $7D_{3/2}$ level of cesium.

In Fig. IV-12 the results of the spatial profile measurements

derived by Abel's inversion techniques, are shown. In Fig. IV-12-A the profile of the population density of Cs* excited to the first excited state is plotted. (The measurements are done in the wing of the line, 10 $\overset{\circ}{A}$ away from the center). The profile of the line intensity from the $7D_{3/2} \rightarrow 6P_{1/2}$ transition is also detected (Fig. IV-12-B). This line is not absorbed and the profile of the light intensity corresponds to the profile of population density of the $7D_{3/2}$ state. By comparing the two profiles in Fig. IV-12-A and Fig. IV-12-B, it appears that the effect of the self absorption on the spatial profile of the population of the $6P_{3/2}$ level is neglegible.

The averaged value of the population density of the $7D_{3/2}$ level obtained from the profile measurement is 25% smaller than the corresponding value given in Fig. IV-11. This can be due to the error of the determination of the discharge diameter and to the fact that the profile measurements and the measurement of the discharge diameter are carried out in two different discharge tubes. As the electron density depends on the square root of the population densities, the error in the electron density is 12%.

The gas temperature can be estimated by the following equation:

$$\vec{\nabla} \cdot (\lambda_{Ar} \vec{\nabla} T_g) = JE. \tag{IV-3}$$

The heat conductivity of argon λ_{Ar} is taken from Ref. 7. For I = 2 A, the profile of T_g is calculated from the measured current density and electric field, assuming cylindrical geometry and λ_{Ar} independent of T_g. Eq. IV-3 is satisfied by a parabolic profile. Assuming at the cylinder wall $T_g = T_w = 520$ K, it follows that T_g on the axis is equal to 1120 K, and that the averaged T_g is equal to 920 K. The average value of T_g can also be estimated from the electron energy equation:

$$JE = 3m_e n_e k (T_e - T_g) \sum_i \frac{\nu_i}{m_i}. \tag{IV-4}$$

The values of J, E, n_e, T_e used in eq. IV-4 are measured values, ν_i is calculated by means of eqs. II-36, II-40. For I = 2 A eq. IV-4 gives $T_g = 950$ K.

The afterglow is obtained after a discharge of 2 A and a wall temperature T_w = 520 K. During the afterglow optical measurements have been carried out. In this case the photoelectron statistical noise of the photomultiplier determines the experimental error and is a limitation of the measurements at low intensities. In order to reduce the statistical error ten afterglows are analyzed for each wave length of interest.
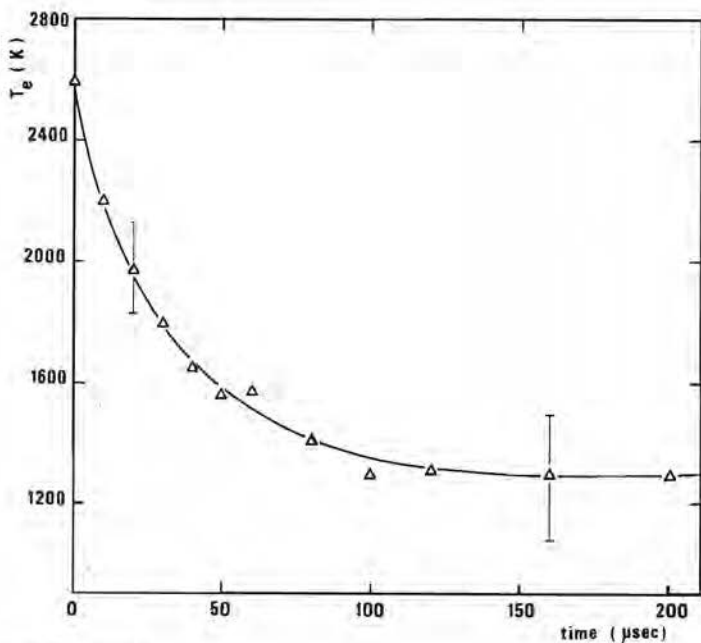

Figure IV-13.
Decay of the electron temperature.

The decay of continuum radiation at 4100, 4450 and 4900 Å has been investigated. From the measured intensities the electron temperature is derived. The error is determined from the obtained values. The electron temperature during the afterglow is shown in Fig. IV-13. T_e decreases during the first 100 μsec approaching the gas temperature T_g, which does not appreciably vary during the afterglow time. The electron
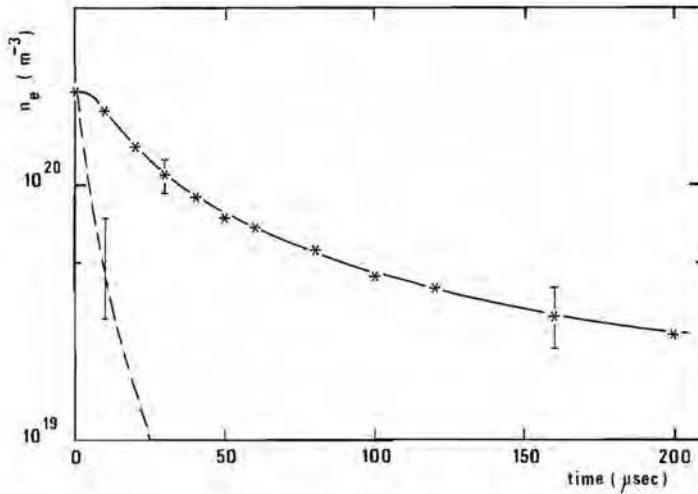
Figure IV-14.
Decay of the electron density: the full line represents the
experimental values of n_e, the broken line represents the value
of n_e given by the Saha relation at the experimental electron
temperature value.

density decay (Fig. IV-14) is slower than the decay of the electron
temperature. During the decay, the experimental value of n_e remains much
larger than the value of n_e given by the Saha relation. In Fig. IV-15
the decay of the population of the $6P_{3/2}$ state and of the $7P_{3/2}$ state
of cesium are shown. They are obtained from the afterglow of the lines
corresponding to the $6P_{3/2} \rightarrow 6S_{1/2}$ transition and to the $7P_{3/2} \rightarrow 6S_{1/2}$
transition. These lines are dominated by pressure broadening (6). Thus
the line profiles do not vary during the afterglow. As discussed in
Sec. IV-3, at any instant their light intensity is proportional to
the decay of the population of the upper state in the corresponding
transition. In the figure the relative decay $n_j(t)/n_j(o)$ is given.
Assuming that these states are in Saha equilibrium with the electrons
during the stationary discharge, the values of $n_j(o)$ can be derived
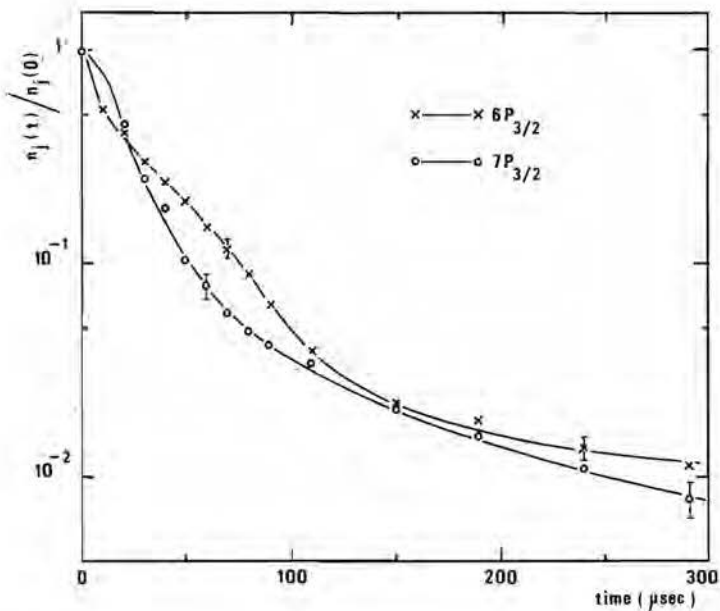from the experimental value of n_e at $t = 0$.

81

Figure IV-15.
Decay of the population density of the $6P_{3/2}$ and of the $7P_{3/2}$
level of cesium.

The afterglow of the diffuse series has been observed and the decay of the population of the $pD_{3/2}$ state of cesium ($p = 7 \div 12$) has been derived. The measured signals are corrected for the line broadening. The decay of the low levels ($p = 7 \div 9$) is always slower with decreasing p, whereas the decay of the high levels ($p = 10 \div 12$) is slower with increasing p for $t < 100$ μsec. For $t > 100$ μsec the high levels decay faster with increasing p (compare Fig. IV-16-A and Fig. IV-16-B).
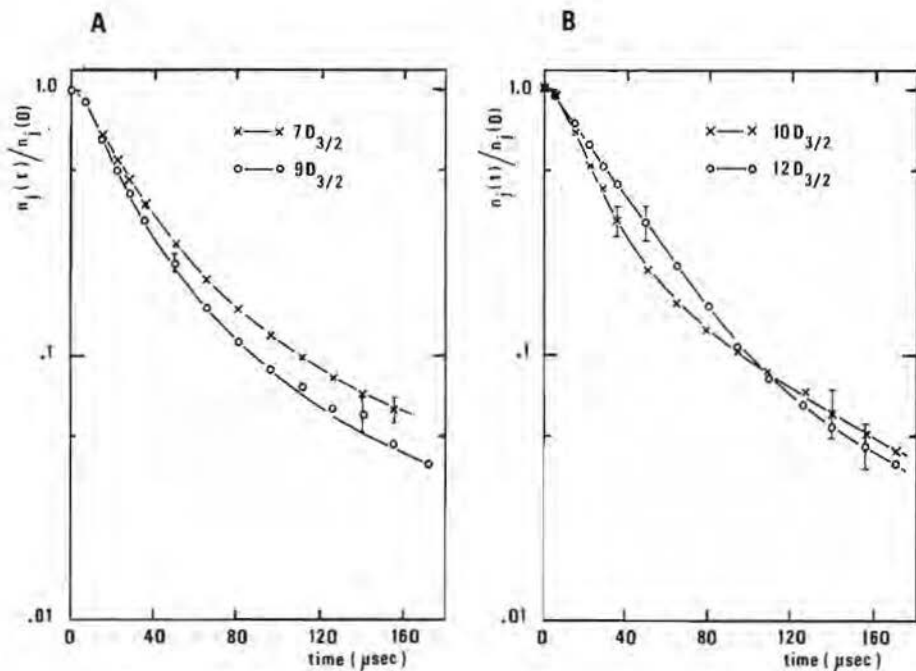
Figure IV-16.

Decay of the population densities of:

A. $7D_{3/2}$ and $9D_{3/2}$ level of cesium.

B. $10D_{3/2}$ and $12D_{3/2}$ level of cesium.

The spatial distribution of the population of the 6P level is measured also during the afterglow. The reason to do this is to see whether the profile of the discharge changes during its decay. The spatial profile is determined during the first 100 µsec of the afterglow. In Fig. IV-17 the profiles at t = 0, t = 30 µsec, t = 60 µsec and t = 90 µsec are shown. The values indicated here are related to the population density measured in the center of the discharge at t = 0. From the figure it appears that the plasma distribution doesn't appreciably vary during the decay.
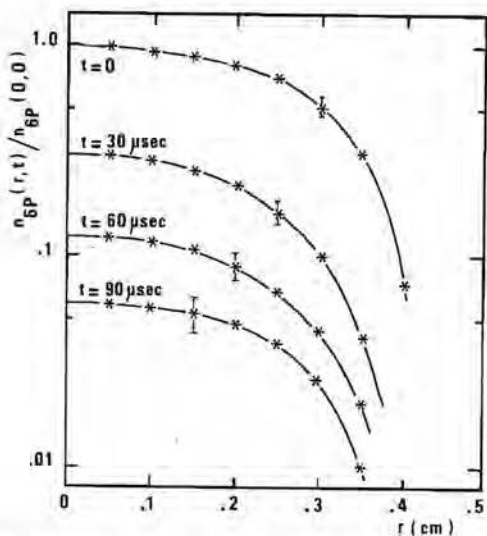
Figure IV-17.

Radial dependence of the population density of the $6P_{3/2}$ level of cesium at several time instants during the afterglow.

IV-6 DISCUSSION OF THE EXPERIMENTAL RESULTS

During the stationary discharge the ground state density and the observed populations of the Cs atom are in Saha equilibrium with the electron density at the measured value of the electron temperature. Hence the conditions for L.T.E. (Local Thermodynamic Equilibrium) are realized.

From the decay of the electron density the graph of $\partial n_e/\partial t$ against n_e^2 is obtained and given in Fig. IV-18. The linear relationship indicates a decay law of the form:

$$\frac{\partial n_e}{\partial t} = \alpha_R n_e^2 \quad ,$$

(IV-10)

where α_R is the recombination coefficient for a two body electron ion process. The value obtained is $\alpha_R = (1.9 \pm 0.6) \times 10^{-16}$ m^3 sec^{-1}. The measured recombination coefficient doesn't show a significant dependance on T_e. The plot in the figure is obtained for values of n_e
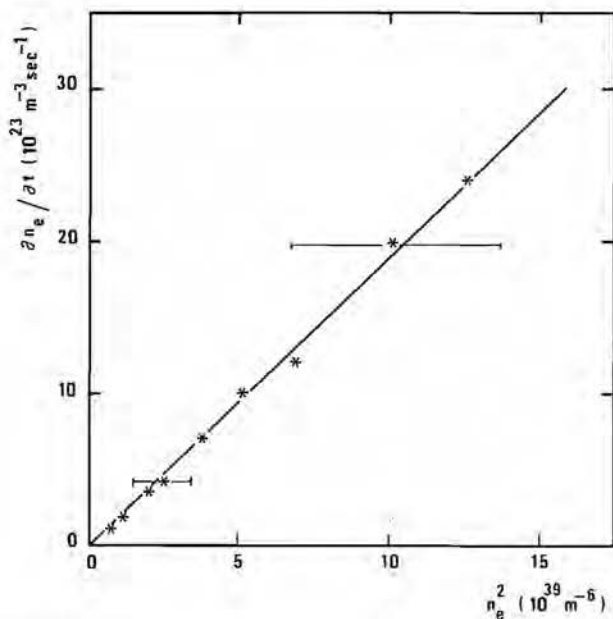
Figure IV-18.
The values of $\partial n_e/\partial t$ against n_e^2 during the first 200 μsec of the afterglow.

measured at t > 30 μsec. The electron temperature here ranges between 1300 and 1800 K. The dependence of the two body radiation recombination coefficient on the electron temperature is given by $T_e^{-\frac{1}{2}}$; a variation of α_R due to the electron temperature variation is not observed. Values of the recombination coefficient were measured by several authors using different techniques [8]. The results of Mohler and Aleskovskii were recorded with probes and spectroscopic techniques in afterglows in cesium vapour at pressures between 10^{-3} and 10^{-1} torr and electron temperatures of 1000 ÷ 2500 K. D'Angelo and Rynn and Wada and Knechtli have reported recombination coefficients deduced from Langmuir probe measurements. Hammer and Aubrey obtained the value of the recombination coefficient by means of atomic beam measurements. The results of these works indicate values in the range $10^{-15} \div 10^{-17}$ m^3 sec^{-1}. The values of α_R predicted by collisional radiative models (see for example the effective recombination coefficient given in

Ref. 9) agree with these values. In Ref. 10 a number of works is listed where recombination coefficients ranging between 10^{-14} and 10^{-12} m^3 sec^{-1} were measured. The fast recombination can be attributed to recombination of molecular cesium ions. The value of α_R obtained in the present experiment agrees with the experimental values predicted by collisional radiative models (as given in Ref. 8) where molecular ions are not included. The disagreement between the results of Ref. 10 and the result of the experiment described here can be attributed to the higher gas temperature and to the lower cesium density in our experiment. In fact in our case the resulting concentration of Cs_2^+ is low.

In Fig. IV-19 the values of the energy gain P_{21}^t due to deexcitations from the first excited state of cesium and the values of the energy flow term P_C^{bt} due to electron electron interactions, obtained during the afterglow, are compared. P_{21}^t and P_C^{bt} are derived from eq. II-29 and eq. II-16 respectively, where for n_2, n_e and T_e the measured values are used. In the first 40 μsec P_C^{bt} is substantially larger than P_{12}^t and apparently the energy gained for the deexcitation of the 6P state of cesium is spread out over the electron energy distribution due to the electron electron interactions. Hence, it has to be expected that for this part of the afterglow the electron distribution remains Maxwellian. For $t > 40$ μsec P_C^{bt} and P_{21}^t are of the same order. For this part of the afterglow the electron electron interactions are not efficient enough for the transfer of the deexcitation energy from the high energetic electrons to the low energetic electrons (compare eq. II-6). The energy distribution function then becomes overpopulated in the tail.

As mentioned above, the observed recombination coefficient reasonably agrees with the values predicted by collisional radiative models where the Maxwellian electron distribution is assumed. In the case of recombination with a non-Maxwellian distribution during the development but with the same initial conditions (i.e. same population and electron densities), the relaxation time does not appreciably change in comparison with that given by a Maxwellian model (compare case 3b to case 2 in Fig. III-3-B). A quantitative analysis of the experimental results by means of the theoretical model is not done. In fact in the model, the electron energy time dependence is assumed to be represented by step functions for T_e and T_t whereas in the afterglow experiments the electron temperature decreases gradually during the first 100 μsec.
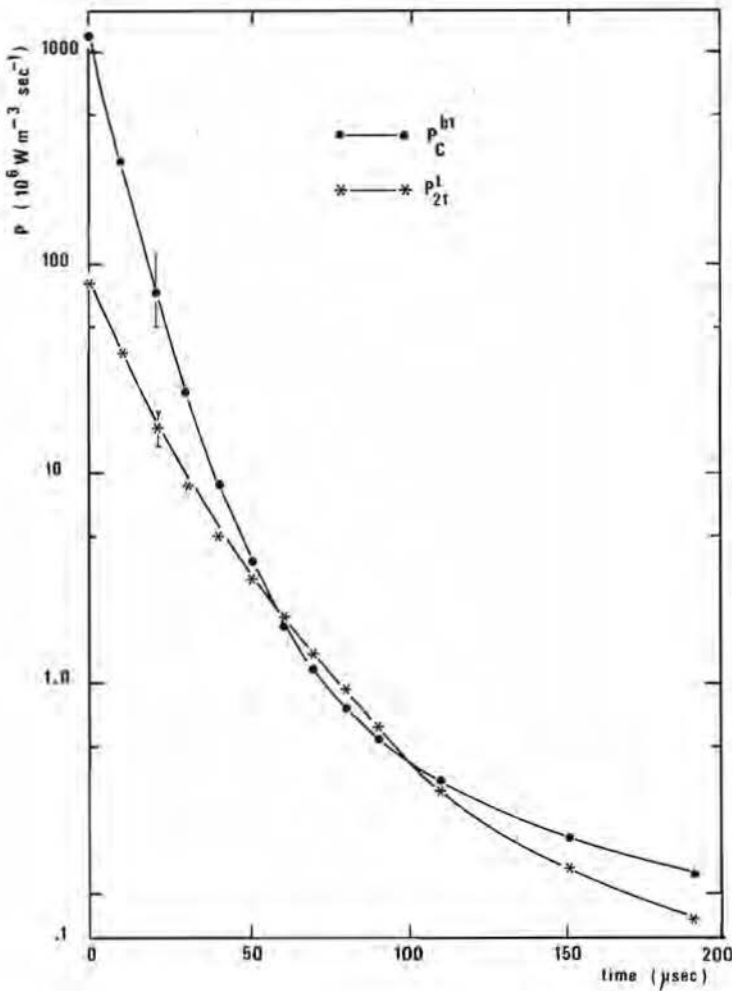
Figure IV-19.

Comparison of the energy flow term P_C^{bt} due to the electron electron interactions and the energy gain term P_{21}^t during the afterglow. For the calculations of P_C^{bt} and P_{21}^t the experimental values of n_2, n_e and T_e are used.

As derived in Chap. III, the excitation and the deexcitation reaction rates for adjacent levels are much larger than those between levels with a large energy gap. Hence the populations of the high excited states depend on collisions with the bulk electrons. Therefore the overpopulated tail of the electron distribution can only influence the low excited states (see Fig. III-2-B). During the early afterglow a slower decay of highly excited states is observed (Fig. IV-16-B). This is a consequence of the increase of the deexcitation time with the decrease of the level quantum number. The electrons first recombine to the high energetic levels, then they flow quickly through the high levels and slowly through the lower ones. Hence electrons are accumulated in the high levels for a certain time. That is indicated also by the results of the time dependent model of Chap. III (compare the slope of n_e and n_{10} of case 3c in Fig. III-2-B). The recombination is then realized through multi-step phenomena.

IV-7 CONCLUDING REMARKS

A stationary arc discharge in an Ar-Cs mixture is experimentally investigated. The argon density is 6.6×10^{24} m^{-3} and the cesium density is 7×10^{21} m^{-3}. The values of the discharge current range from 0.2 to 3 A and correspond to electron densities of $1 \times 10^{20} \div 4 \times 10^{20}$ m^{-3}. During the stationary discharge L.T.E. is observed.

Conditions for deviations from a Maxwellian electron energy distribution are realized during the afterglow. When n_e decreases the electron electron interactions are not efficient enough to thermalize the energy gained by the tail electrons due to the deexcitation from the first excited state. As a consequence the tail of the electron energy distribution becomes overpopulated.

The range of electron temperatures and of electron densities in the inlet region of the MHD gnerator are the same as realized during the afterglow. Hence deviations from the Maxwellian shape of the electron energy distribution have to be expected. During ionization the energy loss caused by excitation to the first excited state of cesium is not thermalized by the electron electron interactions and the tail of the electron distribution becomes depleted.

A recombination coefficient of two body reaction type is measured.

Its value agrees with that given by collisional radiative models. Recombination through multi-step reactions is observed.

REFERENCES

1. HEIMEL, S., "Thermodynamic properties of cesium up to 1500 K", NASA TN-D-2906, (1965).

2. HELLEBREKERS, W.M., "Instability analysis in a nonequilibrium MHD generator", Ph.D. thesis, Eindhoven University of Technology, Eindhoven (1980).

3. HOUBEN, J.W.M.A., "Loss mechanism in an MHD generator", Ph.D. thesis, Eindhoven University of Technology, Eindhoven, (1973).

4. LOCHTE-HOLTGREVEN, W., "Plasma Diagnostics", North-Holland, Amsterdam, (1968);
   HUDDLESTONE, R.H., LEONARD, S.L., "Plasma Diagnostic Techniques", Academic Press, New York, (1965).

5. BORGHI, C.A., and FLINSENBERG, H.J., "Experimental investigation of a steady-state arc discharge in an Ar-Cs MHD generator plasma", Proc. 15th Int. Conf. on Phen. Ion. Gases, Vol. I, p. 329, Minsk, (1981).

6. VAN OOYEN, M.H.F., and HOUBEN, J.W.M.A., "Determination of the electron temperature of a shocktunnel-produced Ar-Cs plasma by the line reversal method using non-resonance lines of Cs", J.Q.S.R.T., Vol. 14, p. 395, (1974).

7. HIRSCHFELEDER, J.O., CURTIS, C.F., and BIRD, R.B., "Molecular Theory of Gases and Liquids", John Wiley, New York, (1954);
   VRUGT, P.J., "Shock tube study of the coefficient of thermal conductivity of helium, neon, argon and krypton", Ph.D. thesis, Eindhoven University of Technology, Eindhoven, (1976), and references here in.

8. MOHLER, F.L., "Recombination of ions in the afterglow of a cesium discharge", J. Res. Natl. Bur. Stand., Vol. 19, p. 447, (1937);
   ALESKOVKII, Yu.M., "Investigation of volume recombination in a cesium plasma, Sovjet Physics JETP, Vol. 17, p. 570, (1963);
   WADA, J.Y. and KNECHTLI, R.C., "Measurements of electron-ion recombination in a thermal cesium plasma", Phys. Rev. Lett., Vol. 10, p. 513, (1963);

D'ANGELO, N., and RYNN, N., "Diffusion and recombination of a
highly ionized cold plasma in a magnetic field", Phys. of Fluids,
Vol. 4, p. 1303, (1961);

HAMMER, J.M., AUBREY, B.B., " Ion beam measurements of cesium
recombination cross section", Phys. Rev., Vol. 141, p. 146, (1966).

9. TAKESHITA, T., GROSSMAN, L.M., "Excitation and ionization proces-
ses in non-equilibrium MHD plasmas", Proc. 4th Int. Symp. on MHD,
Vol. 1, p. 191, Warsaw, (1968).

10. LOEB, L., "Basic Processes in Gasseous Electronics", Univ. of
Calif. Press, (1960);

HARRIS, L.P., "Ionization and recombination in cesium-seeded
plasmas near thermal equilibrium", J. Appl. Phys., vol. 36,
p. 1543, (1965);

HARRIS, J.H., BALFOUR, D., "Microwave cavity studies of ionization
decay in cesium vapour", J. Phys. D., Vol. 1, p. 409, (1968);

SAYER, B., JEANNET, J.C., LOZINGOT, J., and BERLANDE, J., "Colli-
sional and radiative processes in a cesium afterglow", Phys. Rev.
A., Vol. 8, p. 3012, (1973);

SAYER, B., JEANNET, J.C., SAINT-HILAIRE, G., LOZINGOT, J., BER-
LANDE, J., "Recombination processes in a caesium afterglow in the
pressure range $0.06 \leq p_{Cs} \leq 0.4$ Torr.", J. Phys. B., Vol. 8,
p. 503, (1975).

MHD GENERATOR EXPERIMENTS

V-1 INTRODUCTION

In closed cycle MHD generators inlet stagnation temperatures of about 2000 K will be employed. The gas temperature will be considerably lower. For an inlet velocity of 1000 m/sec and for a stagnation temperature of 2000 K, the gas temperature will be 900 K. Accordingly the electron density at the inlet of the generator will be lower than 5×10^{18} m^{-3}. In order to reach a sufficiently high enthalpy extraction, a high non-equilibrium conductivity has to be realized. Corresponding to the finite development time of the non-equilibrium conductivity an inlet relaxation regime appears. The distance between the first loaded electrode pair and the position where the current is equal to 0.63 times its maximum value, is defined as the relaxation length L_R.

At low stagnation temperatures or low magnetic inductions, long relaxation lengths have been observed [1]. A long relaxation length reduces the performance of the generator. One dimensional [2] and two dimensional calculations [3] can not explain the observed slow relaxation. One dimensional calculations predict a steep increase of the current in the entrance region. Two dimensional analyses yield relaxation lengths about equal to the height of the channel. The mentioned calculations suppose a Maxwellian electron distribution. In Chap. II it has been shown that for plasma conditions present in the inlet region of the MHD generator, a deviation from the Maxwellian shape of the electron energy occurs for $n_e \leq 10^{18} \div 10^{19}$ m^{-3}. Conditions in agreement with the model for deviations from a Maxwellian electron distribution are observed in the afterglow experiment described in Chap. IV. For an ionizing plasma with an initial low electron density the electron distribution is expected to be depleted at high energies ($\varepsilon_e > 1.432$ eV) due to the excitations to the first excited state of cesium. The cal-

culations, carried out in Chap. III, yield a longer ionization relaxa-
tion time when deviations from the Maxwellian distribution are taken
into account. For an initial non-Maxwellian electron distribution with
T_e = 2100 K and T_t = 2000 K to a final condition where T_e = T_t = 2300 K
and for a seed fraction of 10^{-3}, a relaxation time of 3×10^{-4} sec is
calculated, whereas in the Maxwellian case the relaxation time is 1.2×10^{-4} sec.

The aim of this chapter is to see whether a non-Maxwellian energy
distribution can explain the long relaxation lengths observed during MHD
conversion experiments. In Sec. V-3 the relaxation region is observed
by means of photographic techniques. In Secs. V-4 and V-5 current voltage
characteristics are obtained by varying the externally applied voltage
to the generator or its external load. These results are analyzed using
a non-Maxwellian model. Finally MHD conversion experiments with pre-
ionization are discussed in Sec. V-6.

V-2 DESCRIPTION OF THE FACILITY

The experiments described in this chapter are carried out in a
5.5 liter MHD generator channel connected to a shock tube (4). In the
shock tube a shock wave is produced in an Ar-Cs test gas. The shock
wave is reflected at the end of the shock tube. The region behind the
reflected shock acts as a reservoir of hot gas during a test time of
5 msec. The stagnation pressure p_s of the Ar-Cs mixture in this region
is measured with a pressure transducer. The stagnation temperature T_s
is derived from the Mach number of the shock wave. The employed stagna-
tion temperature ranges from 3500 K down to 1600 K. The stagnation pres-
sure is kept at about 8 bar during the test time. From a rectangular
hole in the end plate of the shock tube, the gas flows through a nozzle
to the MHD channel. The nozzle Mach number is 2. Two MHD channels have
been employed: channel 1 and channel 2. Both are Faraday type channels
made of Lexan. Both channels have the same dimensions. They have an in-
let cross section of 3.8×11.8 cm^2 and they diverge linearly over 80 cm
to a cross section of 7.8×11.8 cm^2. The electrodes of both channels
are mounted in the parallel walls. Channel 1 has 51 pairs of flat elec-
trodes (width 0.4 cm) mounted flush to the walls. Channel 2 has 32 pairs
of cylindrical electrodes (diameter 0.7 cm) half way countersunk into
the walls. In both cases the electrodes are made of stainless steel.
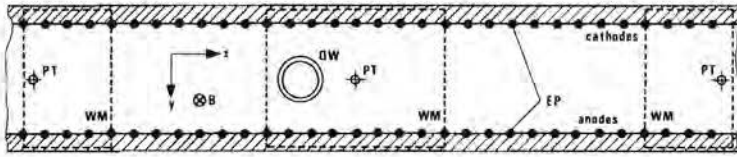The experiments described in Secs. V-3 and V-6 are carried out in channel

Figure V-1.
Side view of the generator channel.
PT: pressure transducers, QW: quartz window,
WM: port of the magnet (dotted lines),
EP: electrode pairs.

2 and the experiments described in Secs. V-4 and V-5 are carried out in channel 1.

In Fig. V-1 a side view of channel 2 is presented. Each electrode pair is separately connected to a load resistance R_L. Three pressure transducers are mounted in the channel, one at the beginning, one in the middle and one at the end. The MHD channel is installed inside a saddle shaped magnet which produces a constant magnetic induction in the duct volume. The direction of the magnetic induction $\vec{B}$ is perpendicolar to the x-y plane. Its maximal attainable value is 3.3 T. A seed ratio of 10^{-3} has been used [5].

V-3 DISCHARGE BEHAVIOUR IN THE IONIZATION RELAXATION REGION

The experiment described in this section is carried out in channel 2. In order to establish the relaxation region in front of the largest port of the magnet (see Fig. V-1), the electrodes of the pairs upstream of the 12th one have not been connected ($R_L = \infty$). The electrodes of the pair 12 to 32 are each connected to a load resistance of 2 Ω.

Electrical currents, Hall voltages and static pressures are measured. In order to study the development of the discharges in the relaxation region, high speed photography is employed. An image converter camera (IMACON) is installed with the optical axis parallel to the magnetic induction and is focused on the side wall of the channel. The camera

is used in two modes: the framing mode and the streak mode (6). In the framing mode, pictures are made of five complete electrode segments. The pictures are taken in a sequence of eight frames. The time interval between the first and the last frame is 35 μsec. The exposure time of each frame is 2.5 μsec. The scheme of the streak photography technique
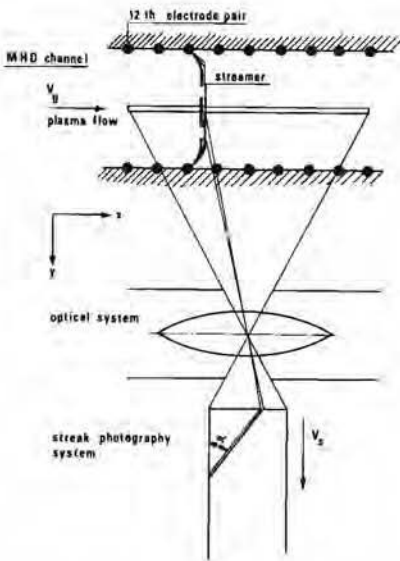

Figure V-2.
Scheme of the streak photo-
graphy arrangement.

employed in this experiment is presented in Fig. V-2. A slit, present in the camera, is projected on the side wall of the channel. The slit is directed in the x-direction and covers 20 cm between the 12th and the 20th electrode pair. The direction of streak velocity is along the y-direction. The streak velocity v_s is 140 m/sec. A small light emitting part of the plasma having a velocity v parallel to the slit, will cause a line on the film. If this velocity is constant, the line will be a straight line under an angle α with the direction of v_s. From the value of α, the velocity v can be derived:

$$v = \frac{v_s}{f} \tan \alpha. \qquad (V-1)$$

Here f is the enlargement of the optical system. The value of f is 0.087.

A number of runs with different parameters, leading to different relaxation lengths have been made. The values of R_L and the main gas-

dynamical parameters are shown in Tab. V-1. The values of the gas
pressure p_g, the gas temperature T_g and the gas velocity u_g indicated
in the table, refer to the position of the 16th electrode pair. The
value of p_g is measured at that location. T_g and u_g are calculated by

Run	L_R (m)	T_s (K)	p_s (bar)	B (T)	T_g (K)	p_g (bar)	u_g (m/sec)	P_{th} (MW)	P_{el} (kW)
3064	0.02	3365	7.27	2.76	1442	0.59	1415	2.9	92.5
3069	0.05	3101	7.80	2.84	1329	0.59	1358	3.0	73.6
3059	0.07	3084	7.23	2.49	1322	0.46	1354	2.8	77.6
3060	0.16	2802	7.32	2.49	1291	0.45	1290	2.7	19.3
3063	0.19	2577	7.36	2.39	1104	0.46	1238	2.6	13.4
3061	>0.45	2562	7.33	2.06	1098	0.50	1234	2.0	3.3

Table V-1.
*Main parameters of the runs for the investigation of the discharge
behaviour in the relaxation region.*

using a one dimensional gasdynamical program (4). The value of the
magnetic induction, the thermal input power P_{th} and the electrical
power output P_{el} are also listed in the table. The current distributions
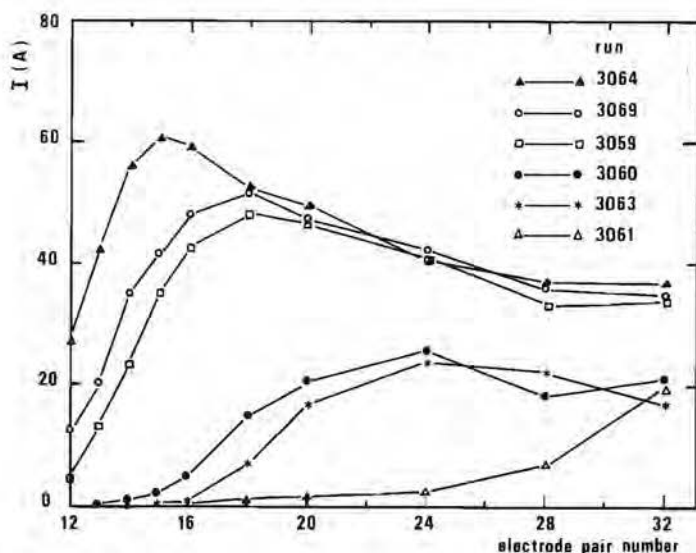

Figure V-3-A.
Current distributions along the channel for the runs of Tab. V-1.

along the channel are given in Fig. V-3-A. From the figure it can be
seen that the relaxation length increases both with the decrease of the
stagnation temperature and with the decrease of the magnetic induction.
(Similar results are found in Ref. 1). The Hall voltage distributions
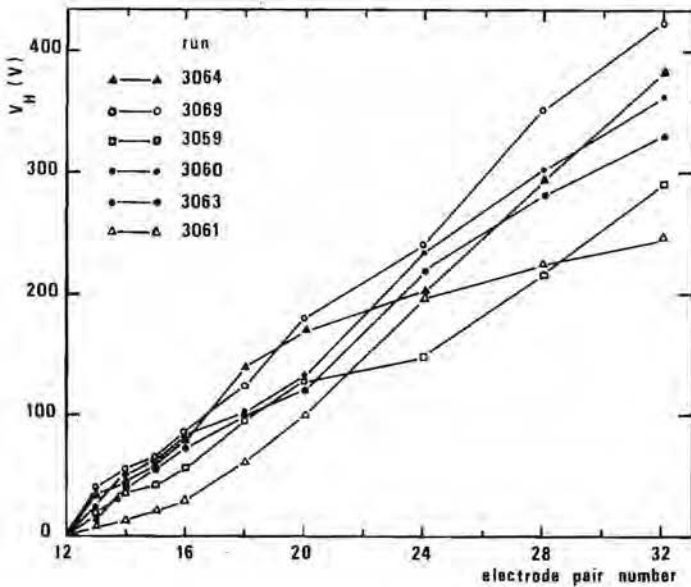along the channel are plotted in Fig. V-3-B. The Hall voltage distribu-

Figure V-3-B.
Hall voltage distributions along the channel for the runs of
Tab. V-1.

tions are obtained from the voltage differences between the anodes. The
distances over which the Hall voltages are measured, are shorter in the
entrance region than further downstream in the channel. No correlation
has been observed between the local Hall field and the relaxation length.

In Fig. V-4 the discharge structure shown by frame photography, is
presented. The discharge is strongly inhomogeneous in the relaxation
region (Fig. V-4a) as well as downstream of the relaxation region (Fig.
V-4b). Apparently the streamers are allready formed in the relaxation
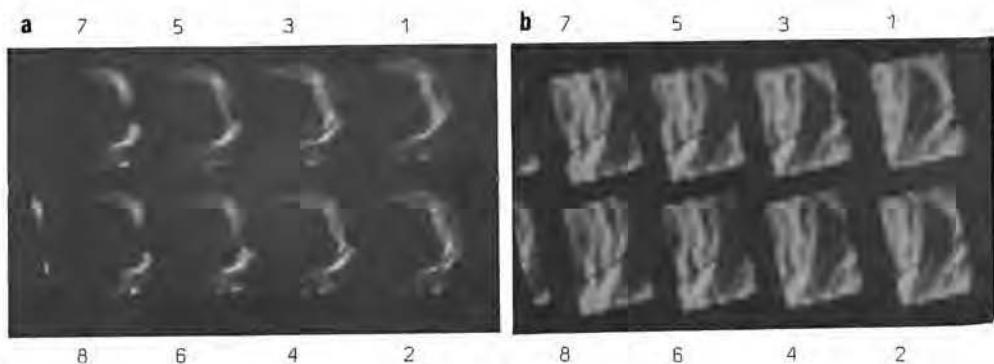region. The difference between Figs. V-4a and V-4b is the downstream

Figure V-4.
Framing pictures of the discharge:
a. in the relaxation region,
b. downstream of the relaxation region.

bending of the discharges. In the relaxation region the discharges are displaced over distances comparable to the channel height which is in agreement with the results of two dimensional calculations (3). In the downstream area the bending is substantially smaller. The streamers, however, do not always start from the first electrode, so that the relaxation length can be longer than the channel height.

Streak pictures of the discharge in the relaxation region are shown in Fig. V-5. They refer to some of the runs listed in Tab. V-1. The discharge is everywhere constricted. The streamers grow by increasing their diameter. Further the pictures confirm the results of the framing pictures that streamers do not always start from the first electrode pair. The relaxation length is determined by two processes: the growth of an individual streamer and the characteristic time necessary to the formation of new streamers. However, the characteristic time for the growth of an individual streamer does not depend on the stagnation temperature and on the magnetic induction whereas the relaxation length depends strongly on these parameters. The comparison of the streak pictures with the current distributions along the generator (Fig. V-3-A) shows that streamers appear as soon as a corresponding minimum current of about 1 A is measured (see Runs 3060 and 3063). Below this minimum value the development of the streamer becomes difficult. As a current constriction in streamer is observed to be approximately 1 cm^2 a current density $J_T \sim 1 \times 10^4$ Am^{-2} corresponds to the minimum current.
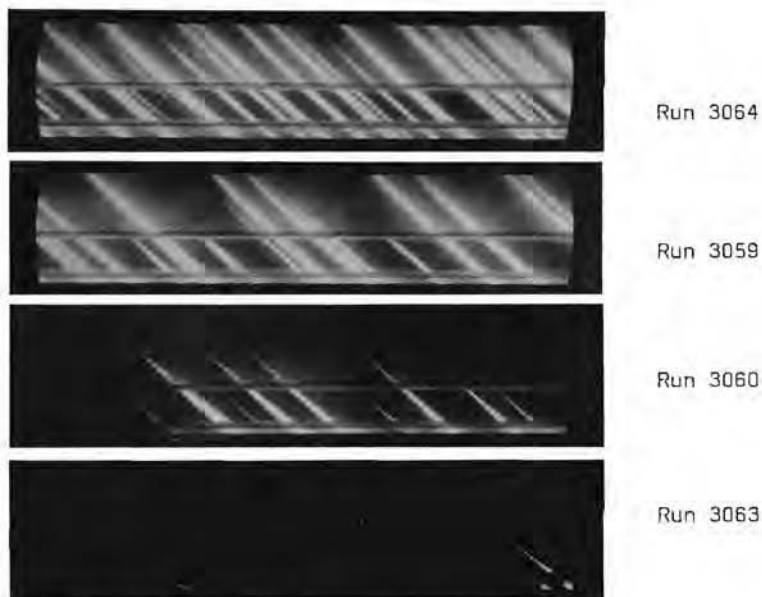
97

Run 3064

Run 3059

Run 3060

Run 3063

Figure V-5.
Streak pictures of the discharge in the entrance region of the
MHD channel.

The velocity of the discharges is derived from the measurement of
the angle α. The values of the streamer velocity for the runs of Fig.
V-5 agree in first order with the gas velocities given in Tab. V-1
(compare for further details Ref. 8).

V-4 BATTERY EXPERIMENT

The non-equilibrium conductivity is built up in the ionization
relaxation region. Here the discharge undergoes a transition from a
low to a high current mode · In order to investigate the current transi-
tion, current voltage characteristics of the discharge at one electrode
pair have been measured (9).

The experiments have been carried out in channel 1. The 33rd elec-
trode pair is connected to a set of accumulators in series with a load
resistance of 1 Ω. The other electrode pairs are operated under open
circuit conditions. The equivalent network of the circuit at the 33rd
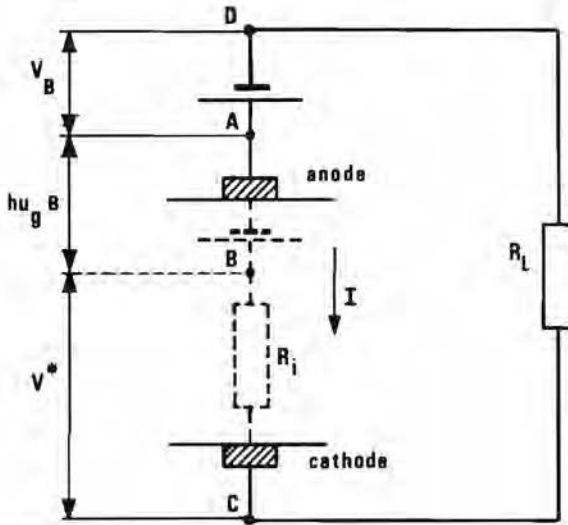electrode pair is given in Fig. V-6. The induced voltage $h u_g B$ (h is

Figure V-6.
Equivalent network for the measurement of the current-voltage
characteristic.

the electrode distance) is introduced in the network as a virtual
battery. The voltage between B and C is given by:

$$V^* = hu_g B + V_B - R_L I. \tag{V-2}$$

Here V_B is the voltage of the external power supply. The current I is
calculated from the measured voltage over the load. The value of
$hu_g B$ is derived from the results of the quasi-one dimensional cal-
culations mentioned in Sec. V-3. (Fig. V-7 shows that a large number
of Faraday voltages are affected by the external power supply. Only
the voltages at the channel entrance and at the very channel exit
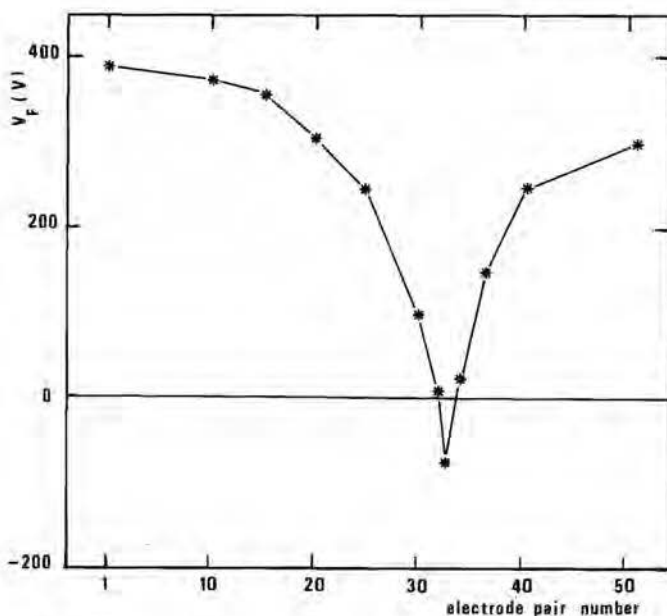approximate $hu_g B$.)

Figure V-7.

Faraday voltage distribution along the channel when the 33rd electrode pair is connected to an external power supply.
$B = 2.6\ T,\ u_g = 1490\ m/sec,\ V_B = 74\ V,\ I = 6.3\ A,\ R_L = 1\ \Omega.$
The induced voltage $hu_g B$ is calculated to be 360 V.

The experiments are carried out at a stagnation temperature of 3500 K. The static pressure at the 33rd electrode pair is 0.3 bar and the gas velocity is 1500 m/sec. Several values of the magnetic induction between 0 and 3 T have been applied.

The resulting I-V* characteristic are given in Fig. V-8 for several values of the magnetic induction. From the figure it can be seen that a minimum voltage V_T^* is necessary to sustain the discharge. Minimum currents I_T of approximately 2 A are measured. Taking as reference the value of I_T found for B = 0 and assuming for the discharge cross section the cross section of the generator segment, a current density $J_T = 2 \times 10^3$ A/m^2 corresponds to the minimum current. The transition voltage V_T^* is strongly affected by the magnetic induction. The value of V_T^* obtained by extrapolation, is plotted as a function of B in Fig. V-9.
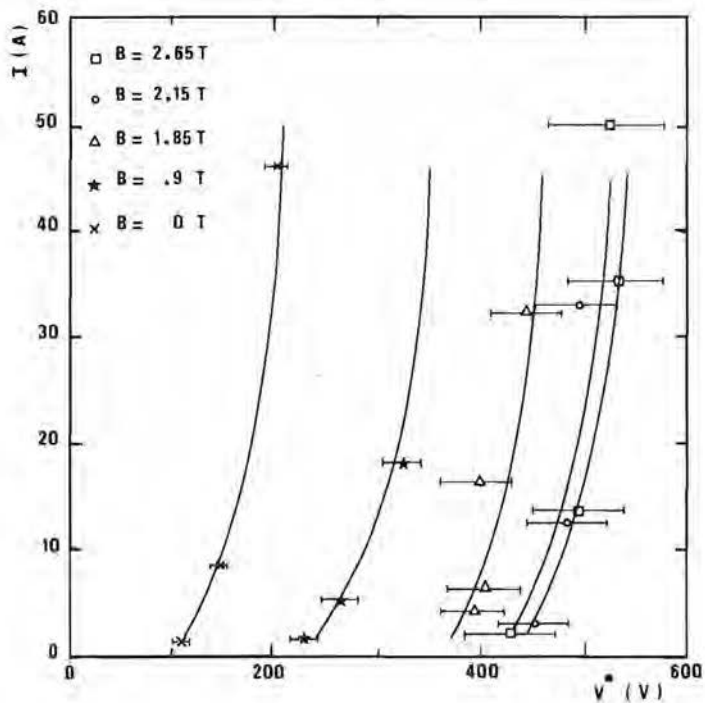
Figure V-8.
Current voltage characteristics at several values of the magnetic
induction. The 33rd electrode pair is connected to an external
power supply and the other electrodes are operated under open
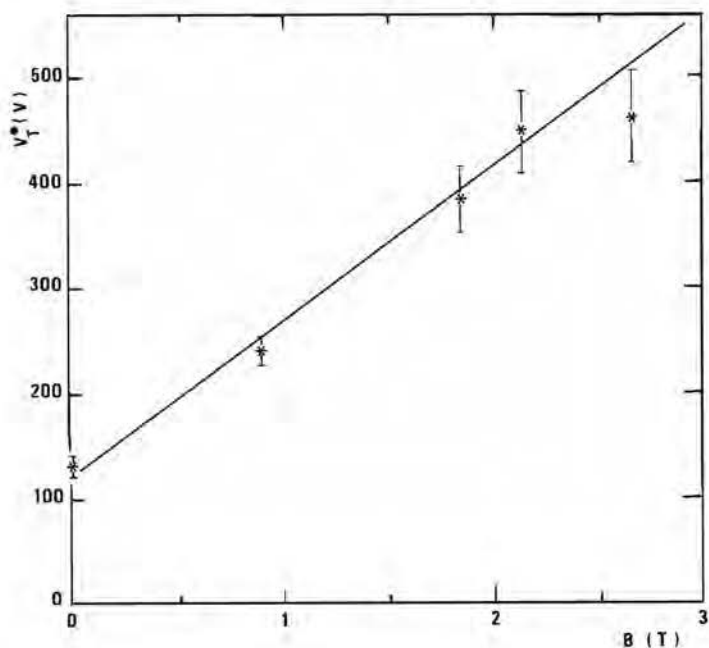circuit conditions (errors determined by the error in u_g).

Figure V-9.
Transition voltage versus magnetic induction.

V-5 LOAD RESISTANCE VARIATION

The aim of the experiment described in this section, is to examine the relation between current and voltage ($V = R_L I$) in real MHD generators (the applied voltage is now equal to zero). Especially low currents are considered in order to study the onset of the discharge. The induced voltages have been kept constant. The load resistances are varied. All electrode pairs are loaded with the same resistance R_L. By changing the load R_L, an I-V characteristic is obtained. Applied values of R_L are: 1, 3, 25, 30, 42, 71, 123 Ω and ∞. Channel 1 has been used for this experiment. The stagnation temperature is 2400 K, the inlet static pressure 1 bar and the magnetic induction 2.7 T. The main plasma conditions of each run are listed in Tab. V-2. Here u_g, T_g and ρ_g refer to values at the entrance of the generator. The Hall voltage V_H is measured between the 1st and the 51st anode.

Run	R_L (Ω)	T_S (K)	B (T)	V_H (V)	u_g (m/sec)	T_g (K)	p_g (bar)	P_{th} (MW)	P_{el} (kW)
2739	1	2390	2.55	570	1043	1024	1.19	3.3	78
2740	3	2320	2.82	471	1136	994	1.16	3.6	122
2745	25	2432	2.65	381	1210	1042	1.09	3.5	42
2749	123	2400	2.80	302	1200	1012	1.13	3.5	0
2742	∞	2432	2.20	181	1260	1042	1.19	3.7	-

Table V-2.
Main parameters of the runs of the experiment with variation of
the load resistance.

In Fig. V-10 the values of the currents are plotted against the measured
voltages between anode and cathode. The currents and voltages indicated
in the figure, are the averaged values from the 20th up to the 40th
electrode pair. For load resistances lower than 25 Ω the current decreases
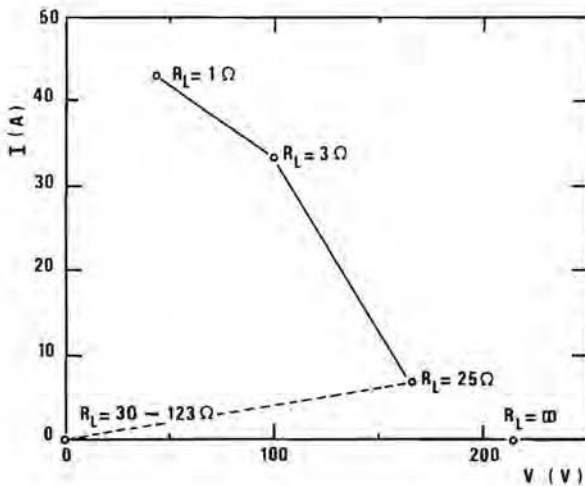continuously with increasing R_L while the voltage increases. For values

Figure V-10.
Current voltage characteristic obtained by variation of the load
resistances.

of R_L between 30 and 123 Ω the current as well as the voltage, becomes
very small. Apparently under these conditions the non-equilibrium con-
ductivity is not established and the internal resistance is much higher
than the load resistance. For $R_L = \infty$ the Faraday open circuit voltage
is measured. As a result of this experiment it can be concluded that
again a transition in the discharge characteristic is found. In this
case the minimum current measured I_T is 6 A. Assuming a constricted
discharge with a cross section of 1 cm^2 a current density $J_T = 6 \times 10^4$
A/m^2 corresponds to the minimum current.

V-6 ENERGY CONVERSION EXPERIMENT WITH PRE-IONIZATION

It has been demonstrated that the development of a sufficiently
high conductivity is strongly dependent on the stagnation temperature,
the magnetic field, as well as on the load resistance. Experiments at low
values of the stagnation temperature show a considerable inlet ionization
relaxation length, which increases strongly with a further decrease of
the inlet stagnation temperature. In order to enhance the non-equilibrium
conditions at the inlet of the generator, pre-ionization can be used.
In this section an experiment at low inlet stagnation temperature using
pre-ionization is described.

The experiment is carried out in channel 2. Load resistances of
1 Ω are used. In Fig. V-11 the scheme of the pre-ionization system is
shown. An external power source is interconnected between the first
electrode pair and the shock tube wall. The stagnation region at the
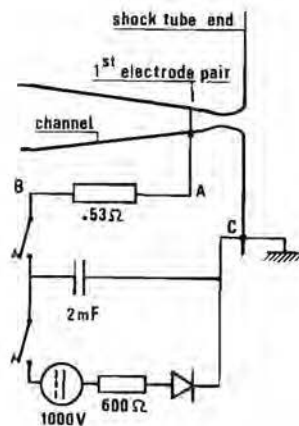end of the shock tube is used as anode. Here the initial electron

Figure V-11.
Electrical circuit of the
pre-ionizer.

density is relatively high due to the high gas density; further the
electron temperature equals the stagnation temperature. An electrolytic
capacitor of 2 mF charged to 1000 V before the run is used as external
power source. During the run the capacitor is discharged over the plasma.
The discharge current flows from the stagnation region through the nozzle
to the first electrode pair over a distance of 40 cm. The pre-ionization
current I_p is derived from the measured voltage between the locations
A and B. The voltage between the location C and A represent the pre-
ionization voltage V_p.

Run	T_S (K)	B (T)	T_g (K)	P_g (bar)	u_g (m/sec)	I_P (A)	P_P (kW)	P_{el} (kW)	P_{th} (MW)
3140	2547	2.66	1091	0.65	1092	50	19	13	2.5
3142	2025	2.28	868	0.54	1097	85	34	15	2.2
3143	1811	2.73	776	0.59	1037	91	50	8	2.2
3150	1610	2.31	690	0.83	987	99	57	3	2.1

Table V-3.
Main parameters of the runs for the pre-ionization experiment.

The main parameters of the runs of this experiment are listed in
Tab. V-3. The electrode current distribution along the channel for each
run is shown in Fig. V-12. Non-equilibrium conductivity is realized at
a stagnation temperature as low as 1610 K in run 3150. The inlet gas
temperature is 690 K. The current at the 2nd electrode pair is 5 A.
The figure shows that long relaxation lengths do no longer occur for
$T_S \geq$ 1811 K when the pre-ionization is applied. The pre-ionization current
used to realize the non-equilibrium conductivity during run 3150 is I_P =
99 A. As the pre-ionization current is along the flow direction outside of
the magnet, it is assumed that I_p fills the whole generator cross
section at the entrance. Hence a corresponding current density J_p =
2×10^4 Am^{-2} is calculated. The current at the 2nd electrode pair is
perpendicular to the magnetic induction and a discharge cross section
of 1 cm^2 is assumed. Hence a current density $J = 5 \times 10^4$ Am^{-2} corresponds
to the current measured here. As can be seen from Tab. V-3, the pre-
ionization power P_p is still a factor of 40 smaller than the thermal
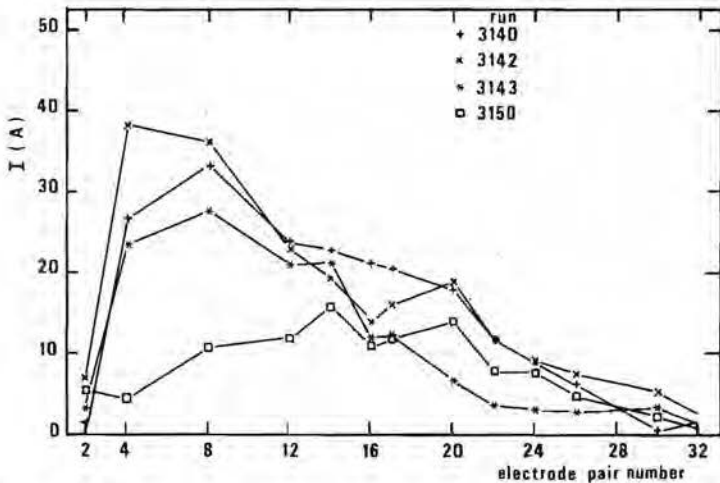input power.

Figure V-12.

Current distributions along the channel in the pre-ionization
experiment. The main parameters of the runs are listed in Tab. V-3.

V-7 DISCUSSION AND CONCLUDING REMARKS

The experiments described in this chapter are made in order to get
information on the onset of the discharges under non-equilibrium con-
ditions in the MHD generator.

In Sec. V-3 an increase of the relaxation length is observed when
the stagnation temperature or the magnetic induction are decreased. For
currents lower than 1 A no streamers appear. As discussed in Sec. V-3
the relaxation length is determined both by the growth of a single
streamer and by the time necessary for the formation of new streamers.
From the observation that the characteristic time of the streamer growth
does not vary for different relaxation lengths it can be concluded that
a long relaxation length is caused by the time to reach the conditions
necessary for the development of streamers rather than by the development
of an individuel streamer. Minimum values of the current necessary to
sustain the discharge, are observed in the experiments of Secs. V-4 and
V-5. In the battery experiment a minimum current of 2 ÷ 5A is found.
It corresponds to different voltages depending on the magnetic induction.
In the load experiment in the MHD generator, by increasing R_L up to 25

the current corresponding to a given induced voltage decreases. For R_L =
30 ÷ 123 Ω the current is lower than I_T and the non-equilibrium conducti-
vity does not develop. The internal resistance is then much larger than
the load resistance. In the open voltage experiment (R_L = ∞) a voltage
equal to $hu_g B$ is measured between anode and cathode.

When pre-ionization is applied, a sufficient non-equilibrium con-
ductivity has been built up at the entrance of the generator. In this
case long relaxation lengths can be prevented. In Tab. V-4 indicative
values of to the minimum current density derived in the experiments of
this chapter are indicated. In the table the values derived from the

Exp. Type	J (10^4 A/m^2)	E (10^3 V/m)	σ (mho/m)	n_e 10^{18} m^{-3})
Bat. exp.	0.2	0.9	2	2
R_L variation	6	2.0	30	33
Relax. exp.	1	2.9	4	4
Pre-ionizer	2.2	1.5	15	16
2nd el. pair	5	2.3	20	21

Table V-4.
Characteristic parameters at the transition from low to high
current.

pre-ionization current and from the current of the 2nd electrode pair
in run 3150 are also indicated. For all experiments, except for the
battery experiment, the electric field E is derived from $V^* = hu_g B + V_B - R_L I$. For the battery experiment E is derived from the I-V^* cha-
racteristic at B = 0 ($V^* = V_B - R_L I$). The value of the electrical con-
ductivity is obtained from J/E. The electron density is then derived
from σ by assuming the momentum collision frequency between electrons
and heavy particles equal to 3×10^{10} sec^{-1} (value corresponding to
T_e = 2000 K). The value of n_e has only an indicative meaning due to
the lack of information of the inhomogeneous structure of the plasma
in the generator at low electron density. In Chap. II a critical value
$n_{ec} = 5 \times 10^{18}$ m^{-3} is found as the threshold between non-Maxwellian
and Maxwellian regime in an Ar-Cs discharge for a seed fraction of 10^{-3}.

From Tab. V-4 it can be seen that the values of n_e corresponding to the minimum current measured in the MHD generator approximate or are larger than n_{ec}. Hence indication is found that the minimum current density observed in the MHD generator experiments is related to the transition from non-Maxwellian to Maxwellian regime. An electron density higher than n_{ec} is obtained, for instance, by means of the pre-ionizer. Here the high current regime is already present at the inlet of the generator. Therefore the generator can work under conditions where Maxwellian electron distribution can be expected and thus non-equilibrium can be built up.

As indicated in Chap. III, for non-Maxwellian conditions the relaxation time increases with respect to the Maxwellian case. When for the latter case a relaxation time of 1.2×10^{-4} is calculated, the non-Maxwellian condition yields a relaxation time of about three times larger. The corresponding relaxation lengths in these cases are 14 and 36 cm respectively for a gas velocity of 1200 m/sec. The non-Maxwellian distribution used in the calculations is derived from the data of the stationary discharge (Chap. II). In the ionizing plasma even stronger deviations from the Maxwellian shape of the electron distribution have to be expected (Chap. III). This results in a further increase of the length of the relaxation region which can fill the whole generator as in run 3061.

REFERENCES

1. VEEFKIND, A., HELLEBREKERS, W.M. BORGHI, C.A., RIETJENS, L.H.T., "Noble gas MHD generator experiments at low stagnation temperatures", Proc. 17th Symp. on Eng. Asp. of MHD, p. H.3.1, Stanford,Calif., (1978).
2. BERTOLINI, E., TOSCHI, R., Mc NAB, I.R., "Relaxation phenomena in MPD generators", Proc. 3rd Int. Symp. on MHD, Vol. 1, p. 533, Salzburg, (1966);
   TAKESHITA, T., GROSSMAN, L.M., "Excitation and ionization processes in non-equilibrium MHD plasmas", Proc. 4th Int. Symp. on MHD, Vol. 1, p. 191, Warsaw, (1968).
3. BLOM, J.H., and HOUBEN, J.W.M.A., "Relaxation length calculations in Ar-Cs mixtures for one- and two-dimensional pre-ionizer geometries", Proc. 5th Int. Symp. on MHD, Vol. 2, p. 65, Munich, (1971);
   HARA, T., VEEFKIND, A., RIETJENS, L.H.Th., "A numerical investigation of the inhomogeneous discharge structure in noble gas MHD channels",

Proc. 19th Symp. on Eng. Asp. of MHD, p. 7.2.1, Tullahoma, Tenn., (1981).

4. VEEFKIND, A., HOUBEN, J.W.M.A., BLOM, J.H., and RIETJENS, L.H.Th., "High-power density experiments in a shock tunnel MHD generator", AIAA J., Vol. 14, p. 118, (1976);
BLOM, J.H., "Relaxation phenomena in an MHD generator with pre-ionizer", Ph. D. Thesis, Eindhoven University of Technology, Eindhoven, (1973).

5. VEEFKIND, A., SENS, A.F.C., WETZER, J.M., "Shock tube investigations on MHD conversion in argon-cesium", Proc. 10th Symp. on Eng. Asp. of MHD, p. 7.3.1, Tullahoma, Tenn., (1981).

6. BORGHI, C.A., SENS, A.F.C., VEEFKIND, A., RIETJENS, L.H.Th., "Experimental investigation on the discharge structure in a noble gas MHD generator", T.H. Report 78-E-79, Eindhoven University of Technology, Eindhoven, (1978).

7. HELLEBREKERS, W.M., VEEFKIND, A., BORGHI, C.A., "Experiments on the nonuniform discharge structure in noble gas MHD generators", Proc. 18th Symp. on Eng. Asp. of MHD, p. D.2.1, Butte, Mont., (1979).

8. SENS, A.F.C. BITYURIN, V.A., WETZER, J.M., VEEFKIND, A., "Investigations on the gasdynamical effects of a non-uniform supersonic flow with streamers in a noble gas MHD generator", to be published, Proc. 20th Symp. Eng. Asp. of MHD, Irwine, Calif., (1982).

9. VEEFKIND, A., BORGHI, C.A., GEUTJENS, A.J., HELLEBREKERS, W.M., MERCK, W.F.H., MESLANO, A.J., SENS, A.F.C., RIETJENS, L.H.Th., "Investigations on the non-equilibrium condition in a shock-tunnel driven noble gas MHD generator", Proc. 7th Int. Conf. on MHD Power Generation, p. L.4.1, Cambridge, Mass., (1980).

CONCLUSIONS

A self consistent model for a stationary discharge has been set up. It predicts deviations from the Maxwellian electron energy distribution for electron densities below a critical density n_{ec} which is generally between 18^{18} and 10^{19} m^{-3}. Then the high energy tail of the electron distribution will be depleted when radiation escapes. As a consequence the ionization degree will be lower when compared to the value given by Maxwellian models.

The main cause of deviations from the Maxwellian distribution is represented by the non-elastic collisions resulting in the transitions between the ground state and the first excited state of cesium. For electron densities larger than n_{ec}, the energy transfer to the tail due to electron electron interaction is much larger than the energy loss due to non-elastic collisions; then the electron energy distribution is Maxwellian. For electron densities lower than n_{ec} both energy transfer processes are of the same order and consequently the electron energy distribution is non-Maxwellian.

When the electron density decreases further below the critical value, the tail of the electron distribution in the stationary discharge becomes more and more depleted. As a consequence of that, when the current density decreases, the discharge has to be sustained by an increasing electric field.

Time dependent calculations of the ionization process, which include deviations from the Maxwellian electron distribution, show at low electron densities relaxation ionization times longer than those resulting from Maxwellian models. This is a consequence of two effects appearing as soon as a non-Maxwellian electron energy distribution has to be taken into account. In this case the densities of the electrons and of the excited states in the initial conditions as well as the rate integrals for excitation and ionization are lower than when calculated

under the Maxwellian assumption.

An arc discharge in an Ar-Cs mixture is experimentally investigated. Under stationary conditions the current range is $0.2 \div 3$ A and corresponds to electron densities of $1 \times 10^{20} \div 4 \times 10^{20}$ m^{-3}. During the stationary discharge L.T.E. is observed.

Conditions for deviations from a Maxwellian electron energy distribution are realized during the afterglow of the discharge. For low values of n_e ($\lesssim 10^{19}$ m^{-3}) the electron interactions are not efficient enough to thermalize the energy gained by the tail electrons owing to the de-excitations from the first excited state. Consequently the tail of the electron distribution becomes overpopulated. As the values of T_e and n_e in the inlet region of the MHD generator are of the same order as realized during the afterglow, deviations from the Maxwellian shape of the electron energy distribution have to be expected there too. During the ionization of the plasma the energy loss caused by the excitation to the first excited state of cesium is not thermalized by the electron electron interactions and the tail of the electron distribution becomes depleted.

Minimum values of the current are measured in MHD generator experiments. They correspond to a current density J_T and related electron density, where a transition from the non-Maxwellian to the Maxwellian regime is expected. When the current density is larger than J_T, the electron distribution is Maxwellian. When the current density is lower than J_T, the electron distribution is non-Maxwellian. In the latter case the electron distribution is underpopulated at the high energies and the onset of the non-equilibrium becomes difficult. The relaxation ionization process is retarded and leads to a long relaxation length.

For stagnation temperatures of 2400, 2000 and 1800 K and a stagnation pressure of 8 bar, electron densities of 3.4×10^{20}, 4.5×10^{19} and 1.2×10^{19} m^{-3} are obtained in the stagnation region of the shock tube. These values lead to electron densities of 4.2×10^{19}, 5.6×10^{18} and 1.5×10^{18} m^{-3} and to a pressure of 1 bar in the entrance region of the MHD generator. In the experiments at a magnetic field of 3 T and with a seed ratio of 10^{-3} (see Ref. 1 Chap. V), a short relaxation length (~ 1 cm) has been observed for T_S = 2400 K. The relaxation length increases to 15 cm for T_S = 2000 K. A limiting case is given for T_S = 1800 K where L_R is 55 cm. The value of n_{ec} calculated for a

seed fraction of 10^{-3} is 5×10^{18} m^{-3}. In the first case (T_S = 2400 K) the inlet electron density is larger than n_{ec} and the discharge develops from a Maxwellian initial condition. The non-equilibrium conductivity is easily built up. For the second case (T_S = 2000 K) the inlet electron density is about equal to the critical electron density n_{ec} where the transition between non-Maxwellian and Maxwellian regime is expected. The onset of the discharge is more difficult than in the former case but the non-equilibrium regime can still be built up in a reasonable distance from the inlet of the generator. However, when the inlet n_e is smaller than n_{ec} (T_S = 1800 K) the onset of the non-equilibrium regime becomes critical. Below 1800 K it is not possible to obtain a sufficient non-equilibrium conductivity without increasing the inlet electron density by means of a proper pre-ionizer (Sec. V-6).

SAMENVATTING

In dit werk wordt het begin van de ontwikkeling van het niet-even-
wichtsgeleidingsvermogen in het ingangsgebied van een edelgas-MHD-genera-
tor zowel theoretisch als experimenteel onderzocht. Het relaxatie-proces
dat uitmondt in de niet-evenwichtstoestand hangt hoofdzakelijk af van het
aantal ionisaties per volume per tijd. Bij lage gastemperaturen wordt het
ionisatie-relaxatieproces de beperkende faktor voor de werking van de
generator.

Afwijkingen van de Maxwellse vorm van de energieverdeling van de
elektronen zijn bij lage temperaturen van invloed op een ontlading. De
inelastische botsingen die de overgangen van de grondtoestand naar de
eerste aangeslagen toestand van het cesium atoom veroorzaken, leiden tot
een verlies van electronen met hoge energieën. Bij lage elektronendicht-
heden is de thermalisatie door elektron-elektron botsingen niet efficient
genoeg om dit verlies te compenseren, zodat de staart van de elektronen-
verdeling ontvolkt wordt. Het gevolg hiervan is een afname van het aantal
ionisaties per volume per tijd, dat immers volgt uit het aantal botsingen
van cesium atomen met elektronen van hoge energie. Hierdoor bouwt de elek-
tronendichtheid zich minder snel op dan verwacht wordt volgens theorieën
die een Maxwellse verdeling gebruiken.

Eerst wordt een in zichzelf consistent model opgesteld van een ontla-
ding in een mengsel van argon en cesium bij atmosferische drukken. Vol-
gens het model ontstaan afwijkingen van de Maxwellse verdeling van de
elektronen bij elektronendichtheden lager dan $10^{18} \div 10^{19}$ m^{-3} indien
straling kan ontsnappen. In hoofdstuk III worden afwijkingen van de Max-
wellverdeling van de elektronen opgenomen in een model waarmee bereke-
ningen worden uitgevoerd aan het tijdafhankelijk gedrag van de elektro-
nendichtheid en van de bezettingen van aangeslagen toestanden zoals dat
volgt op een verandering van de elektronenenergie. Er wordt door deze the-
orie een toename van de karakteristieke tijd voor ionisatie-relaxatie
verwacht.

In een ontladingsexperiment zijn twee omstandigheden onderzocht: een
stationaire boogontlading en het nalichten ervan. De hoogste waarde van
de elektrondichtheid die is verkregen onder stationaire condities is

4×10^{20} m^{-3}, de laagste is 1×10^{20} m^{-3}. Gedurende de stationaire ont-
lading is L.T.E. waargenomen. Lagere elektronendichtheden zijn geme-
ten gedurende het nalichten van de ontlading. De waarden van n_e en T_e
die dan gerealiseerd worden komen overeen met die welke zich voordoen in
het ingangsgebied van de MHD-generator. Gedurende het nalichten van de
ontlading komt het plasma in een toestand die aanleiding geeft tot afwij-
kingen van de Maxwellse vorm van de energieverdeling van de elektronen.

Een experimenteel onderzoek naar de overgang van lage naar hoge
stroom in de MHD-generator wordt in hoofdstuk V beschreven. De omstandig-
heden bij het ontstaan van de niet-evenwichtstoestand komen overeen met
die welke zich voordoen bij de overgang van de niet-Maxwellse naar de
Maxwellse toestand. Voor een lage ingangswaarde van n_e ($\lesssim 5 \times 10^{18}$ m^{-3})
wordt een niet-Maxwellse elektronenverdeling verwacht waardoor de niet-
evenwichtstoestand moeilijk opgebouwd kan worden. Het gevolg hiervan is
dat de relaxatielengte groter wordt. Bij een magnetische induktie van
3 T en een ingangswaarde van n_e kleiner dan 5×10^{18} m^{-3} worden relaxatie-
lengten gevonden die groter zijn dan 50 cm. Als de ingangswaarde van n_e
gelijk is aan 5×10^{18} m^{-3} dan is de relaxatielengte 15 cm. Hogere in-
gangswaarden van n_e leiden tot kortere relaxatielengten.

ACKNOWLEDGEMENTS

CURRICULUM VITAE

The author of this work was born the 17th of March, 1951 at Massa Lombarda (Italy). In July, 1970 he received the school-leaving certificate of the Scientific Liceum "G. Ricci Curbastro" (Lugo di Romagna). In February, 1976 he took the degree in Nuclear Engineering at the University of Bologna. The title of the graduation thesis is: "Stability of a nuclear reactor with N coupled junctions and power counterreaction". From March 1976 to February 1978 he was research assistant at the University of Bologna, Laboratorio di Ingegneria Magnetofluidodinamica. The research carried out is based on the gasdynamical performance of a shock tube. From January to August 1977 he worked as a guest at the Eindhoven University of Technology within the co-operation between University of Bologna and Eindhoven University of Technology on MHD Power Generation. The topic of the research is: Discharge structure in a noble gas MHD generator. From March 1978 to May 1982 he worked as research fellow at the Eindhoven University of Technology, Department of Electrical Engineering, Division Direct Energy Conversion. The research is based on the building up of the non-equilibrium conductivity in a noble gas MHD generator plasma and has led to the present thesis.

-1-

The building up of the non-equilibrium regime in noble gas MHD
generators is achieved through a transition from a regime where
the electron energy distribution is described by a non-Maxwellian
function with a depressed tail to a regime where the electron
energy distribution is described by a Maxwellian function.

-2-

When the non-equilibrium has been built up in a noble gas MHD
generator, the plasma is in a state of local thermodynamic
equilibrium.

-3-

Due to the large line broadening compared to the optical resolution
of the monochromator, in many experiments the observed line inten-
sities resulting from the high states of cesium appear to be low.
This is not caused by the depletion of the high states as stated
by several authors.

> For excmple: E.E. Antonov et al., High Temp.,
> Vol. 14, p. 1032, 1975.

-4-

The strongly non-linear dependence of the ionization process on
electron density, favours the growth of the current constricted
in streamers observed in noble gas MHD generators.

-5-

It is possible to describe the establishment of the non-equilibrium
conductivity through volume relaxation phenomena assuming charge
neutrality.

-6-

The main difference between open cycle and closed cycle MHD generators
is the way to achieve the necessary electrical conductivity of the
flow. In open cycle the required conductivity is realized at the gas
temperature and is already present at the inlet of the generator

whereas in closed cycle the non-equilibrium conductivity has to be built up by the Joule heating inside the generator.

-7-

The order which man attributes to natural phenomena is only a means of man to know them. The consciousness that nature does not know that order is the basis of scientific work.

> See also: A.M.S. Boethius, "De consolatione philosophiae", ca. 524; L. Wittgenstein, "Tractatus Logico-Philosophicus", 1921.

-8-

The evolution has no aim.

> See also: C. Darwin, "On the evolution of species", 1859.

-9-

The worth of a man for the community in which he lives depends on the contributions of his sentiments, his thoughts and his actions to the development and the life of the other men.

> A. Einstein, "Mein Weltbild", 1934.

-10-

The shortage of energy is one of the major problems that modern technology tries to solve. On the other hand modern technology requires larger and larger quantities of energy.

-11-

At present, Italy is struck by two kinds of terrorism: the terrorism of weapons and the terrorism of information. The latter is much more dangerous as no police can fight it.

-12-

To do something new within a tradition is a contradiction but sometimes new ideas can arise from traditional practices.

Eindhoven, 1 juni 1982.   C.A. Borghi